#467

SO-11A, 11B, 11C, 11D

NO NEW I.D.'s

Table of Contents

---

1. INTRODUCTION:

The documentation for this data set was originally on paper, kept in NSSDC's Data Set Catalogs (DSCs). The paper documentation in the Data Set Catalogs have been made into digital images, and then collected into a single PDF file for each Data Set Catalog. The inventory information in these DSCs is current as of July 1, 2004. This inventory information is now no longer maintained in the DSCs, but is now managed in the inventory part of the NSSDC information system. The information existing in the DSCs is now not needed for locating the data files, but we did not remove that inventory information.

The offline tape datasets have now been migrated from the original magnetic tape to Archival Information Packages (AIP's).

A prior restoration may have been done on data sets, if a requestor of this data set has questions; they should send an inquiry to the request office to see if additional information exists.

2. ERRATA/CHANGE LOG:

NOTE: Changes are made in a text box, and will show up that way when displayed on screen with a PDF reader.

When printing, special settings may be required to make the text box appear on the printed output.

Version	Date	Person	Page	Description of Change
01				
02				

3 LINKS TO RELEVANT INFORMATION IN THE ONLINE NSSDC INFORMATION SYSTEM:

http://nssdc.gsfc.nasa.gov/nmc/

[NOTE: This link will take you to the main page of the NSSDC Master Catalog. There you will be able to perform searches to find additional information]

4. CATALOG MATERIALS:

a. Associated Documents To find associated documents you will need to know the document ID number and then click here. http://nssdcftp.gsfc.nasa.gov/miscellaneous/documents/

b. Core Catalog Materials

REQ. AGENT	RAND NO.	ACQ. AGENT
DEW		HKH

SO-11A, 11B, 11C, 11D

This data set catalog consists of 6 data tapes. The tapes are 6250 BPI, 9 track, EBCDIC and contain 1 file of data each. They were created on an IBM 360/75 computer.

SO-11A

D#	C#
D-39850	C-21061
D-39851	C-21062

SO-11B

D-39852	C-21037
D-39853	C-21038

SO-11C

D-39854	C-21039

SO-11D

D-39870*	C-21019*

* These tapes contain binary data.

SO-11A

Corrected by HKH/NSSDC

POGO LOW LATITUDE ANOMALY FIELD DATA SET

This tape contains a subset of data from the POGO (Polar Orbiting Geophysical Observatory: OGO-2, OGO-4, OGO-6) satellites. This data set was created utilizing the data set originally derived by Regan, Cain, and Davis [J. Geophys. Res., Feb. 10, 1975, Vol. 80, No. 5, pg. 794-802].

The original data selection contained only data with $K_p \leq 2^+$, and then limited the data to ±50° geographic latitude, and altitude below 700 km. Data taken between 0900 and 1500 hours local time was excluded to avoid most of the effects of the equatorial electrojet. Magnetic field values obtained from a main core field model (POGO 0272), were subtracted from the observed satellite data to yield raw anomaly field data.

The raw anomaly field data for each pass of the satellite has an estimate of the field due to magnetospheric sources removed. The potential function, from which the estimate is derived, is

$$V = a\,[(r/a)\,e + (a/r)^2\,i]\quad(\cos\theta) \qquad (1)$$

where a = mean radius of the Earth = 6371.2 km

r = position of the satellite relative to the center of the Earth

θ = colatitude

This form of potential best reproduces the estimated disturbances due to magnetospheric sources. A modified magnetic field value, ΔB, is then determined by subtracting a computed field value, determined by the potential function, from the raw anomaly field value. The variables, i and e, in Equation (1) are solved for by a method which results in the best fit, in a least squares sense, to the satellite pass in question, from -50° to +50° latitude. The computed field value is included on this data tape designated as "magnetospheric field correction".

In addition to the magnetospheric field correction, a first or second degree polynomial is fit to the ΔB value for each satellite pass. This polynomial fit was determined necessary [Mayhew, J. Geophys., 45, pg. 119-128, 1979] in order to bring anomaly data from separate satellite passes over the same geographic region into internal consistency. For the present data, this correction is made in three segments for each pass; 0° to 50° latitude, -25° to +25 latitude, and -50° to 0° latitude. Comparison of overlapping segments indicates good agreement over most of the overlapping region of each segment. The greatest disagreement is near the end points. The coefficients of the polynomial fits are included on the tape.

In general, to reconstruct what is believed to be a good estimate of the anomaly field, one should take the anomaly field value (F (5,N) on the tape) and subtract from it the magnetospheric field correction (F (6,N)), and the field from the polynomial correction (not included on the tape). These calculations have been done, and the estimated anomaly field, for each segment, are included on the tape (F (8,N), F (9,N), and F (10,N)).

The field generated from the polynomial fit may be computed by:

a) determining the latitude of the satellite at the time the raw magnetic field value was taken.

b) determining into which segment of the three segments this value of latitude fits "best".

c) using the given coefficients of a quadratic polynomial of the given segment ([A(1), A(2), A(3)] for the segment covering latitudes 0° to 50°, [A(4), A(5), A(6)] for the segment covering latitudes -25° to +25°, [A(7), A(8), A(9)] for the segment covering latitudes -50°

to 0°) and the independent variable, latitude (F(2,N), construct and solve the resulting polynomial:

$$FIT = A(M) + A(M+1) * F(2,N) + A(M\ 2) * F(2,N)^2$$

For M=1, 4, or 7. (For those tapes where a linear fit is removed A(3), A(6), and A(9) are all zero.)

TAPE INFORMATION

The satellite data is on two files of one tape. The first file contains ascending satellite data, and the second file contains descending satellite data. This tape is in EBCDIC format, generated on an IBM S/360-91 computer with the following Job Control Language:

```
UNIT = 800, DISP = (NEW, KEEP), LABEL = (1, NL),
DCB  = (RECFM = FB, LRECL = 80, BLKSIZE = 800, DEN = 2)
VOL  = SER = XXXXXX
```

Subject to change

The UNIT address identifies the tape drive to be used to read the 9-track, 800 bpi density magnetic tape.

The DISP parameter specifies the disposition of the tape. The NEW subparameter specifies that the data set did not exist before this job step. The KEEP subparameter specifies that the data set is to be kept on this tape volume if this step abnormally terminates.

The LABEL parameter specifies additional information about what is written on the tape. The numeric subparameter specifies that the data sets begin with file 1, at the beginning of the tape, immediately after the reflector strip. The NL subparameter specifies that the tape does not have a system or user label. (The tapemarks between files of non-labeled tapes are one byte in length).

The DCB parameter specifies data control block information. RECFM = FB specifies the record format as being in fixed block lengths. LRECL = 80 specifies the logical record length as 80 bytes. BLKSIZE = 800 specifies the block length as 800 bytes (10 logical records). There is an inter record gap of 5/8" between blocks. DEN = 2 specifies the density of the tape as 800 bpi.

The VOL parameter specifies the volume serial number of the tape as XXXXXX to correspond to the external label on the tape. Since there is no internal label, this number is arbitrary.

The data for each satellite pass is contained in a series of three types of 80 byte (card formatted) records created with the following write statements.

I. Header Information: (number of records = 1)

```
      WRITE (9,200) MJD,ISAT,IHO,NPTS,EQLON
  200 FORMAT (4I10, F15.8)
```

where:
- MJD = Modified Julian Date (11/2/79 = 44179)
- ISAT = Number of the OGO satellite which made the data measurement (either OGO-2, OGO-4, or OGO-6)
- IHO = Half-orbit number for an OGO satellite. A half-orbit is defined here as the partial orbit of the satellite from one of the Earth's poles to the opposite pole. This number is uniquely associated with a satellite pass for the specified satellite only.
- NPTS = Number of observations for this satellite pass.
- EQLON = Longitude of the satellite as it passes the equator in degrees.

II. Polynomial fit information: (number of records = 1)

```
      WRITE (9,201) (A(K), K = 1,9)
  201 FORMAT (9F8.4)
```

where: A(1), A(2), and A(3) are the coefficients of the constant, linear, and quadratic terms, respectively, of the quadratic polynomial fit of the data as a function of latitude. The latitude boundaries of

the data fit by the polynomial function for this satellite pass are 0° and 50°.

A(4), A(5), and A(6) are values similar to A(1), A(2), and A(3), respectively, but the latitude boundaries of the data fit by the polynomial function for this satellite pass are -25° and +25°.

A(7), A(8), and A(9) are values similar to A(1), A(2), and A(3), respectively, but the latitude boundaries of the data fit by the polynomial function for this satellite pass are -50° and 0°.

III. Data Information: (number of records = NPTS)

```
      WRITE (9,202) ((IF(1,N), F(2,N), F(3,N), F(4,N),
     *               F(5,N), F(6,N), IF(7,N), F(8,N),
     *               F(9,N), F(10,N)), N = 1, NPTS)
  202 FORMAT (I8, 5F8.4, I8, 3F8.4)
```

where: IF (1,N) = Time of day in milliseconds (0 to 86400000)

F (2,N) = Latitude of the satellite for this observation point (in degrees)

F (3,N) = Longitude of the satellite for this observation point (in degrees)

F (4,N) = Altitude of the satellite for this observation point (in kilometers) above the Earth's surface (6371.2)

F (5,N) = Raw anomaly field value (before corrections) (measured in gammas, $1\gamma = 1 \times 10^{-9}$ tesla)

F (6,N) = Magnetospheric field correction (in gammas)

IF (7,N) = Magnetic activity index, K_p (see attached Magnetic Activity Index Chart)

F (8,N) = Anomaly field value, in gammas, corrected for the magnetospheric field and with a linear or quadratic fit removed. The data is bounded by latitudes 0° and 50° for this satellite pass

F (9,N) = Anomaly field value, in gammas, similar to F (8,N) but the data is bounded by latitudes -25° and +25° for this satellite pass

F (10,N) = Anomaly field value, in gammas, similar to F (8,N) but the data is bounded by latitudes -50° and 0° for this satellite pass

The tape structure is:

HEADER	~~40~~ 80 BYTES (55 used)	SATELLITE PASS 1
	MJD - ~~10~~8 Bytes	
	ISAT - ~~10~~8 Bytes	
	IHO - ~~10~~8 Bytes	
	NPTS - ~~10~~8 Bytes	
	EQLON fill - ~~10~~15 2.5 Bytes	
POLY.FIT	~~72~~ 80 BYTES (72 used)	
	A(K), K = 1,9 - 8 Bytes Each fill 8 Bytes	
DATA	80 x NPTS BYTES	
	IF (1,N) - 8 Bytes	
	F (2,N) - 8 Bytes	
	F (3,N) - 8 Bytes	
	F (4,N) - 8 Bytes	
	F (5,N) - 8 Bytes	

DATA	80 x NPTS BYTES (Cont'd.)	
	F (6,N) - 8 Bytes	
	IF (7,N) - 8 Bytes	
	F (8,N) - 8 Bytes	
	F (9,N) - 8 Bytes	
	F (10,N) - 8 Bytes	
HEADER	80 ~~40~~ BYTES	SATELLITE
POLY.FIT	80 ~~72~~ BYTES	PASS 2
DATA	80 x NPTS BYTES	
HEADER	80 ~~40~~ BYTES	SATELLITE
POLY.FIT	80 ~~72~~ BYTES	PASS 3
DATA	80 x NPTS BYTES	

(etc.)

MAGNETIC ACTIVITY INDEX CHART

(TRANSFORMED K_p)

K_p	IF (7,N)
0	0
0+	3
1-	7
1°	10
1+	13
2-	17
2°	20
2+	23

corrected by HKH/NSSDC

SO-11B

POGO HIGH LATITUDE ANOMALY FIELD DATA SET

This tape contains a subset of data from the POGO (Polar Orbiting Geophysical Observatory: OGO-2, OGO-4, and OGO-6) satellites. This data set is similar to the POGO Low Latitude Anomaly Field Data Set, which utilized the data set originally derived by Regan, Cain, and Davis [J. Geophys. Res., Feb. 10, 1975, Vol. 80, No. 5, pg. 794-802].

The data was limited to an altitude below 600 km, and geographic position above 50 degrees latitude, for the North Polar Data Set, and below -50 degrees latitude, for the South Polar Data Set.

In order to eliminate non-crustal fields, data was excluded from the data set if the modified magnetic field values, ΔB values, were greater than 20 gammas ($= 1 \times 10^{-9}$ tesla) in magnitude, under the assumption that the presence of such fields indicates a condition of magnetic disturbance. Visual analysis of the data in polar plot form enabled further exclusion of "noisy" data due to polar disturbances. Closely overlapping satellite passes were analyzed for consistency in the value of ΔB.

After these corrections to the data set had been completed, a first or second degree polynomial was fit to the ΔB (as a function of time) for each satellite pass. This polynomial fit was determined necessary [Mayhew, J. Geophys., 45, pg. 119-128, 1979] in order to bring anomaly data from separate satellite passes over the same geographic region into internal consistency.

In general, to reconstruct what is believed to be a good estimation of the anomaly field, one should take the raw ΔB value (not on the tape) and subtract from it the field from the polynomial correction. These calculations have been done, and the estimated anomaly field is included on the tape (F (7,N)).

TAPE INFORMATION

The two data sets are on two tapes. One tape is the North Polar Data Set, and the other tape is the South Polar Data Set. The tapes are in EBCDIC format, generated on an IBM S/360-91 computer with the following Job Control Language.

```
UNIT = 800, DISP = (NEW, KEEP), LABEL = (1, NL)
DCB  = (RECFM = FB, LRECL = 80, BLKSIZE = 800, DEN = 2),
VOL  = SER = XXXXX
```

The UNIT address identifies the tape drive to be used to read the 9-track, 800 bpi density magnetic tape.

The DISP parameter specifies the disposition of the tape. The NEW subparameter specifies that the data set did not exist before this job step. The KEEP subparameter specifies that the data set is to be kept on this tape volume if this step abnormally terminates.

The LABEL parameter specifies additional information about what is written on the tape. The numeric subparameter specifies that the data set begins with file 1, at the beginning of the tape, immediately after the reflector strip. The NL subparameter specifies that the tape does not have a system or user label. (The tapemarks between files on non-labeled tapes are 1 byte in length.)

The DCB parameter specifies data control block information. RECFM = FB specifies the record format as being in fixed block lengths, EBCDIC format. LRECL = 80 specifies the logical record length as 80 bytes maximum. BLKSIZE = 800 specifies the block length as 800 bytes (10 logical records). There is an inter-record gap of 5/8 inch between blocks. DEN = 2 specifies the density of the tape as 800 bpi.

The VOL parameter specifies the volume serial number of the tape as XXXXX, to correspond to the external label on the tape. Since there is no internal label, this number is arbitrary.

The data for each satellite pass is contained in a series of two types of 80 byte (card formatted) records, created with the following write statements.

I. Header Information: (number of records = 1)

```
      WRITE (9,300) MJD, IHO, NPTS
  300 FORMAT (3I10)
```

Where: MJC = Modified Julian Date (11/2/79 = 44179)

IHO = Half-orbit number for an OGO satellite A half-orbit is defined here as the partial orbit of the satellite from one of the Earth's poles to the opposite pole. This number is uniquely associated with a satellite pass for the specified satellite only.

NPTS = Number of observations for this satellite pass.

II. Data Information: (number of records = NPTS)

```
      WRITE (9,301) ((IF (1, N), F (2,N), F (3,N),
     *               F (4, N), F (5,N), IF (5,N), F (7, N),
                     F (8, N)), N = 1, NPTS)
  301 FORMAT (I8, 3F8.4, F8.1, I8, 2F8.4)
```

Where: IF (1, N) = Time of day in milliseconds (0 to 86400000).

F (2, N) = Latitude of the satellite for this observation point. (In degrees)

F (3, N) = Longitude of the satellite for this observation point. (In degrees)

F (4, N) = Altitude of the satellite for this observation point (in kilometers). Above the Earth's surface (5371.2 km).

F (5, N) = Total magnetic field value as observed by the satellite (measured in gammas, $1\gamma = 1 \times 10^{-9}$ tesla.)

IF (6, N) = Magnetic activity index, Kp (see attached Magnetic Activity Index Chart).

F (7,N) = Anomaly field value with a linear or quadratic fit removed (in gammas).

F (8,N) = Magnetic local time (in hours).

The tape structure is:

HEADER	~~24~~ 80 BYTES (30 used)	SATELLITE PASS 1
	MJD - ~~10~~ 10 Bytes	
	IHO - 10~~8~~ Bytes	
	NPTS - 10~~8~~ Bytes	
	Fill 50 Bytes	
DATA	80 ~~64~~ x NPTS BYTES (64 used)	
	IF (1, N) - 8 Bytes	
	F (2, N) - 8 Bytes	
	F (3, N) - 8 Bytes	
	F (4, N) - 8 Bytes	
	F (5, N) - 8 Bytes	
	IF (6, N) - 8 Bytes	
	F (7, N) - 8 Bytes	
	F (8, N) - 8 Bytes	
	Fill 16 Bytes	
HEADER	80 ~~24~~ BYTES	SATELLITE PASS 2
DATA	80 ~~64~~ x NPTS BYTES	
HEADER	80 ~~24~~ BYTES	SATELLITE PASS 3
DATA	80 ~~64~~ x NPTS BYTES	

(etc.)

MAGNETIC ACTIVITY INDEX CHART
(TRANSFORMED K_p)

K_p	IF (6, N)
0	0
0+	3
1-	7
1°	10
1+	13
2-	17
2°	20
2+	23
3-	27

POGO LOW LATITUDE AVERAGE ANOMALY FIELD DATA SET

SO-11C

This tape contains POGO average anomaly field and equivalent source anomaly field data computed at the centers of 2 X 2 degree grids within $\pm$ 50° geographic latitude. This data was created in the following three steps:

STEP 1 : 2 X 2 grids were constructed with centers at (longitude,latitude) = (0,-49), (0,-47),....,(0,+49), (2,-49),....,(2,+49),....,(358,-49),....,(358,+49). The average anomaly field, average altitude, and the number of observations were then computed for each grid from each of the three segments of POGO low latitude anomaly field data. (Segment 1 covers 0° to 50° latitude range, Segment 2 covers -25° to 25° latitude range and Segment 3 covers -50° to 0° latitude range.)

STEP 2 : Three segments of average data were combined in one data set to cover latitude range -50° to+50°. The data for latitude range (-50° to -17°) was selected from segment 3, likewise latitude range (-11 to +11) from segment 2 and latitude range (+17 to +50) from segment 1. The data for the latitude range (-17 to -11) was obtained by averaging segments 3 and 2 and similarly latitude range (+11 to +17) was obtained by averaging segments1 and 2.

STEP 3 : The equivalent source magnetic anomaly field values and its components were computed at each grid center (for 500 Km constant altitude), using the techniques described in the documentation of the Equivalent Source Magnetic Anomaly Program (ESMAP) (Reference 1). The latitude (at the center of grid), the longitude, average altitude, number of observations within grid, the anomaly field, the equivalent source anomaly

field, the radial component, the colatitudinal component and the longitudinal component of the field were written onto a magnetic tape.

1. Computer Sciences Corporation, Equivalent Source Magnetic Anomaly Program R. Horner 1980
NSSDC Ref. No: B32937-000A
Also: CSC/TM-80/6180

TAPE INFORMATION

The POGO low latitude anomaly field data is on one file of tape OF3103. This tape is in EBCDIC format, generated on GSFC - SACC IBM/360-91 computer with the following Job Control Launguage (JCL) :

```
UNIT=800,DISP=(NEW,KEEP),LABEL=(1,NL,,OUT),
DCB=(RECFM=FB,LRECL=80,BLKSIZE=800,DEN=2),
VOL=SER=OF3103
```

Subject to change

Each record was created with the following write statement:

```
WRITE(26,200) ALAT,ALON,ALT,FNO,PUDA,DB,DBR,DBT,DBP
200  FORMAT(9F8.3)
```

where:
- ALAT = Latitude in degrees at the center of the grid
- ALON = Longitude in degrees at the center of the grid
- ALT = Average ~~latitude~~ altitude in KM
- FNO = Number of observations within the grid
- PUDA = Average anomaly field (POGO) over the grid
- DB = Equivalent source anomaly field over the grid
- DBR = Radial component of the equivalent source anomaly field
- DBT = Colatitudinal component of the equivalent source anomaly field
- DBP = Longitudinal component of the equivalent source anomaly field

DB is difference in magnitudes, not magnitude of vector difference.

Rec'd 5/9/80
HKH

SP-11D

SELECTED POGO DATASET

The SELECTED POGO dataset is a collection of observations made by the OGO-2, -4, and -6 satellites. The bulk of the dataset is comprised of 47384 observations which went into the POGO 2/72 field model. Added to this were OGO-6 magnetic field values taken from intervals from 1969-1971. Desired time intervals were selected from quiet ($|F|<10$ gamma) and moderately quiet ($10<|F|<30$ gamma) periods of magnetic activity. The data contains 95700 quiet time observations, and 29000 observations from moderately quiet activity periods. The data is not time ordered. All data is contained on one file in the order: quiet data, moderately quiet data, and POGO 2/72 data. The geodetic quantities reflect an adopted earth flattening of 1/298.3 and equatorial radius 6378.155km.

A subset of this database was chosen to derive a new magnetic field model designated POGO 2/79. This subset consisted of every tenth OGO-6 quiet observation (9570), every other OGO-6 moderately quiet observation (14546), and every POGO 2/72 observation (47384) for a total of 71500 scalar observations. The overall rms of fit to the data is 6 nT.

day 40222 = Jan 1 of 1969

9DBE = 40382 = June 9 of 1969

$$\begin{array}{r} 40382 \\ -40222 \\ \hline 160 \end{array}$$

160 = June 9 of 1969

Reed 5/9/80
HKH

SAMPLE TAPE READ

SOURCE CODE

```
Integer *4 IA(10,100)
Real *4 A(10,100)
Equivalence (A(1,1), (IA(1,1)

Read (10)A
```

JOB CONTROL LANGUAGE

Data is written in IBM/360 binary.

```
//FT10F001 DD UNIT=9TRACK, DISP=(ØLD,KEEP), LABEL=(01,NL,,IN),
//  DCB=(RECFM=VBS, LRECL=4004, BLKSIZE=4008, DEN=3)
//  VØL=SER=DUMMY
```

FORMAT DESCRIPTION

1.	IA(1,I):	Modified Julian Day	I*4
2.	IA(2,I):	Milliseconds of day	I*4
3.	A(3,I):	Geodetic Latitude	R*4
4.	A(4,I):	Longitude	R*4
5.	A(5,I):	Geodetic Altitude	R*4
6.	IA(6,I):	Satellite number	I*4

= 5 OGO-6 Quiet
= 5 OGO-6 Moderately Quiet
= 1 OGO-2 (POGO 2/72)
= 2 OGO-4 (POGO 2/72)
= 3 OGO-6 (POGO 2/72)

7.	IA(7,1):	Data Code (=1)	I*4
8.	A(8,I):	Scalar Field Value	R*4
9.	A(9,I):	Not Used (=0.)	R*4
10.	A(10,I):	Not Used (=0.)	R*4

Reprinted from

Canadian Journal of Earth Sciences

Réimpression du

Journal canadien des sciences de la terre

Comparisons of magnetic anomalies of lithospheric origin measured by satellite and airborne magnetometers over western Canada

R. A. LANGEL, R. L. COLES, AND M. A. MAYHEW

Volume 17 • Number 7 • 1980

Pages 876–887

National Research Council Canada

Conseil national de recherches Canada

Comparisons of magnetic anomalies of lithospheric origin measured by satellite and airborne magnetometers over western Canada[1]

R. A. LANGEL
Geophysics Branch, National Aeronautics and Space Administration, Goddard Space Flight Center, Greenbelt, MD 20771, U.S.A.
R. L. COLES
Earth Physics Branch, Department of Energy, Mines and Resources, Ottawa, Ont., Canada K1A 0Y3
AND
M. A. MAYHEW
Business and Technological Systems, Inc., Seabrook, MD 20801, U.S.A.

Received October 11, 1979
Revision accepted March 7, 1980

Crustal magnetic anomaly data from the Orbiting Geophysical Observatories 2, 4, and 6 (Pogo) satellites are compared with upward-continued aeromagnetic data between 50–85°N latitude and 220–260°E longitude. Agreement is good, both in anomaly location and in amplitude, giving confidence that it is possible to proceed with the derivation and interpretation of satellite anomaly maps in all parts of the globe. The data contain a magnetic high over the Alpha ridge suggesting continental composition and a magnetic low over the southern Canada basin and northern Canadian Arctic Islands (Sverdrup basin). The low in the Sverdrup basin corresponds to a region of high heat flow, suggesting a shallow Curie isotherm. A ridge of high field, with two distinct peaks in amplitude, is found over the northern portion of the platform deposits and a relative high is located in the central portion of the Churchill Province. No features are present to indicate a magnetic boundary between Slave and Bear Provinces, but a trend change is evident between Slave and Churchill Provinces. South of 60° latitude a broad magnetic low is located over very thick (40–50 km) crust, interpreted to be a region of low magnetization.

On compare les données recueillies par les satellites OGO 2, 4 et 6 (Pogo) sur les anomalies magnétiques dans la croûte avec un prolongement vers le haut des données aéromagnétiques situées entre les latitudes 50–85°N et les longitudes 220–260°E. L'accord est bon à la fois pour la localisation des anomalies et leur amplitude, ce qui permet d'être optimiste quant à la possibilité de procéder à la confection et à l'interprétation de cartes d'anomalies magnétiques par satellite dans toutes les parties du globe. Les données contiennent un pic magnétique sur la crête Alpha suggérant une composition continentale et une dépression magnétique sur le bassin du sud du Canada et dans les îles de l'Arctique canadien au nord (le bassin de Sverdrup). La dépression dans le bassin de Sverdrup correspond à une région de flux thermique élevé ce qui laisse supposer une isotherme de Curie à faible profondeur. Une crête de champ intense avec deux pics distincts dans l'amplitude se retrouve dans la partie nord des dépôts de plate-forme et un sommet relatif est localisé dans la portion centrale de la province de Churchill. Il n'y a rien qui indique une limite magnétique entre les provinces de l'Esclave et de l'Ours, il y a un changement évident entre les provinces de Churchill et de l'Esclave. Au sud de la latitude 60°N, on observe une vaste dépression magnétique située sur une croûte très épaisse (40–50 km) et qu'on interprète comme une région de faible aimantation.

[Traduit par le journal]

Can. J. Earth Sci., 17, 876–887 (1980)

Introduction

In recent years it has been realized that crustal magnetic anomalies exist which are of longer wavelengths than those investigated by exploration geophysicists and that these longer wavelength (greater than 50 km) anomalies are indicative of geologic and tectonic features in the deep crust (Pakiser and Zietz 1965; Zietz *et al.* 1966; Shuey *et al.* 1973; Hall 1974; Krutikhovskaya and Pashkevich 1977).

With the publication of the paper by Regan *et al.* (1975) it was demonstrated that long wavelength lithospheric anomalies could be mapped successfully from satellites. That map showed a global distribution of anomalies of about 500–3000 km scale size which were never before mapped and whose very existence was in most cases discovered for the first time. Although this map was distorted by variations in altitude over the data set and by contamination from magnetospheric fields, Regan *et al.* were able to demonstrate that the probable source of the anomalies is indeed the lithosphere.

[1]Contribution from the Earth Physics Branch No. 854.

0008-4077/80/070876-12$01.00/0

TABLE 1. Some characteristics of the Pogo orbits

Satellite	Launch date	Inclination	Perigee (km)	Apogee (km)
OGO 2 (1965 81A)	October 14, 1965	87.3°	410	1510
OGO 4 (1967 73A)	July 28, 1967	86.0°	410	910
OGO 6 (1969 51A)	June 5, 1969	82.0°	400	1100

Subsequently, Regan and Marsh (in preparation) have collected ancillary data and derived a quantitative model of an anomaly located in central Africa. Analysis techniques for this type of data are rapidly becoming available (Bhattacharyya 1977; Mayhew 1978, 1979).

While analysis of data at lower latitudes has proceeded (Regan and Marsh, in preparation; Mayhew 1979), nothing has been published dealing with anomalies measured by satellite at the higher latitudes. The reason for this is that at low latitudes the external (magnetospheric/ionospheric) fields are mainly of longer wavelength than the anomalies being mapped, and can be readily filtered from the data, thus isolating the anomaly fields. This remains true as long as data within about 3 h of local noon are not utilized. At high latitudes, however, ionospheric currents occur at all local times and are very often present even during magnetically quiet periods of time. Further, these currents result in fields of the same spatial scale as the anomalies of interest, thus complicating the problem of isolating the anomaly fields. This paper is a report on an attempt to isolate the anomaly fields at satellite altitude for such high latitudes, and in particular over that part of Canada between 50–85°N latitude and 220–260°E longitude. To gauge the success of this attempt, the resulting anomaly map is compared to aeromagnetic data upward continued to satellite altitude, 500 km.

The Satellite Data

A survey of the near-Earth magnetic field was carried out by the Polar Orbiting Geophysical Observatories (OGO 2, 4, and 6), also known as the Pogo satellites (Langel 1973, 1974). Some characteristics of the Pogo orbits are given in Table 1. Orbiting Geophysical Observatory 2 acquired data from launch until October 2, 1967; OGO 4 from launch until January 19, 1969; and OGO 6 from launch until August 29, 1970 and then sporadically until June 1971. Each satellite completed about 15 revolutions each day. Orbiting Geophysical Observatory 2 and OGO 4 acquired a data point every 0.5 s and OGO 6 every 0.288 s.

The measured magnetic field, $\boldsymbol{B}$, is the vector sum of magnetic fields from several sources. These are the main (core) field of the Earth, $\boldsymbol{M}$, the variable field due to ionospheric and magnetospheric currents, $\boldsymbol{D}$, and the field originating in the lithosphere of the Earth, $\boldsymbol{A}$. In this study the main field is represented by a spherical harmonic model, $\boldsymbol{M}_c$, of degree and order 13, designated Pogo(02/72) and described in the Appendix. It should be noted that this model is intended primarily as a representation of the main field of the Earth for the time span of the Pogo data. The degree and order were chosen on the basis of studies by Phillips (J. Phillips, personal communication, 1978), Cain *et al.* (1974), and Cain (1976), which indicate that a 13th degree and order representation is sufficient to represent the main field without unduly distorting the anomaly field. Any such choice is, of course, a compromise and no exact separation is possible.

Orbiting Geophysical Observatories 2, 4, and 6 measured the magnitude but not the direction of the field $\boldsymbol{B}$. The quantity analyzed is thus the residual field

$$\Delta B = |\boldsymbol{B}| - |\boldsymbol{M}_c|$$

This residual field contains contributions from: (1) any inaccuracy in modeling the core field $\boldsymbol{M}$ with $\boldsymbol{M}_c$, (2) the external field, $\boldsymbol{D}$, and (3) the lithospheric field, $\boldsymbol{A}$. Contributions from $\boldsymbol{D}$ are minimized by elimination of all data in which the residual field was considered to be dominantly due to $\boldsymbol{D}$. This elimination was accomplished on a pass by pass basis in two steps. (A pass is defined as a continuous set of data beginning when the satellite goes above 50° latitude and ending when it again goes below 50° on the other side of the pole.) Firstly, if the magnitude of the residual field, ΔB, exceeds 20 nT (nanotesla) at any place in the pass, the entire pass is rejected. Secondly, the remaining passes are visually intercompared to attempt to distinguish the time invariant features, the lithospheric field $|\boldsymbol{A}|$, from the time varying external field $|\boldsymbol{D}|$, and passes with significant contribution from the latter are not used in the anomaly map. A total of 271 "quiet" passes remained and were used in deriving the anomaly map. After performing these operations the internal agreement of passes which are nearly coincident geographically is substantial, which indicates the presence and reality of the crustal

anomalies. However, significant differences of wavelength more than 2000–3000 km still remain between coincident passes. This is similar to the results of Mayhew (1979) over the continental United States. His solution was to remove a polynomial function separately from each individual pass. Only passes with several thousand kilometres of data were used. This function is determined by a least squares fit to that pass. The procedure of Mayhew was followed with the data presented here except that Mayhew chose a quadratic function whereas we have chosen a linear function. The function chosen is a matter of subjective judgement. The difference between the linear and quadratic functions for these data is not substantial. We are, of course, left with an anomaly field with arbitrary zero. After the data selection and trend removal, individual residual field data points were averaged in an equal-area grid superimposed over an equal-area map of the area of interest. The grid is square and the distance along each side is equivalent to 3° of latitude. Figure 1 shows the density distribution of the data used in the averages. The resulting averaged residual anomaly map, contoured at 2 nT intervals, is shown in Fig. 2*a*. Results in the southwest portion of the map, between 220–240° longitude and 50–60°N latitude, are to be regarded with caution because of the sparseness of data as shown in Fig. 1. The residuals plotted in Fig. 2*a* are not at a common altitude but are at the altitudes determined in each block over which the data were averaged. The average altitude varies from 440–560 km, with mean near 520 km. A map reduced to common altitude is discussed later in the paper.

The anomalies range from a maximum of 14 nT at about 85° latitude to a minimum of −11 nT at 50° latitude and 239° longitude.

The Airborne Magnetometer Data

The airborne magnetic field data considered here have been acquired by the Earth Physics Branch of the Department of Energy, Mines and Resources, Ottawa, since 1969 in a series of airborne vector magnetometer surveys, each survey covering 2×10^6 to 4×10^6 km^2 at a typical altitude of 3.5 km above sea level, with excursions giving a range of 2.5–6.0 km. The instrumentation and survey details have been variously described by Haines and Hannaford (1972, 1974, 1976) and Hannaford and Haines (1974). Discussions of the data have been given by Haines *et al.* (1971), Riddihough *et al.* (1973), Coles *et al.* (1976), and Coles and Haines (1979).

The data were obtained in three separate surveys

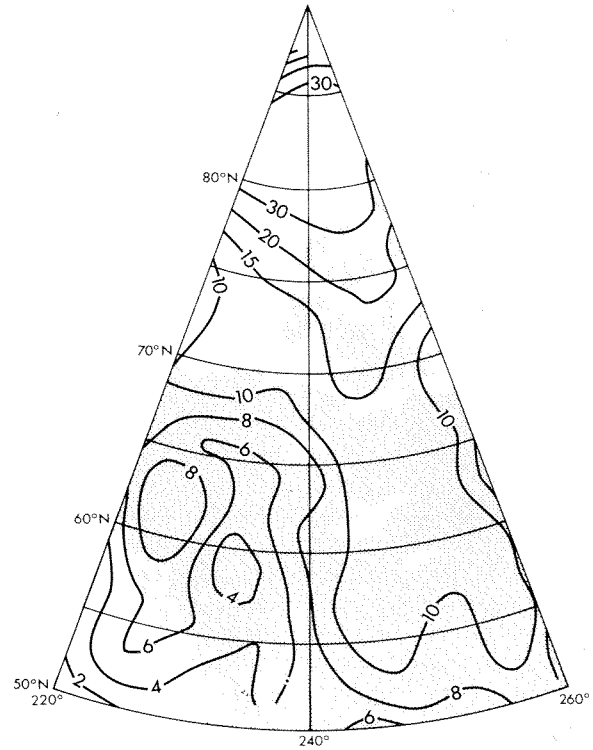

FIG. 1. Density of distribution of Pogo data, as number of points in averages.

flown at approximately 2 year intervals. In order to remove level differences due to secular change, a reference field has been removed. Coles (1979) has shown that the best available reference field models for this region and for this interval of time are based on the Pogo data. The model chosen was the Pogo(02/72) model, i.e., the same reference field used for the satellite data. Coles also demonstrated a way of correcting for inadequacies in the secular change terms of the reference model in its application to the airborne data. The residual data values are, in effect, adjusted to a single epoch. At each magnetic observatory in or near the survey region, the change in average quiet day field level from the epoch of the survey to the updated epoch is compared with the change in value of the field model between the two epochs. This comparison leads to a low-degree polynomial correction surface to be applied to the data residuals. The airborne data residuals were upward continued to 500 km in order to compare them with the satellite data. A more detailed discussion of this procedure is given by Coles and Haines (1979).

At high geomagnetic latitudes, differences between scalar and vertical component regional anomaly fields are minor (Langel 1974). The vertical

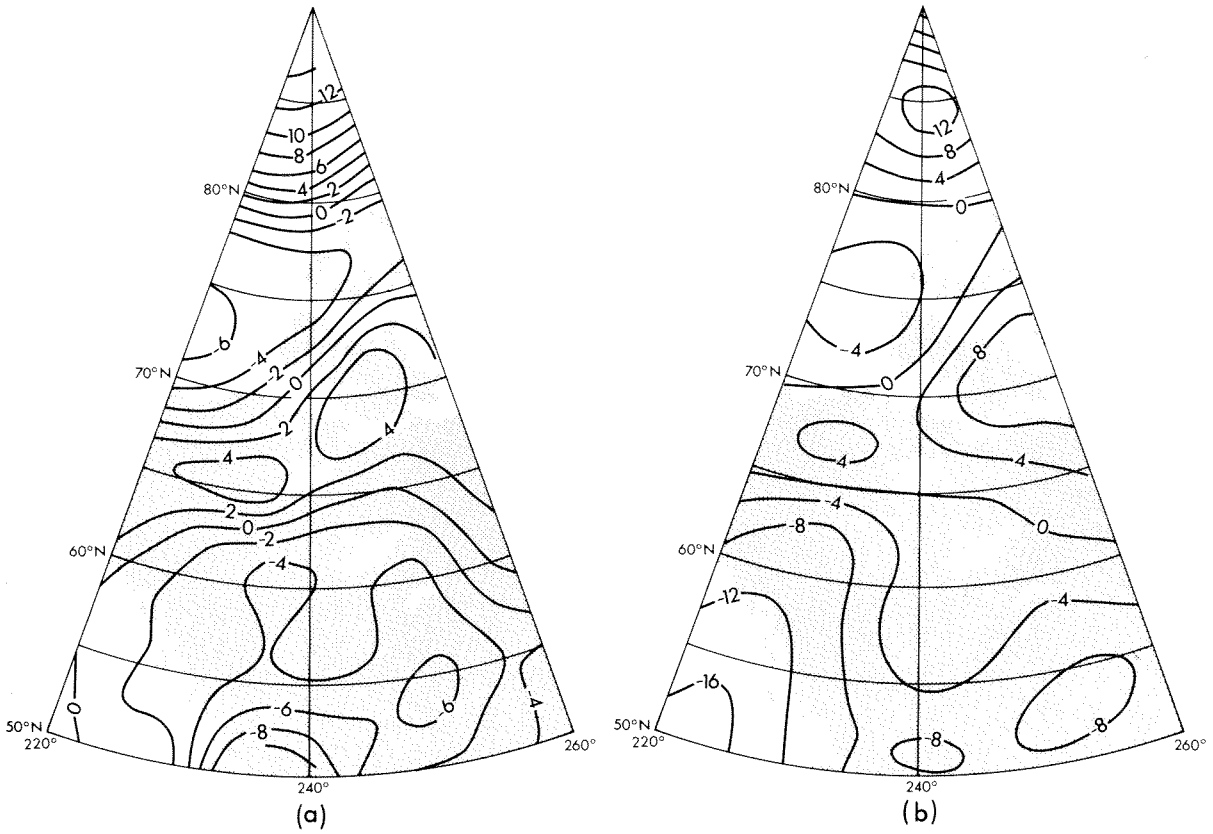

FIG. 2. Comparison of (*a*) averaged scalar magnetic anomalies from Pogo data with (*b*) upward-continued aeromagnetic vertical component anomaly data (500 km altitude).

component airborne data were used for the upward continuation because the data coverage is more complete than the scalar data coverage, and because the scalar field is not strictly harmonic. The input data to the upward continuation were in the form of averages of vertical component residuals along flight tracks over 5 min of time (about 35 km distance). The data points are shown in Fig. 3, and Fig. 4 is a contoured map prepared from the 5 min averaged data.

The data averages were each associated with an area determined by the spacing (35 km) multiplied by the mean flight-line spacing in the region of each data average. Although the original data were only along flight lines, the approximation is sufficient for the present purposes. No corrections for variations in flight altitude have been incorporated.

The basic equation for upward continuation from a sphere can be approximately represented, for the vertical component Z_p at point P, by

$$Z_p = \frac{R^2 - R_0^2}{4\pi R} \sum \frac{Z_i}{\rho_i^3} \Delta S_i$$

where the summation is over all data points i, each associated with an area ΔS_i and field value Z_i. R is the geocentric distance to the point P, R_0 is the radius of the Earth, and ρ_i is the distance from P to the point i. The data values, Z_i, are residuals relative to the reference field. The residual field beyond the data area is assumed to be zero and, therefore, has no contribution to the summation. This is an assumption, of course, which limits the accuracy of the upward continuation. Coles and Haines (1979) discuss this point in more detail; however, the actual total contribution from distant points beyond the data area is small (less than about 2 nT for most parts of the area), since the integral of the residual field over a large region tends to zero.

The data (5600 points) have been upward continued to 100, 300, and 500 km (Figs. 5, 2*b*). As the altitude increases, the anomalies become smoother and reduced in amplitude. Broad features, however, persist through the series of figures.

Comparison of the Anomaly Maps

There is good agreement between the satellite

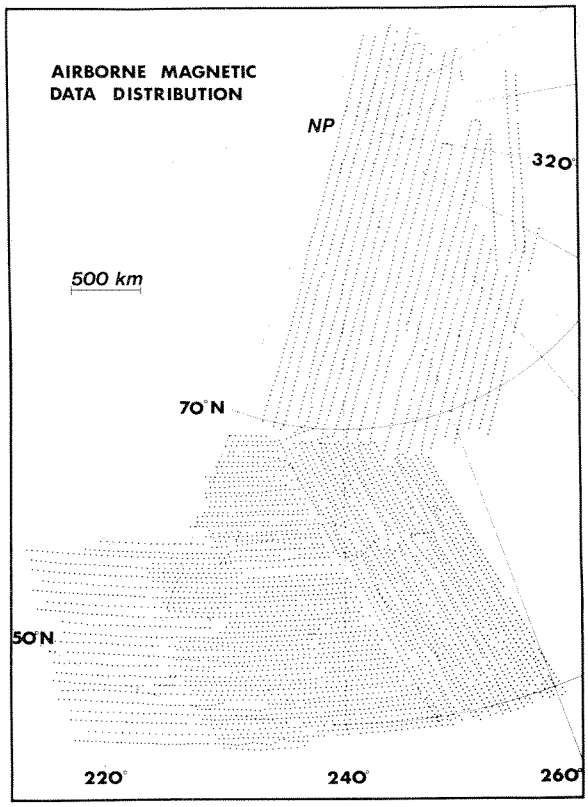

FIG. 3. Relative distribution of aeromagnetic data.

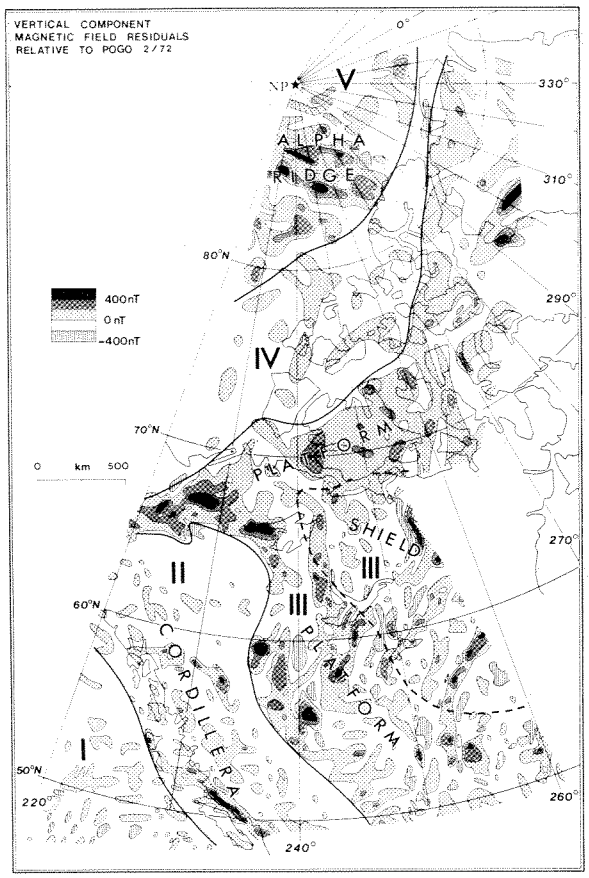

FIG. 4. Residuals of aeromagnetic data at an altitude of 3 km. Roman numerals designate regions of differing characteristics as described in the text.

and airborne data in their common spectral region. The agreement is excellent in the north, with a high anomaly north of 80°N, a low region between about 70 and 80°N, and a north-easterly trending ridge of high field centered near 65–67°N in the west and extending to about 70°N in the east. A south-trending, relatively positive area extends between 55 and 62°N at a longitude of about 240°. In the southwest the agreement is not as good, with a large gradient evident in the airborne-derived map. Nevertheless, the indications are of a relatively low field over the southwestern Cordillera region in Canada. The agreement in anomaly amplitudes is also very good, except in the southwest corner. This comparison gives a confirmation over a sub-continental size region of the reality of the anomalies derived from satellite data. This is particularly important for this region of the Earth where contaminating fields from high latitude currents are strong and it indicates that we have been successful in separating the anomaly fields from fields due to those currents.

The reason for the discrepancy in the southwest between the two maps is not clear. The method of upward continuation is not a major factor since different analyses of the original data also indicate a similar discrepancy (Coles and Haines 1979). The Pogo anomaly map is determined relative to a model also derived from Pogo data, so one would not expect trends of 10–20 nT to be present in that map. Either the available satellite data are consistently high in this region (the density of satellite passes is very low here), or the airborne data (one particular survey) are consistently low.

Effect of Model Removed

Any bias in the field model utilized to estimate the core field may be reflected as an error in anomaly maps derived by this method. This would be the case, for example, if the higher order terms of the model utilized were negatively correlated with the anomalies derived. Obviously, some error is introduced simply because the spectra of core and crustal fields overlap so that it is not possible to do a clean separation. We believe that, if anything, our results are biased by removing too much long

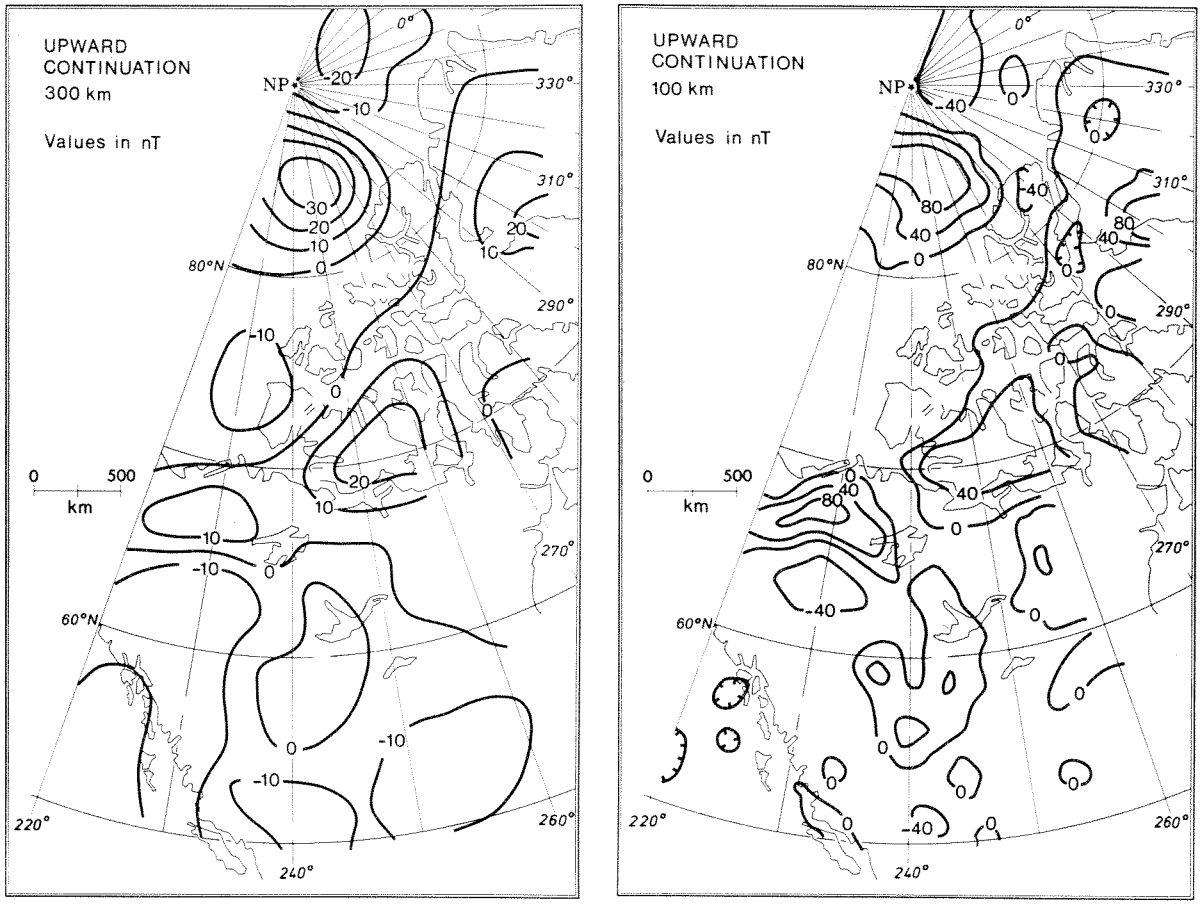

FIG. 5. Upward continuation of aeromagnetic data.

wavelength field rather than too little, because of the pass by pass linear trend removal.

We have two indications that field model biases are not significantly contaminating our results. Firstly, Coles *et al.* (1976, Fig. 2) subtracted the vertical component of the International Geomagnetic Reference Field (IGRF) from the vertical component of the Pogo(02/72) model (erroneously designated Pogo(6/71) in their paper). This difference plot shows *no* correlation with the derived anomaly maps. Secondly, we have recomputed the satellite anomaly map utilizing the Pogo(06/74) field model (Cain *et al.* 1974) which is of degree and order 22. This map is presented here as Fig. 6. Comparison with Fig. 2*a* shows that the greatest differences are in the southwest corner of the map—already noted to be suspect. All other features remain relatively unchanged except for subtle longer wavelength effects. We believe this indicates that any biases due to the degree of the field models used are negligible.

Geologic Implications

It is not our intention to present a detailed interpretation of the magnetic anomaly maps shown here. Interpretations of the aeromagnetic data have already been published (Haines *et al.* 1971; Riddihough *et al.* 1973; Coles *et al.* 1976). In this section we wish to contrast the different viewpoints offered by the aeromagnetic and satellite magnetic data and to illustrate the use of the satellite data in making geologic inferences.

Examination of Fig. 4 shows changes in the character of the anomaly patterns from region to region, often delineating geologic boundaries. Such changes are clearly apparent between the Cordillera and the platform, i.e., between regions II and III and between the platform of region III and the thick sediments, both onshore and offshore, of region IV. The character changes most evident are (1) changes from high magnetic relief to low magnetic relief and (2) changes in the trends of the anomalies. Because most of the high relief features are positive

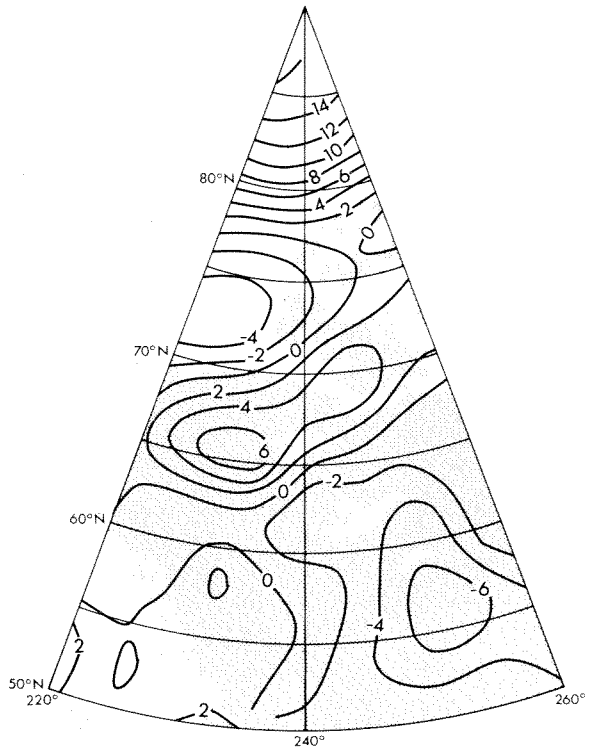

FIG. 6. Averaged magnetic anomaly map from Pogo data, using a 22nd degree spherical harmonic model to remove the core field.

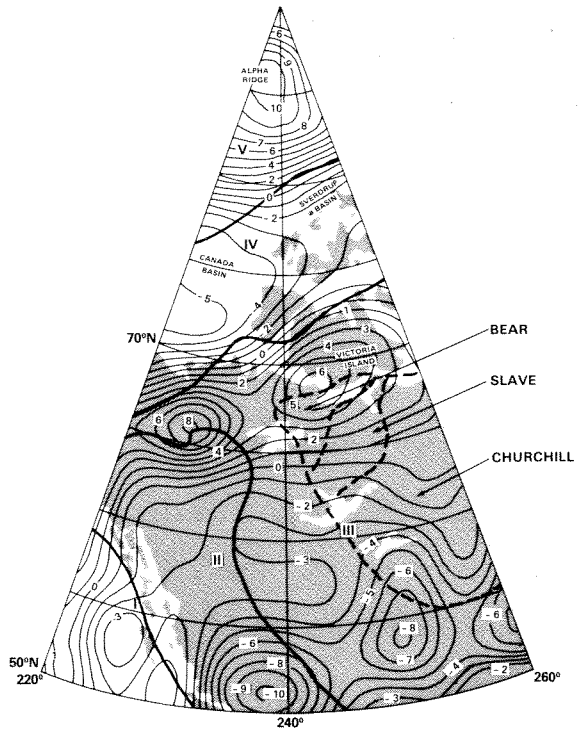

FIG. 7. Reduction of Pogo anomaly map to an altitude of 500 km using an equivalent source representation (reference field is Pogo(02/72)). The contour interval is 1 nT.

there is also an apparent contrast between regions of predominantly positive and predominantly negative fields. Figure 7 shows the satellite field, now reduced to common altitude using an equivalent source representation (Mayhew 1978, 1979). In contrast to Fig. 4, the satellite map shows only the contrasts between the predominantly positive and negative regions. The aeromagnetic data clearly contain all of the information in the satellite data and more and are able to delineate boundaries more definitively. However, the satellite map (or an upward-continued aeromagnetic map) gives a clearer picture of broad trends and can serve as a guide in discerning those same trends in the lower altitude data. In the following paragraphs we will discuss the various "regions" delineated by the satellite anomalies (Fig. 7) compared with those delineated by the aeromagnetic data (Fig. 4) and known geologic provinces.

At the very north of the map the satellite data show a prominent high of about 12 nT magnitude. This is centered on the Alpha ridge of the Arctic Basin. The airborne survey also shows a broad positive in this region but is punctuated by a complex series of intense positive anomalies nearly parallel to the trend of the ridge. These extend both north and south of the ridge and are all contained within the area of positive field as seen by Pogo. This region has also been surveyed by Vogt *et al.* (1979) who concluded that the principal magnetic anomalies in this region are topographic effects in a normally magnetized basement with high magnetization intensity (20–30 A/m). The broader picture afforded by the satellite data supports the existence of a region of highly magnetized crust and partially outlines its extent. Unfortunately, the satellite data do not extend above 87° latitude so the northern portion of this region is not mapped. The upward-continued aeromagnetic data indicate that it terminates at about 88° latitude.

The Alpha ridge has been variously interpreted as a subduction zone (Herron *et al.* 1974), as an extinct center of sea-floor spreading (Churkin 1973; Vogt and Ostenso 1970; Hall 1973; Tailleur 1973; Vogt and Avery 1974), or as subsided continental crust (Eardley 1961; King *et al.* 1966; Taylor 1978). DeLaurier (1978) rejects the hypotheses of a subduction zone or a center of sea-floor spreading on the basis of a comparison of the measured relief with the relief expected from a cooling model, because of a lack of seismic activity, and because active accretion is inconsistent with the known

marine fossils and sediment thickness. Vogt *et al.* (1979) also examine these questions and conclude that on the basis of the airborne magnetic data it is not possible to rule out any of the three hypotheses. In addition to the arguments noted above against a spreading center or subduction zone, they claim that the depth of the Alpha ridge argues against it being a subsided shield.

Taylor (1978) suggests that the Alpha ridge is an aseismic ridge similar to the Lord Howe Rise, which is continental in nature, in the southwest Pacific. In fact, the satellite data show a similar positive anomaly over the Lord Howe Rise (Regan *et al.* 1975). Coles *et al.* (1978) and Sweeney *et al.* (1978) note that the positive long-wavelength anomaly over the Alpha ridge is consistent with a region of crust of continental composition since most of the major long-wavelength positive anomalies detected by satellites are associated with continental crust, both in shield areas and in regions such as Broken Ridge in the Indian Ocean (Regan *et al.* 1975).

To the south of the Alpha ridge and its environs the satellite map shows a broad negative over the southern Canada Basin and the northern Canadian Arctic Islands. The aeromagnetic data in this region are remarkably free from shorter wavelength anomalies. Geologically, this is a region of deep (3–12 km) sediments (Sweeney *et al.* 1978) resulting in a greater depth to basement which may account for the lack of shorter wavelength anomalies in the aeromagnetic data (Riddihough *et al.* 1973). The southern 0 nT contour of this region is close to the edge of the craton but both bathymetric (Sweeney *et al.* 1978) and seismic (Sweeney *et al.* 1978; Berry and Barr 1971; Sander and Overton 1965; Overton 1970; Berry 1973) data show that the transition from continental to oceanic crust, the Canada Basin, takes place well within the region of negative anomaly. Comparison of Fig. 7 with the bathymetry (Sweeney *et al.* 1978) indicates that over much of its length the −4 nT contour nearly coincides with the continental slope. Thus, the central low of the negative anomaly is located over oceanic crust. The eastward extension of this magnetic low is over the Sverdrup basin, where refraction data (Sander and Overton 1965; Overton 1970; Forsyth *et al.* 1979) indicate sediments reaching 12 km. Forsyth *et al.* note that "Based on heat flow measurements taken in bore-holes throughout the Sverdrup Basin, A. S. Judge has estimated that maximum temperatures are 600 to 650°C at 20 km and 850 to 900°C at 30 km (personal communication)." Judge noted higher than average heat flow values for the central Sverdrup basin. Thus, the magnetite Curie isotherm is well up into a thickly sedimented crust in this region which could account for the relative negative magnetic anomaly. The cause of the negative anomaly over the Canada Basin is unknown. Future refinement of the satellite data over the rest of the Arctic will be required to see if the negative anomaly is coextensive with the entire Amerasian Basin.

An elongated region of high magnetic field (Fig. 7) is located near 65° latitude at 220°E longitude in the west and extends to 71° latitude at 260°E longitude. This "high" occurs over the northern portion of the platform deposits on the Precambrian craton and can be resolved into two maxima. In the east the positive anomaly extends southward over the northern parts of the exposed shield. Considering the two highs over the platform deposits, comparison with Fig. 4 shows positive anomalies in the aeromagnetic data in these regions but of significantly different character. In the east, over Victoria Island, there is no concentration of short-wavelength anomalies, whereas in the west, the broad positive background is punctuated by narrow regions of intense positive short-wavelength anomalies. This region of large amplitude anomalies extends around the top of region II (Fig. 4) and has been interpreted to indicate that the crystalline continental basement extends far to the west of the exposed and known buried shield (Coles *et al.* 1976). This regional difference seems to be reflected in the heat flow data (although a good thermal model is not yet available and the available data are sparse) in that the available heat flow values near the western field maximum are considerably higher than those near the eastern maximum. This difference in heat flow between two magnetic highs of nearly equal amplitude indicates that the long-wavelength anomalies, at least to the east of the Cordillera, do not correlate well with heat flow and, therefore, are not indicative of variations in the depth to the Curie isotherm. For comparison, in the United States good heat flow vs. long-wavelength anomaly correlation is evident in the tectonically active region west of the Cordillera (Mayhew, in preparation), whereas in the more stable region to the east of the Cordillera the extremely sparse heat flow data do not seem to correlate with the long-wavelength magnetic anomalies.

Just to the south of the double maximum the contour lines are relatively featureless with a northeasterly trend. In particular, no features are present marking the boundary between Bear and Slave Provinces. Below 67° latitude a trend change is evident between Slave and Churchill Provinces and, near the eastern border of the map, a relative

high extends through the central portion of the Churchill Province. This relative high is not clearly defined in the aeromagnetic data, which do not extend as far east as the satellite data.

South of about 60–63° the satellite anomaly map is everywhere negative, highly negative in some regions. The low altitude data of Fig. 4 show that large portions of this area are relatively free of large amplitude short-wavelength anomalies. A relative negative anomalous region can be caused by one or a combination of three things: very low rock magnetization, a shallow Curie isotherm, or a high reversed remanent magnetization. The latter is extremely unlikely for a geographic region of this size; reversed magnetizations for regions this size are neither expected nor found in practice. Although sparse, the existing heat flow data are at or below normal values, with no indication of a shallow Curie isotherm. Thus the crust in this region, which is 40–50 km thick (Chandra and Cumming 1972; Berry 1973), most likely has very low average rock magnetization over most of its area. The satellite data show a relative high at about 57–60° latitude and 238–241° longitude. This is reflected in the low latitude aeromagnetic data (Fig. 4) as a cluster of magnetic highs east of the Cordillera, and in fact the Cordillera is outlined by their western boundary. Most of this region of "highs" is underlain by sedimentary cratonic cover rocks, reaching several kilometres thickness in the west. Some deep drill holes exist to the east of the Cordillera within both the area of short-wavelength intense positive anomalies and the area further southeast, free of such anomalies. The magnetizations of basement rocks from the bottoms of the drill holes have been measured (R. A. Burwash, personal communication, 1974; R. L. Coles, unpublished data, 1975). Although sparse, the magnetization values outside the area of short-wavelength positive anomalies are lower on average than what appears to be typical for shield areas, whereas within the area of short-wavelength "highs," much of the crystalline basement is highly magnetic.

Summary

Aeromagnetic and satellite magnetic data have been presented and compared for western Canada. Such a comparison at these geomagnetic latitudes is important because both data types are affected by fields from external (ionospheric and magnetospheric) sources. Such external fields are particularly troublesome to the satellite data where, even after careful data selection, external fields are undoubtedly present on most data passes. The close agreement between the two data types indicates that it is possible to extract the anomaly "signal" from the satellite data and that the anomalies so defined are indeed crustal in origin. We believe it is now possible to proceed in confidence with the derivation and interpretation of satellite anomaly maps in all parts of the globe.

Both averaging of satellite data and upward continuation of aeromagnetic data serve to filter out details in the field. For aeromagnetic data this is not a problem since one can compare with results for lower altitudes. Derivation of an equivalent source representation of the satellite data preserves most of the information content of the data, as is apparent from comparison of Fig. 7 and Fig. 2*a*. Broad interpretative comparison of the equivalent source field with known geologic and geophysical data has indicated that it is indeed indicative of important features in the crust and can aid in the solution of such problems as the nature and origin of the Alpha ridge and the nature of the crystalline basement underlying sedimentary cover.

Acknowledgements

We would like to thank M. K. Hutchinson, R. Horner, D. Love, and B. Draper for their efforts in data preparation and display, and G. V. Haines and G. D. Mead for valuable discussion and review of the manuscript.

BARRACLOUGH, D. R., HARWOOD, J. M., LEATON, B. R., and MALIN, S. R. C. 1975. A model of the geomagnetic field at epoch 1975. Geophysical Journal of the Royal Astronomical Society, **43**, pp. 645–659.

BERRY, M. J. 1973. Structure of the crust and upper mantle in Canada. Tectonophysics, **20**, pp. 183–201.

BERRY, M. J., and BARR, K. G. 1971. A seismic refraction profile across the polar continental shield of the Queen Elizabeth Islands. Canadian Journal of Earth Sciences, **8**, pp. 360–374.

BHATTACHARYYA, B. K. 1977. Reduction and treatment of magnetic anomalies of crustal origin in satellite data. Journal of Geophysical Research, **82**, pp. 3379–3390.

CAIN, J. C. 1976. Introductory remarks. Abstract. EOS, Transactions of the American Geophysical Union, **57**, p. 907.

CAIN, J. C., DAVIS, W. M., and REGAN, R. D. 1974. An $N = 22$ model of the geomagnetic field. Abstract. EOS, Transactions of the American Geophysical Union, **56**, p. 1108.

CHANDRA, N. N., and CUMMING, G. L. 1972. Seismic refraction studies in western Canada. Canadian Journal of Earth Sciences, **9**, pp. 1099–1109.

CHURKIN, M. 1973. Geologic concepts of Arctic Ocean Basin. *In* Arctic geology. *Edited by* M. G. Pitcher. American Association of Petroleum Geology, Memoir 19, pp. 485–499.

COLES, R. L. 1979. Some comparisons among geomagnetic field models, observatory data and airborne magnetometer data: implications for broad scale anomaly studies over Canada. Journal of Geomagnetism and Geoelectricity, **31**, pp. 459–478.

COLES, R. L., and HAINES, G. V. 1979. Long-wavelength magnetic anomalies over Canada, using polynomial and upward continuation techniques. Journal of Geomagnetism and Geoelectricity, **31**, pp. 545–566.

COLES, R. L., HAINES, G. V., and HANNAFORD, W. 1976. Large

scale magnetic anomalies over western Canada and the Arctic: a discussion. Canadian Journal of Earth Sciences, **13**, pp. 790–802.

COLES, R. L., HANNAFORD, W., and HAINES, G. V. 1978. Magnetic anomalies and the evolution of the Arctic. *In* Arctic geophysical review. *Edited by* J. F. Sweeney. Publication of the Earth Physics Branch, Energy, Mines and Resources, Ottawa, Ont., **45**, pp. 51–66.

DELAURIER, J. M. 1978. The Alpha ridge is not a spreading centre. *In* Arctic geophysical review. *Edited by* J. F. Sweeney. Publication of the Earth Physics Branch, Energy, Mines and Resources, Ottawa, Ont., **45**, pp. 87–90.

EARDLEY, A. J. 1971. History of geologic thought on the origin of the Arctic Basin. *In* Geology of the Arctic. *Edited by* G. O. Raesh. University of Toronto Press, Toronto, Ont., pp. 223–249.

FORSYTH, D. A., MAIR, J. A., and FRASER, I. 1979. Crustal structure of the central Sverdrup basin. Canadian Journal of Earth Sciences, **16**, pp. 1581–1598.

HAINES, G. V., and HANNAFORD, W. 1972. Magnetic anomaly maps of British Columbia and the adjacent Pacific Ocean. Publication of the Earth Physics Branch, Energy, Mines and Resources, Ottawa, Ont., **42**, pp. 211–228.

——— 1974. A three-component aeromagnetic survey of the Canadian Arctic. Publication of the Earth Physics Branch, Energy, Mines and Resources, Ottawa, Ont., **44**, pp. 209–234.

——— 1976. A three-component aeromagnetic survey of Saskatchewan, Alberta, Yukon and the District of Mackenzie. Earth Physics Branch, Geomagnetic Series No. 8, Ottawa, Ont. 34 p.

HAINES, G. V., HANNAFORD, W., and RIDDIHOUGH, R. P. 1971. Magnetic anomalies over British Columbia and the adjacent Pacific Ocean. Canadian Journal of Earth Sciences, **8**, pp. 387–391.

HALL, D. H. 1974. Long-wavelength aeromagnetic anomalies and deep crustal magnetization in Manitoba and northwestern Ontario, Canada. Journal of Geophysics, **40**, pp. 403–430.

HALL, J. K. 1973. Geophysical evidence for ancient sea floor spreading from Alpha Cordillera and Mendeleyev Ridge. *In* Arctic geology. *Edited by* M. G. Pitcher. American Association of Petroleum Geology, Memoir 19, Tulsa, OK.

HANNAFORD, W., and HAINES, G. V. 1974. A three-component aeromagnetic survey of British Columbia and the adjacent Pacific Ocean. Publication of the Earth Physics Branch, Energy, Mines and Resources, Ottawa, Ont. **44**, pp. 323–379.

HERRON, E. M., DEWEY, J. F., and PITMAN, W. C., III. 1974. Plate tectonics model for the evolution of the Arctic. Geology, **2**, pp. 377–380.

International Association of Geomagnetism and Aeronomy (IAGA) DIVISION 1 STUDY GROUP 1976. International geomagnetic reference field 1975. EOS, Transactions of the American Geophysical Union, **57**, pp. 120–121.

KING, E. R., ZIETZ, I., and ALLDREDGE, L. R. 1966. Magnetic data on the structure of the central Arctic region. Geological Society of America Bulletin, **77**, pp. 619–646.

KRUTIKHOVSKAYA, Z. A., and PASHKEVICH, I. K. 1977. Magnetic model for the Earth's crust under the Ukrainian shield. Canadian Journal of Earth Sciences, **14**, pp. 2718–2728.

LANGEL, R. A. 1973. A study of high latitude magnetic disturbance. Technical Note BN-767, Institute for Fluid Dynamics and Applied Mathematics, University of Maryland, College Park, MD.

——— 1974. Near-Earth magnetic disturbance in total field at high latitudes 1. Summary of data from OGO 2, 4, and 6. Journal of Geophysical Research, **79**, pp. 2363–2371.

MAYHEW, M. A. 1978. A computer program for reduction of Pogo satellite magnetic anomaly data to common elevation and to the pole. Contract Report, NASA Contract NAS 5-41625-B.

——— 1979. Inversion of satellite magnetic anomaly data. Journal of Geophysics, **45**, pp. 119–128.

——— In preparation. Satellite-derived equivalent magnetization of the United States.

MEAD, G. D. 1979. An evaluation of recent internal field models. *In* Quantitative modeling of magnetospheric processes. *Edited by* W. P. Olson. Geophysics Monograph, **21**, pp. 110–117.

OVERTON, A. 1970. Seismic refraction surveys, western Queen Elizabeth Islands and polar continental margin. Canadian Journal of Earth Sciences, **7**, pp. 346–363.

PAKISER, L. C., and ZIETZ, I. 1965. Transcontinental crustal and upper mantle structure. Review of Geophysics, **3**, pp. 505–520.

PEDDIE, N. W., and FABIANO, E. B. 1976. A model of the geomagnetic field for 1975. Journal of Geophysical Research, **81**, pp. 2539–2542.

REGAN, R. D., and MARSH, B. D. In preparation. The Bangui anomaly: its geological origin.

REGAN, R. D., CAIN, J. C., and DAVIS, W. M. 1975. A global magnetic anomaly map. Journal of Geophysical Research, **80**, pp. 794–802.

RIDDIHOUGH, R. P., HAINES, G. V., and HANNAFORD, W. 1973. Regional magnetic anomalies of the Canadian Arctic. Canadian Journal of Earth Sciences, **10**, pp. 147–163.

SANDER, G. W., and OVERTON, A. 1965. Deep seismic refraction investigations in the Canadian Arctic archipelago. Geophysics, **30**, pp. 87–96.

SHUEY, R. T., SCHELLINGER, D. R., JOHNSON, E. H., and ALLEY, L. G. 1973. Aeromagnetics and the transition between the Colorado Plateau and the Basin Range province. Geology, **1**, pp. 107–110.

SWEENEY, J. F., COLES, R. L., DELAURIER, J. M., FORSYTH, D. A., IRVING, E., JUDGE, A., SOBCZAK, L. W., and WETMILLER, R. J. 1978. Arctic geophysical review—a summary. Publication of the Earth Physics Branch, Energy, Mines and Resources, Ottawa, Ont., **45**, pp. 101–108.

TAILLEUR, I. L. 1973. Probable rift origin of Canada Basin, Arctic Ocean. *In* Arctic geology. *Edited by* M. G. Pitcher. American Association of Petroleum Geology, Memoir 19, pp. 526–535.

TAYLOR, P. T. 1978. Low-level aeromagnetic data across the western Arctic basin. Abstract. EOS, Transactions of the American Geophysical Union, **59**, p. 268.

VOGT, P. R., and AVERY, O. E. 1974. Tectonic history of the Arctic basins: partial solutions and unsolved mysteries. *In* Marine geology and oceanography of the Arctic seas. *Edited by* Y. Hermann. Springer-Verlag, New York, NY, pp. 83–117.

VOGT, P. R., and OSTENSO, N. A. 1970. Magnetic and gravity profiles across the Alpha Cordillera and their relations to arctic sea floor spreading. Journal of Geophysical Research, **75**, pp. 4925–4937.

VOGT, P. R., TAYLOR, P. T., KOVACS, L. C., and JOHNSON, G. L. 1979. Detailed aeromagnetic investigation of the Arctic basin. Journal of Geophysical Research, **84**, pp. 1071–1089.

ZIETZ, I., KING, E. R., GEDDES, W., and LIDIAK, E. G. 1966. Crustal study of a continental strip from the Atlantic Ocean to the Rocky Mountains. Geological Society of America Bulletin, **77**, pp. 1427–1448.

Appendix

The spherical harmonic analysis used to represent the Earth's main field in this study is designated Pogo(02/72). The data set utilized in the derivation

TABLE A1. Pogo (02/72) coefficients, epoch 1960

n	m	g_n^m	h_n^m	$\dot{g}_n^m$	$\dot{h}_n^m$	n	m	g_n^m	h_n^m	$\dot{g}_n^m$	$\dot{h}_n^m$
1	0	−30456.2	0.0	23.47	0.0	9	8	10.3	4.7	−1.09	−1.09
1	1	−2180.3	5819.0	12.67	−8.84	9	9	−6.5	8.6	1.45	−1.06
2	0	−1546.2	0.0	−23.09	0.0	10	0	−2.1	0.0	0.05	0.0
2	1	2996.2	−1994.0	0.53	−4.20	10	1	−1.7	3.5	−0.14	−0.17
2	2	1605.2	203.2	−2.19	−17.71	10	2	1.5	0.3	0.05	0.07
3	0	1304.8	0.0	−2.29	0.0	10	3	−4.1	0.3	−0.05	0.17
3	1	−1982.6	−443.9	−11.86	8.18	10	4	−3.4	4.8	0.22	0.14
3	2	1305.6	222.6	−2.08	3.02	10	5	9.3	−2.7	−0.42	−0.14
3	3	886.7	−156.7	−5.50	−2.99	10	6	5.7	2.2	−0.12	−0.20
4	0	961.4	0.0	−1.11	0.0	10	7	2.8	−5.4	−0.33	0.38
4	1	811.7	136.7	−1.15	2.96	10	8	0.6	8.7	−0.04	−0.67
4	2	496.7	−276.6	−2.69	0.96	10	9	0.9	−7.0	0.39	0.91
4	3	−381.7	16.2	−1.05	0.54	10	10	4.0	−9.3	−0.48	0.63
4	4	264.5	−259.9	−2.66	−1.39	11	0	2.4	0.0	0.01	0.0
5	0	−222.7	0.0	0.89	0.0	11	1	−0.2	1.3	−0.09	0.01
5	1	358.9	11.7	0.30	0.98	11	2	−1.9	2.6	0.00	0.04
5	2	242.9	118.4	1.52	1.75	11	3	5.0	−1.8	−0.17	−0.00
5	3	−28.1	−111.4	−0.97	−2.99	11	4	−2.4	−4.2	0.20	−0.19
5	4	−140.6	−101.2	−2.37	0.84	11	5	−1.2	1.5	0.18	0.14
5	5	−95.2	119.1	4.86	−3.81	11	6	−4.0	−3.9	0.47	0.54
6	0	46.0	0.0	−0.02	0.0	11	7	3.7	−1.0	−0.28	−0.05
6	1	59.1	−9.0	0.32	−0.21	11	8	−0.0	−3.0	0.33	0.44
6	2	−0.1	−106.8	1.36	−0.46	11	9	−0.7	−5.3	−0.26	0.37
6	3	−243.2	61.5	2.83	1.28	11	10	−3.6	−3.8	0.80	0.36
6	4	−3.3	−26.5	0.58	−1.42	11	11	5.4	−8.7	−0.28	1.28
6	5	−0.1	−20.3	0.11	1.59	12	0	−0.5	0.0	−0.15	0.0
6	6	−102.1	−4.4	−1.01	0.30	12	1	0.3	1.1	−0.03	−0.08
7	0	71.1	0.0	−0.15	0.0	12	2	0.4	0.1	−0.13	0.05
7	1	−51.6	−52.9	−0.29	−1.68	12	3	0.2	1.9	−0.02	0.03
7	2	3.9	−27.3	−0.32	0.18	12	4	1.6	0.3	−0.15	−0.10
7	3	12.3	−7.2	0.28	0.11	12	5	0.4	−0.6	0.02	0.04
7	4	−39.9	1.4	1.85	1.01	12	6	0.1	0.4	−0.11	−0.02
7	5	0.9	17.6	−0.46	0.36	12	7	−2.3	−1.3	0.20	0.13
7	6	−4.0	−35.1	2.25	1.80	12	8	0.7	−1.3	−0.04	0.25
7	7	39.7	−47.5	−5.78	4.11	12	9	0.3	2.7	−0.13	−0.30
8	0	8.9	0.0	0.36	0.0	12	10	−0.5	−0.6	0.06	−0.07
8	1	3.9	11.1	0.24	−0.35	12	11	−4.4	4.8	0.44	−0.55
8	2	−4.6	−12.7	0.41	−0.20	12	12	−5.4	−4.6	0.80	0.40
8	3	−11.0	8.8	−0.01	−0.48	13	0	1.1	0.0	−0.10	0.0
8	4	−0.3	−15.4	−0.51	−0.34	13	1	0.7	1.8	−0.15	−0.23
8	5	6.2	8.1	0.04	−0.36	13	2	0.7	0.7	−0.00	−0.05
8	6	−5.5	19.6	0.34	0.14	13	3	−0.6	0.6	0.00	0.06
8	7	12.3	6.1	−0.01	−1.44	13	4	1.0	−0.3	−0.09	0.00
8	8	−6.8	−35.1	1.49	2.05	13	5	0.7	−0.7	−0.03	0.08
9	0	11.4	0.0	−0.31	0.0	13	6	0.9	0.9	−0.13	−0.19
9	1	7.8	−22.0	0.12	−0.08	13	7	−1.0	−0.2	0.10	0.09
9	2	3.4	14.7	−0.26	−0.01	13	8	0.8	0.1	−0.16	−0.10
9	3	−12.3	2.1	0.01	0.42	13	9	2.2	0.3	−0.20	0.06
9	4	17.0	1.2	−0.73	−0.51	13	10	3.5	3.6	−0.49	−0.45
9	5	1.2	−1.7	−0.22	−0.25	13	11	−1.5	6.9	0.17	−0.79
9	6	8.1	18.5	−1.15	−1.30	13	12	−8.5	−6.2	0.88	0.63
9	7	−9.1	18.2	1.70	−0.90	13	13	3.3	−11.4	−0.15	1.14

NOTE: Units are nT and nT/year.

of this field model is identical to that used for the Pogo(08/71) field model (Langel 1973, 1974) except that no data from 1970 were used in the derivation of Pogo(02/72). The fitting procedure used 47 485 data points that were fit with the coefficients given in Table A1 to a root mean square residual of 6.2 nT. The distribution of residuals is given in Table A2, and pertinent statistics relative to data from the three satellites in Table A3.

The model generation assumed a spheroidal Earth with mean radius of 6371.0 km, equatorial radius of 6378.16 km, and a flattening factor of 1/298.25.

Because it was not designed as a predictive

TABLE A2. Distribution of residuals

Range (nT)	−60 to −50	−50 to −40	−40 to −30	−30 to −20	−20 to −10	−10 to 0	0 to 10	10 to 20	20 to 30	30 to 40
Number of points	2	4	25	216	2562	19 113	23 692	1831	28	2

TABLE A3. Statistics for OGO 2, OGO 4, and OGO 6

	Number of points	RMS (nT)	Mean (nT)	Standard deviation about mean (nT)
OGO 2	12 773	5.17	0.263	5.16
OGO 4	18 431	6.80	0.088	6.80
OGO 6	16 281	6.25	−0.063	6.21

model, Pogo(02/72) does not include data from observatories to aid in determination of the secular variation. It is, however, suitable for some uses at times past 1971. Mead (1979) has recently evaluated four field models for the epoch 1973–1976, well past the time span of the data utilized to create the models. The models evaluated were Pogo(08/71), IGS/75 (Barraclough *et al.* 1975), AWC/75 (Peddie and Fabiano 1976), and IGRF 1975 (IAGA 1976). He concluded that the first three were all about equally accurate and much superior to IGRF 1975. Both AWC/75 and IGS/75 are slightly better than Pogo(08/71). An extension of Mead's result shows that Pogo(02/72) is of comparable accuracy to Pogo(08/71) for the interval 1973–1976.

Reprinted from

Canadian Journal of Earth Sciences

Réimpression du

Journal canadien des sciences de la terre

Comparisons of magnetic anomalies of lithospheric origin measured by satellite and airborne magnetometers over western Canada

R. A. LANGEL, R. L. COLES, AND M. A. MAYHEW

Volume 17 • Number 7 • 1980

Pages 876–887

National Research Council Canada

Conseil national de recherches Canada

Comparisons of magnetic anomalies of lithospheric origin measured by satellite and airborne magnetometers over western Canada[1]

R. A. LANGEL
Geophysics Branch, National Aeronautics and Space Administration, Goddard Space Flight Center, Greenbelt, MD 20771, U.S.A.
R. L. COLES
Earth Physics Branch, Department of Energy, Mines and Resources, Ottawa, Ont., Canada K1A 0Y3
AND
M. A. MAYHEW
Business and Technological Systems, Inc., Seabrook, MD 20801, U.S.A.

Received October 11, 1979
Revision accepted March 7, 1980

Crustal magnetic anomaly data from the Orbiting Geophysical Observatories 2, 4, and 6 (Pogo) satellites are compared with upward-continued aeromagnetic data between 50–85°N latitude and 220–260°E longitude. Agreement is good, both in anomaly location and in amplitude, giving confidence that it is possible to proceed with the derivation and interpretation of satellite anomaly maps in all parts of the globe. The data contain a magnetic high over the Alpha ridge suggesting continental composition and a magnetic low over the southern Canada basin and northern Canadian Arctic Islands (Sverdrup basin). The low in the Sverdrup basin corresponds to a region of high heat flow, suggesting a shallow Curie isotherm. A ridge of high field, with two distinct peaks in amplitude, is found over the northern portion of the platform deposits and a relative high is located in the central portion of the Churchill Province. No features are present to indicate a magnetic boundary between Slave and Bear Provinces, but a trend change is evident between Slave and Churchill Provinces. South of 60° latitude a broad magnetic low is located over very thick (40–50 km) crust, interpreted to be a region of low magnetization.

On compare les données recueillies par les satellites OGO 2, 4 et 6 (Pogo) sur les anomalies magnétiques dans la croûte avec un prolongement vers le haut des données aéromagnétiques situées entre les latitudes 50–85°N et les longitudes 220–260°E. L'accord est bon à la fois pour la localisation des anomalies et leur amplitude, ce qui permet d'être optimiste quant à la possibilité de procéder à la confection et à l'interprétation de cartes d'anomalies magnétiques par satellite dans toutes les parties du globe. Les données contiennent un pic magnétique sur la crête Alpha suggérant une composition continentale et une dépression magnétique sur le bassin du sud du Canada et dans les îles de l'Arctique canadien au nord (le bassin de Sverdrup). La dépression dans le bassin de Sverdrup correspond à une région de flux thermique élevé ce qui laisse supposer une isotherme de Curie à faible profondeur. Une crête de champ intense avec deux pics distincts dans l'amplitude se retrouve dans la partie nord des dépôts de plate-forme et un sommet relatif est localisé dans la portion centrale de la province de Churchill. Il n'y a rien qui indique une limite magnétique entre les provinces de l'Esclave et de l'Ours, il y a un changement évident entre les provinces de Churchill et de l'Esclave. Au sud de la latitude 60°N, on observe une vaste dépression magnétique située sur une croûte très épaisse (40–50 km) et qu'on interprète comme une région de faible aimantation.

[Traduit par le journal]

Can. J. Earth Sci., 17, 876–887 (1980)

Introduction

In recent years it has been realized that crustal magnetic anomalies exist which are of longer wavelengths than those investigated by exploration geophysicists and that these longer wavelength (greater than 50 km) anomalies are indicative of geologic and tectonic features in the deep crust (Pakiser and Zietz 1965; Zietz *et al.* 1966; Shuey *et al.* 1973; Hall 1974; Krutikhovskaya and Pashkevich 1977).

With the publication of the paper by Regan *et al.* (1975) it was demonstrated that long wavelength lithospheric anomalies could be mapped successfully from satellites. That map showed a global distribution of anomalies of about 500–3000 km scale size which were never before mapped and whose very existence was in most cases discovered for the first time. Although this map was distorted by variations in altitude over the data set and by contamination from magnetospheric fields, Regan *et al.* were able to demonstrate that the probable source of the anomalies is indeed the lithosphere.

[1]Contribution from the Earth Physics Branch No. 854.

0008-4077/80/070876-12$01.00/0

TABLE 1. Some characteristics of the Pogo orbits

Satellite	Launch date	Inclination	Perigee (km)	Apogee (km)
OGO 2 (1965 81A)	October 14, 1965	87.3°	410	1510
OGO 4 (1967 73A)	July 28, 1967	86.0°	410	910
OGO 6 (1969 51A)	June 5, 1969	82.0°	400	1100

Subsequently, Regan and Marsh (in preparation) have collected ancillary data and derived a quantitative model of an anomaly located in central Africa. Analysis techniques for this type of data are rapidly becoming available (Bhattacharyya 1977; Mayhew 1978, 1979).

While analysis of data at lower latitudes has proceeded (Regan and Marsh, in preparation; Mayhew 1979), nothing has been published dealing with anomalies measured by satellite at the higher latitudes. The reason for this is that at low latitudes the external (magnetospheric/ionospheric) fields are mainly of longer wavelength than the anomalies being mapped, and can be readily filtered from the data, thus isolating the anomaly fields. This remains true as long as data within about 3 h of local noon are not utilized. At high latitudes, however, ionospheric currents occur at all local times and are very often present even during magnetically quiet periods of time. Further, these currents result in fields of the same spatial scale as the anomalies of interest, thus complicating the problem of isolating the anomaly fields. This paper is a report on an attempt to isolate the anomaly fields at satellite altitude for such high latitudes, and in particular over that part of Canada between 50–85°N latitude and 220–260°E longitude. To gauge the success of this attempt, the resulting anomaly map is compared to aeromagnetic data upward continued to satellite altitude, 500 km.

The Satellite Data

A survey of the near-Earth magnetic field was carried out by the Polar Orbiting Geophysical Observatories (OGO 2, 4, and 6), also known as the Pogo satellites (Langel 1973, 1974). Some characteristics of the Pogo orbits are given in Table 1. Orbiting Geophysical Observatory 2 acquired data from launch until October 2, 1967; OGO 4 from launch until January 19, 1969; and OGO 6 from launch until August 29, 1970 and then sporadically until June 1971. Each satellite completed about 15 revolutions each day. Orbiting Geophysical Observatory 2 and OGO 4 acquired a data point every 0.5 s and OGO 6 every 0.288 s.

The measured magnetic field, $\boldsymbol{B}$, is the vector sum of magnetic fields from several sources. These are the main (core) field of the Earth, $\boldsymbol{M}$, the variable field due to ionospheric and magnetospheric currents, $\boldsymbol{D}$, and the field originating in the lithosphere of the Earth, $\boldsymbol{A}$. In this study the main field is represented by a spherical harmonic model, $\boldsymbol{M}_c$, of degree and order 13, designated Pogo(02/72) and described in the Appendix. It should be noted that this model is intended primarily as a representation of the main field of the Earth for the time span of the Pogo data. The degree and order were chosen on the basis of studies by Phillips (J. Phillips, personal communication, 1978), Cain *et al.* (1974), and Cain (1976), which indicate that a 13th degree and order representation is sufficient to represent the main field without unduly distorting the anomaly field. Any such choice is, of course, a compromise and no exact separation is possible.

Orbiting Geophysical Observatories 2, 4, and 6 measured the magnitude but not the direction of the field $\boldsymbol{B}$. The quantity analyzed is thus the residual field

$$\Delta B = |\boldsymbol{B}| - |\boldsymbol{M}_c|$$

This residual field contains contributions from: (1) any inaccuracy in modeling the core field $\boldsymbol{M}$ with $\boldsymbol{M}_c$, (2) the external field, $\boldsymbol{D}$, and (3) the lithospheric field, $\boldsymbol{A}$. Contributions from $\boldsymbol{D}$ are minimized by elimination of all data in which the residual field was considered to be dominantly due to $\boldsymbol{D}$. This elimination was accomplished on a pass by pass basis in two steps. (A pass is defined as a continuous set of data beginning when the satellite goes above 50° latitude and ending when it again goes below 50° on the other side of the pole.) Firstly, if the magnitude of the residual field, ΔB, exceeds 20 nT (nanotesla) at any place in the pass, the entire pass is rejected. Secondly, the remaining passes are visually intercompared to attempt to distinguish the time invariant features, the lithospheric field $|\boldsymbol{A}|$, from the time varying external field $|\boldsymbol{D}|$, and passes with significant contribution from the latter are not used in the anomaly map. A total of 271 "quiet" passes remained and were used in deriving the anomaly map. After performing these operations the internal agreement of passes which are nearly coincident geographically is substantial, which indicates the presence and reality of the crustal

anomalies. However, significant differences of wavelength more than 2000–3000 km still remain between coincident passes. This is similar to the results of Mayhew (1979) over the continental United States. His solution was to remove a polynomial function separately from each individual pass. Only passes with several thousand kilometres of data were used. This function is determined by a least squares fit to that pass. The procedure of Mayhew was followed with the data presented here except that Mayhew chose a quadratic function whereas we have chosen a linear function. The function chosen is a matter of subjective judgement. The difference between the linear and quadratic functions for these data is not substantial. We are, of course, left with an anomaly field with arbitrary zero. After the data selection and trend removal, individual residual field data points were averaged in an equal-area grid superimposed over an equal-area map of the area of interest. The grid is square and the distance along each side is equivalent to 3° of latitude. Figure 1 shows the density distribution of the data used in the averages. The resulting averaged residual anomaly map, contoured at 2 nT intervals, is shown in Fig. 2*a*. Results in the southwest portion of the map, between 220–240° longitude and 50–60°N latitude, are to be regarded with caution because of the sparseness of data as shown in Fig. 1. The residuals plotted in Fig. 2*a* are not at a common altitude but are at the altitudes determined in each block over which the data were averaged. The average altitude varies from 440–560 km, with mean near 520 km. A map reduced to common altitude is discussed later in the paper.

The anomalies range from a maximum of 14 nT at about 85° latitude to a minimum of −11 nT at 50° latitude and 239° longitude.

The Airborne Magnetometer Data

The airborne magnetic field data considered here have been acquired by the Earth Physics Branch of the Department of Energy, Mines and Resources, Ottawa, since 1969 in a series of airborne vector magnetometer surveys, each survey covering 2×10^6 to 4×10^6 km^2 at a typical altitude of 3.5 km above sea level, with excursions giving a range of 2.5–6.0 km. The instrumentation and survey details have been variously described by Haines and Hannaford (1972, 1974, 1976) and Hannaford and Haines (1974). Discussions of the data have been given by Haines *et al.* (1971), Riddihough *et al.* (1973), Coles *et al.* (1976), and Coles and Haines (1979).

The data were obtained in three separate surveys

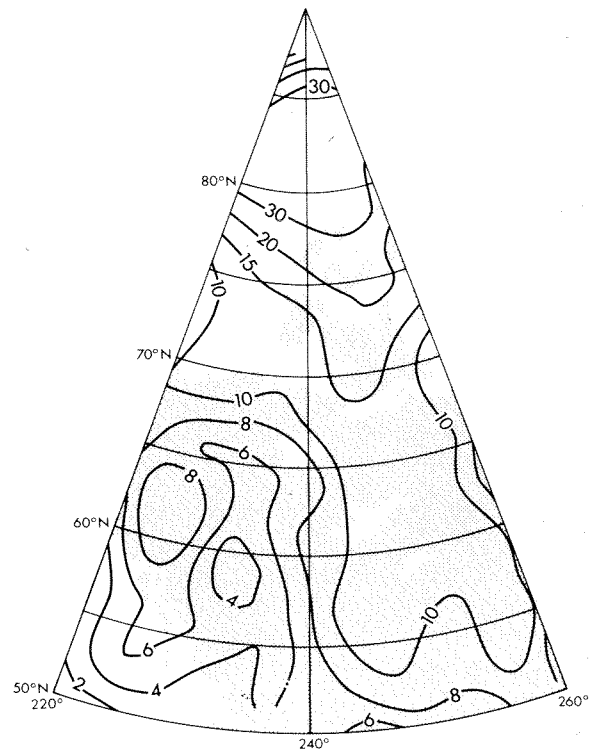

FIG. 1. Density of distribution of Pogo data, as number of points in averages.

flown at approximately 2 year intervals. In order to remove level differences due to secular change, a reference field has been removed. Coles (1979) has shown that the best available reference field models for this region and for this interval of time are based on the Pogo data. The model chosen was the Pogo(02/72) model, i.e., the same reference field used for the satellite data. Coles also demonstrated a way of correcting for inadequacies in the secular change terms of the reference model in its application to the airborne data. The residual data values are, in effect, adjusted to a single epoch. At each magnetic observatory in or near the survey region, the change in average quiet day field level from the epoch of the survey to the updated epoch is compared with the change in value of the field model between the two epochs. This comparison leads to a low-degree polynomial correction surface to be applied to the data residuals. The airborne data residuals were upward continued to 500 km in order to compare them with the satellite data. A more detailed discussion of this procedure is given by Coles and Haines (1979).

At high geomagnetic latitudes, differences between scalar and vertical component regional anomaly fields are minor (Langel 1974). The vertical

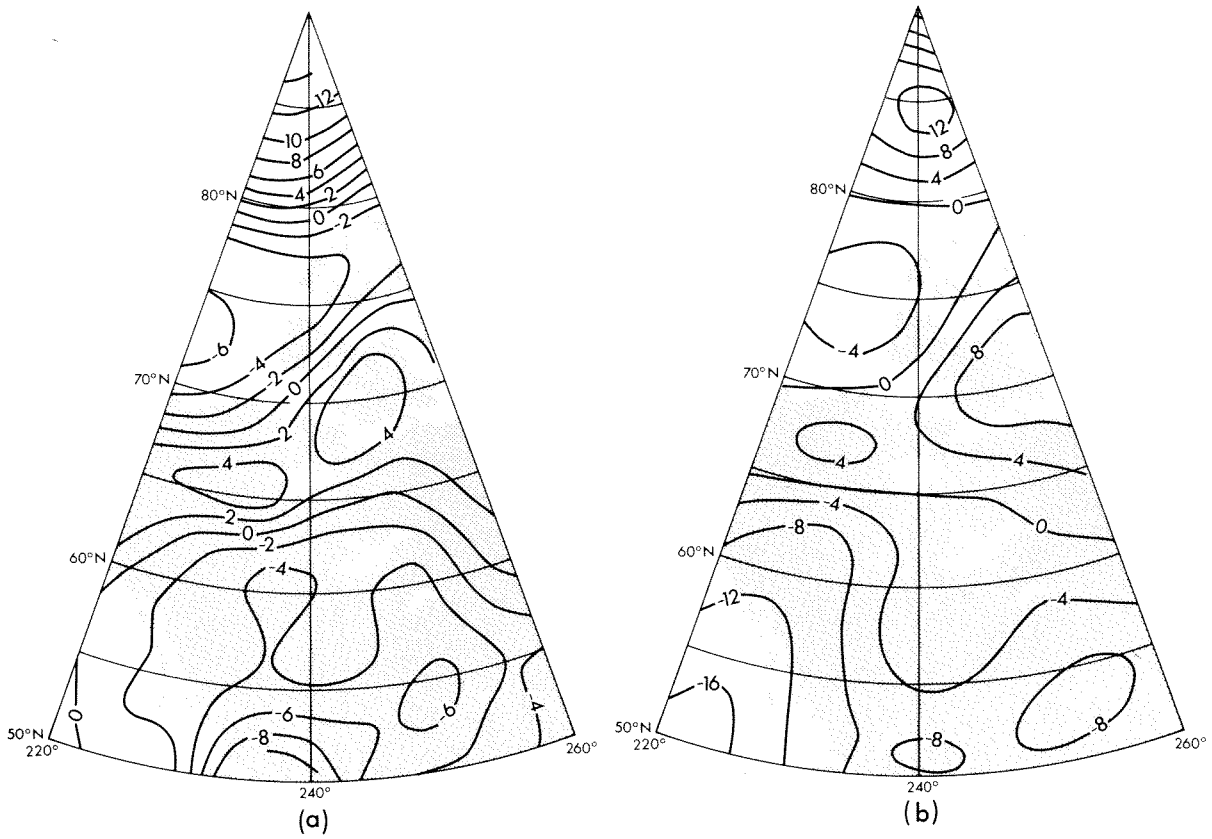

FIG. 2. Comparison of (*a*) averaged scalar magnetic anomalies from Pogo data with (*b*) upward-continued aeromagnetic vertical component anomaly data (500 km altitude).

component airborne data were used for the upward continuation because the data coverage is more complete than the scalar data coverage, and because the scalar field is not strictly harmonic. The input data to the upward continuation were in the form of averages of vertical component residuals along flight tracks over 5 min of time (about 35 km distance). The data points are shown in Fig. 3, and Fig. 4 is a contoured map prepared from the 5 min averaged data.

The data averages were each associated with an area determined by the spacing (35 km) multiplied by the mean flight-line spacing in the region of each data average. Although the original data were only along flight lines, the approximation is sufficient for the present purposes. No corrections for variations in flight altitude have been incorporated.

The basic equation for upward continuation from a sphere can be approximately represented, for the vertical component Z_p at point P, by

$$Z_p = \frac{R^2 - R_0^2}{4\pi R} \sum \frac{Z_i}{\rho_i^3} \Delta S_i$$

where the summation is over all data points i, each associated with an area ΔS_i and field value Z_i. R is the geocentric distance to the point P, R_0 is the radius of the Earth, and ρ_i is the distance from P to the point i. The data values, Z_i, are residuals relative to the reference field. The residual field beyond the data area is assumed to be zero and, therefore, has no contribution to the summation. This is an assumption, of course, which limits the accuracy of the upward continuation. Coles and Haines (1979) discuss this point in more detail; however, the actual total contribution from distant points beyond the data area is small (less than about 2 nT for most parts of the area), since the integral of the residual field over a large region tends to zero.

The data (5600 points) have been upward continued to 100, 300, and 500 km (Figs. 5, 2*b*). As the altitude increases, the anomalies become smoother and reduced in amplitude. Broad features, however, persist through the series of figures.

Comparison of the Anomaly Maps

There is good agreement between the satellite

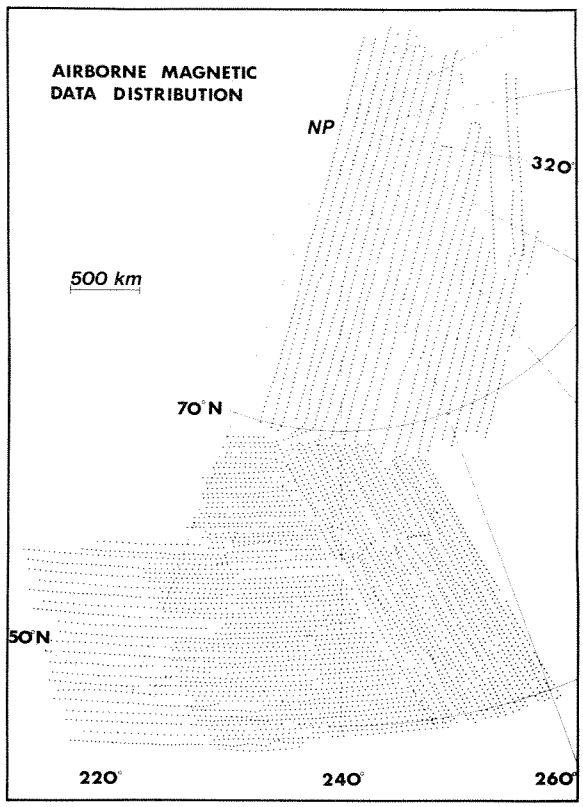

FIG. 3. Relative distribution of aeromagnetic data.

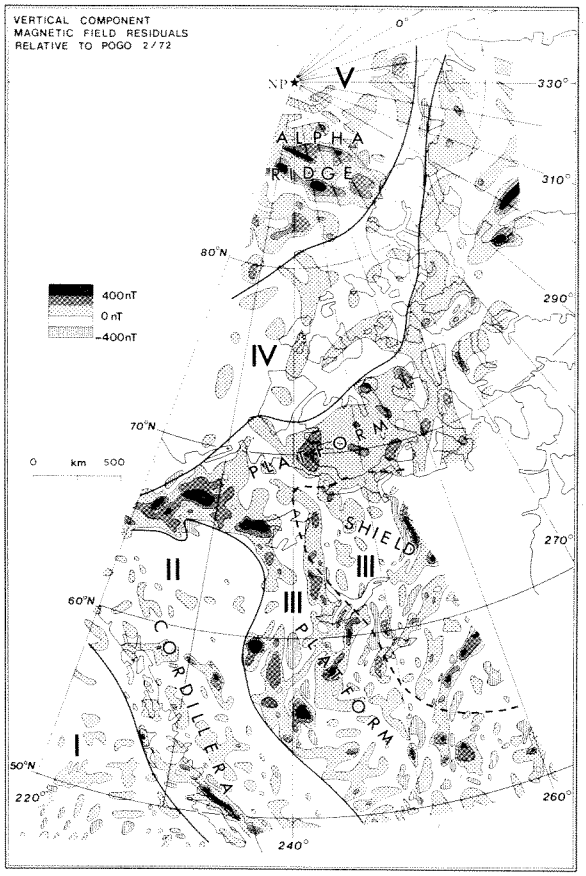

FIG. 4. Residuals of aeromagnetic data at an altitude of 3 km. Roman numerals designate regions of differing characteristics as described in the text.

and airborne data in their common spectral region. The agreement is excellent in the north, with a high anomaly north of 80°N, a low region between about 70 and 80°N, and a north-easterly trending ridge of high field centered near 65–67°N in the west and extending to about 70°N in the east. A south-trending, relatively positive area extends between 55 and 62°N at a longitude of about 240°. In the southwest the agreement is not as good, with a large gradient evident in the airborne-derived map. Nevertheless, the indications are of a relatively low field over the southwestern Cordillera region in Canada. The agreement in anomaly amplitudes is also very good, except in the southwest corner. This comparison gives a confirmation over a sub-continental size region of the reality of the anomalies derived from satellite data. This is particularly important for this region of the Earth where contaminating fields from high latitude currents are strong and it indicates that we have been successful in separating the anomaly fields from fields due to those currents.

The reason for the discrepancy in the southwest between the two maps is not clear. The method of upward continuation is not a major factor since different analyses of the original data also indicate a similar discrepancy (Coles and Haines 1979). The Pogo anomaly map is determined relative to a model also derived from Pogo data, so one would not expect trends of 10–20 nT to be present in that map. Either the available satellite data are consistently high in this region (the density of satellite passes is very low here), or the airborne data (one particular survey) are consistently low.

Effect of Model Removed

Any bias in the field model utilized to estimate the core field may be reflected as an error in anomaly maps derived by this method. This would be the case, for example, if the higher order terms of the model utilized were negatively correlated with the anomalies derived. Obviously, some error is introduced simply because the spectra of core and crustal fields overlap so that it is not possible to do a clean separation. We believe that, if anything, our results are biased by removing too much long

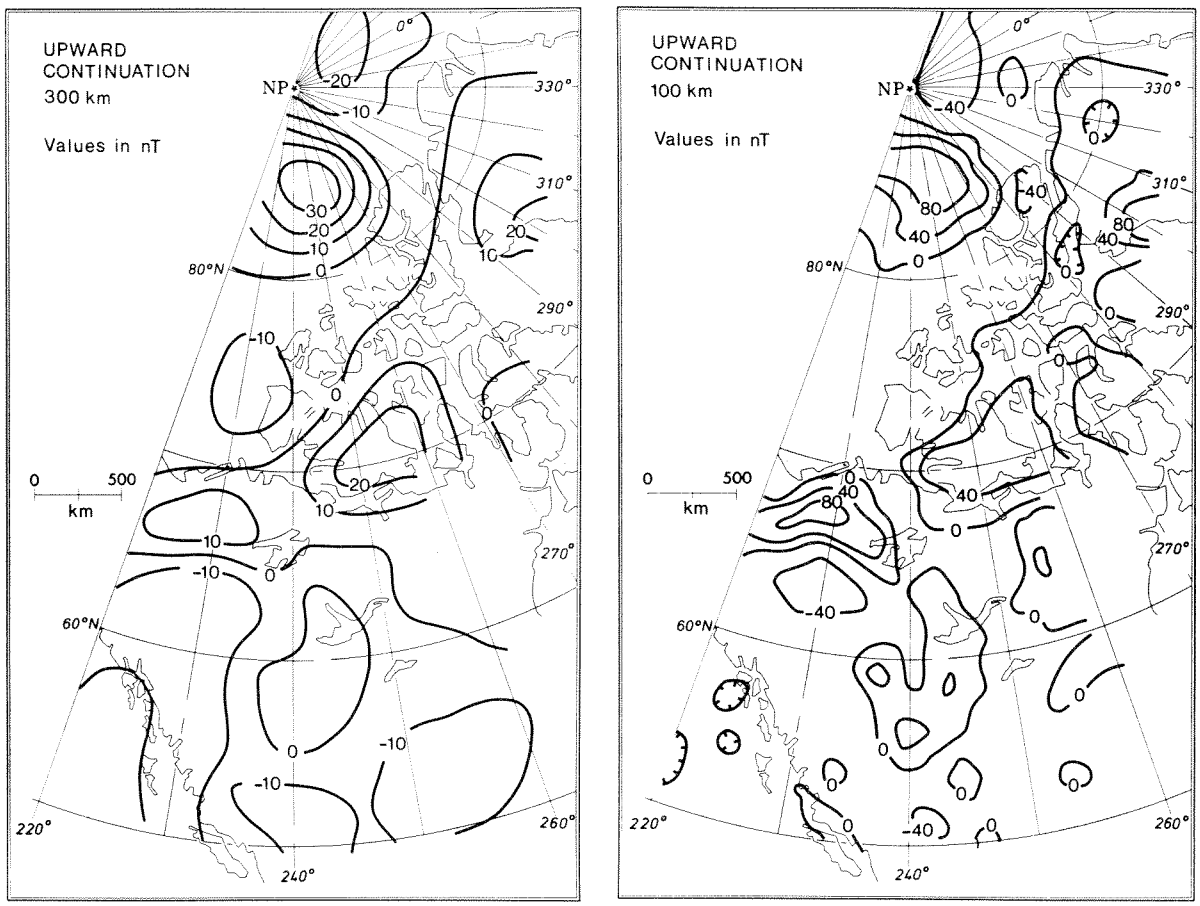

FIG. 5. Upward continuation of aeromagnetic data.

wavelength field rather than too little, because of the pass by pass linear trend removal.

We have two indications that field model biases are not significantly contaminating our results. Firstly, Coles *et al.* (1976, Fig. 2) subtracted the vertical component of the International Geomagnetic Reference Field (IGRF) from the vertical component of the Pogo(02/72) model (erroneously designated Pogo(6/71) in their paper). This difference plot shows *no* correlation with the derived anomaly maps. Secondly, we have recomputed the satellite anomaly map utilizing the Pogo(06/74) field model (Cain *et al.* 1974) which is of degree and order 22. This map is presented here as Fig. 6. Comparison with Fig. 2*a* shows that the greatest differences are in the southwest corner of the map—already noted to be suspect. All other features remain relatively unchanged except for subtle longer wavelength effects. We believe this indicates that any biases due to the degree of the field models used are negligible.

Geologic Implications

It is not our intention to present a detailed interpretation of the magnetic anomaly maps shown here. Interpretations of the aeromagnetic data have already been published (Haines *et al.* 1971; Riddihough *et al.* 1973; Coles *et al.* 1976). In this section we wish to contrast the different viewpoints offered by the aeromagnetic and satellite magnetic data and to illustrate the use of the satellite data in making geologic inferences.

Examination of Fig. 4 shows changes in the character of the anomaly patterns from region to region, often delineating geologic boundaries. Such changes are clearly apparent between the Cordillera and the platform, i.e., between regions II and III and between the platform of region III and the thick sediments, both onshore and offshore, of region IV. The character changes most evident are (1) changes from high magnetic relief to low magnetic relief and (2) changes in the trends of the anomalies. Because most of the high relief features are positive

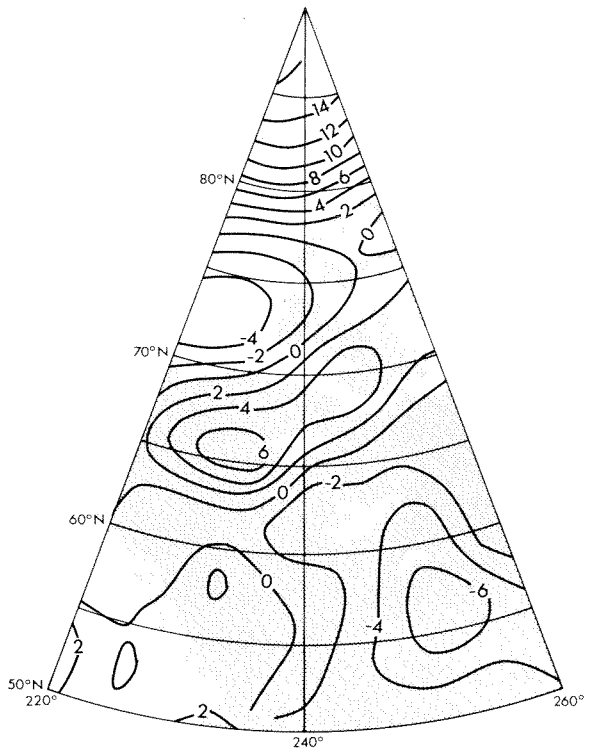

FIG. 6. Averaged magnetic anomaly map from Pogo data, using a 22nd degree spherical harmonic model to remove the core field.

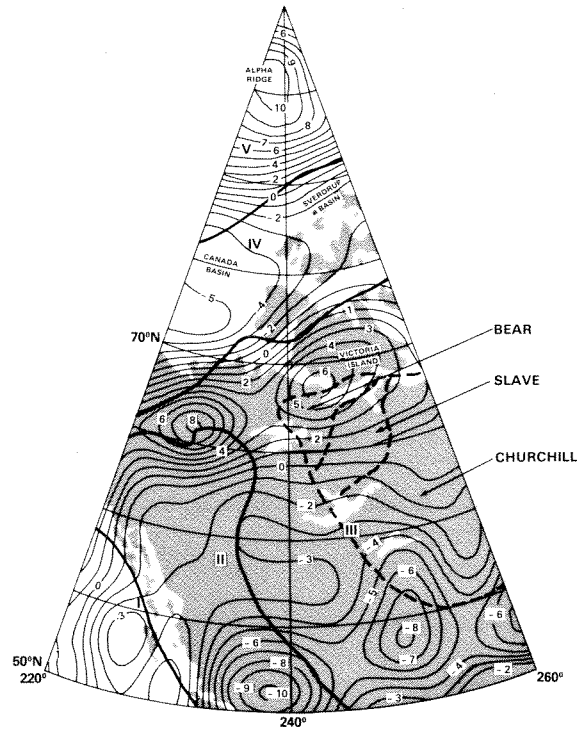

FIG. 7. Reduction of Pogo anomaly map to an altitude of 500 km using an equivalent source representation (reference field is Pogo(02/72)). The contour interval is 1 nT.

there is also an apparent contrast between regions of predominantly positive and predominantly negative fields. Figure 7 shows the satellite field, now reduced to common altitude using an equivalent source representation (Mayhew 1978, 1979). In contrast to Fig. 4, the satellite map shows only the contrasts between the predominantly positive and negative regions. The aeromagnetic data clearly contain all of the information in the satellite data and more and are able to delineate boundaries more definitively. However, the satellite map (or an upward-continued aeromagnetic map) gives a clearer picture of broad trends and can serve as a guide in discerning those same trends in the lower altitude data. In the following paragraphs we will discuss the various "regions" delineated by the satellite anomalies (Fig. 7) compared with those delineated by the aeromagnetic data (Fig. 4) and known geologic provinces.

At the very north of the map the satellite data show a prominent high of about 12 nT magnitude. This is centered on the Alpha ridge of the Arctic Basin. The airborne survey also shows a broad positive in this region but is punctuated by a complex series of intense positive anomalies nearly parallel to the trend of the ridge. These extend both north and south of the ridge and are all contained within the area of positive field as seen by Pogo. This region has also been surveyed by Vogt *et al.* (1979) who concluded that the principal magnetic anomalies in this region are topographic effects in a normally magnetized basement with high magnetization intensity (20–30 A/m). The broader picture afforded by the satellite data supports the existence of a region of highly magnetized crust and partially outlines its extent. Unfortunately, the satellite data do not extend above 87° latitude so the northern portion of this region is not mapped. The upward-continued aeromagnetic data indicate that it terminates at about 88° latitude.

The Alpha ridge has been variously interpreted as a subduction zone (Herron *et al.* 1974), as an extinct center of sea-floor spreading (Churkin 1973; Vogt and Ostenso 1970; Hall 1973; Tailleur 1973; Vogt and Avery 1974), or as subsided continental crust (Eardley 1961; King *et al.* 1966; Taylor 1978). DeLaurier (1978) rejects the hypotheses of a subduction zone or a center of sea-floor spreading on the basis of a comparison of the measured relief with the relief expected from a cooling model, because of a lack of seismic activity, and because active accretion is inconsistent with the known

marine fossils and sediment thickness. Vogt *et al.* (1979) also examine these questions and conclude that on the basis of the airborne magnetic data it is not possible to rule out any of the three hypotheses. In addition to the arguments noted above against a spreading center or subduction zone, they claim that the depth of the Alpha ridge argues against it being a subsided shield.

Taylor (1978) suggests that the Alpha ridge is an aseismic ridge similar to the Lord Howe Rise, which is continental in nature, in the southwest Pacific. In fact, the satellite data show a similar positive anomaly over the Lord Howe Rise (Regan *et al.* 1975). Coles *et al.* (1978) and Sweeney *et al.* (1978) note that the positive long-wavelength anomaly over the Alpha ridge is consistent with a region of crust of continental composition since most of the major long-wavelength positive anomalies detected by satellites are associated with continental crust, both in shield areas and in regions such as Broken Ridge in the Indian Ocean (Regan *et al.* 1975).

To the south of the Alpha ridge and its environs the satellite map shows a broad negative over the southern Canada Basin and the northern Canadian Arctic Islands. The aeromagnetic data in this region are remarkably free from shorter wavelength anomalies. Geologically, this is a region of deep (3–12 km) sediments (Sweeney *et al.* 1978) resulting in a greater depth to basement which may account for the lack of shorter wavelength anomalies in the aeromagnetic data (Riddihough *et al.* 1973). The southern 0 nT contour of this region is close to the edge of the craton but both bathymetric (Sweeney *et al.* 1978) and seismic (Sweeney *et al.* 1978; Berry and Barr 1971; Sander and Overton 1965; Overton 1970; Berry 1973) data show that the transition from continental to oceanic crust, the Canada Basin, takes place well within the region of negative anomaly. Comparison of Fig. 7 with the bathymetry (Sweeney *et al.* 1978) indicates that over much of its length the −4 nT contour nearly coincides with the continental slope. Thus, the central low of the negative anomaly is located over oceanic crust. The eastward extension of this magnetic low is over the Sverdrup basin, where refraction data (Sander and Overton 1965; Overton 1970; Forsyth *et al.* 1979) indicate sediments reaching 12 km. Forsyth *et al.* note that "Based on heat flow measurements taken in bore-holes throughout the Sverdrup Basin, A. S. Judge has estimated that maximum temperatures are 600 to 650°C at 20 km and 850 to 900°C at 30 km (personal communication)." Judge noted higher than average heat flow values for the central Sverdrup basin. Thus, the magnetite Curie isotherm is well up into a thickly sedimented crust in this region which could account for the relative negative magnetic anomaly. The cause of the negative anomaly over the Canada Basin is unknown. Future refinement of the satellite data over the rest of the Arctic will be required to see if the negative anomaly is coextensive with the entire Amerasian Basin.

An elongated region of high magnetic field (Fig. 7) is located near 65° latitude at 220°E longitude in the west and extends to 71° latitude at 260°E longitude. This "high" occurs over the northern portion of the platform deposits on the Precambrian craton and can be resolved into two maxima. In the east the positive anomaly extends southward over the northern parts of the exposed shield. Considering the two highs over the platform deposits, comparison with Fig. 4 shows positive anomalies in the aeromagnetic data in these regions but of significantly different character. In the east, over Victoria Island, there is no concentration of short-wavelength anomalies, whereas in the west, the broad positive background is punctuated by narrow regions of intense positive short-wavelength anomalies. This region of large amplitude anomalies extends around the top of region II (Fig. 4) and has been interpreted to indicate that the crystalline continental basement extends far to the west of the exposed and known buried shield (Coles *et al.* 1976). This regional difference seems to be reflected in the heat flow data (although a good thermal model is not yet available and the available data are sparse) in that the available heat flow values near the western field maximum are considerably higher than those near the eastern maximum. This difference in heat flow between two magnetic highs of nearly equal amplitude indicates that the long-wavelength anomalies, at least to the east of the Cordillera, do not correlate well with heat flow and, therefore, are not indicative of variations in the depth to the Curie isotherm. For comparison, in the United States good heat flow vs. long-wavelength anomaly correlation is evident in the tectonically active region west of the Cordillera (Mayhew, in preparation), whereas in the more stable region to the east of the Cordillera the extremely sparse heat flow data do not seem to correlate with the long-wavelength magnetic anomalies.

Just to the south of the double maximum the contour lines are relatively featureless with a northeasterly trend. In particular, no features are present marking the boundary between Bear and Slave Provinces. Below 67° latitude a trend change is evident between Slave and Churchill Provinces and, near the eastern border of the map, a relative

high extends through the central portion of the Churchill Province. This relative high is not clearly defined in the aeromagnetic data, which do not extend as far east as the satellite data.

South of about 60–63° the satellite anomaly map is everywhere negative, highly negative in some regions. The low altitude data of Fig. 4 show that large portions of this area are relatively free of large amplitude short-wavelength anomalies. A relative negative anomalous region can be caused by one or a combination of three things: very low rock magnetization, a shallow Curie isotherm, or a high reversed remanent magnetization. The latter is extremely unlikely for a geographic region of this size; reversed magnetizations for regions this size are neither expected nor found in practice. Although sparse, the existing heat flow data are at or below normal values, with no indication of a shallow Curie isotherm. Thus the crust in this region, which is 40–50 km thick (Chandra and Cumming 1972; Berry 1973), most likely has very low average rock magnetization over most of its area. The satellite data show a relative high at about 57–60° latitude and 238–241° longitude. This is reflected in the low latitude aeromagnetic data (Fig. 4) as a cluster of magnetic highs east of the Cordillera, and in fact the Cordillera is outlined by their western boundary. Most of this region of "highs" is underlain by sedimentary cratonic cover rocks, reaching several kilometres thickness in the west. Some deep drill holes exist to the east of the Cordillera within both the area of short-wavelength intense positive anomalies and the area further southeast, free of such anomalies. The magnetizations of basement rocks from the bottoms of the drill holes have been measured (R. A. Burwash, personal communication, 1974; R. L. Coles, unpublished data, 1975). Although sparse, the magnetization values outside the area of short-wavelength positive anomalies are lower on average than what appears to be typical for shield areas, whereas within the area of short-wavelength "highs," much of the crystalline basement is highly magnetic.

Summary

Aeromagnetic and satellite magnetic data have been presented and compared for western Canada. Such a comparison at these geomagnetic latitudes is important because both data types are affected by fields from external (ionospheric and magnetospheric) sources. Such external fields are particularly troublesome to the satellite data where, even after careful data selection, external fields are undoubtedly present on most data passes. The close agreement between the two data types indicates that it is possible to extract the anomaly "signal" from the satellite data and that the anomalies so defined are indeed crustal in origin. We believe it is now possible to proceed in confidence with the derivation and interpretation of satellite anomaly maps in all parts of the globe.

Both averaging of satellite data and upward continuation of aeromagnetic data serve to filter out details in the field. For aeromagnetic data this is not a problem since one can compare with results for lower altitudes. Derivation of an equivalent source representation of the satellite data preserves most of the information content of the data, as is apparent from comparison of Fig. 7 and Fig. 2*a*. Broad interpretative comparison of the equivalent source field with known geologic and geophysical data has indicated that it is indeed indicative of important features in the crust and can aid in the solution of such problems as the nature and origin of the Alpha ridge and the nature of the crystalline basement underlying sedimentary cover.

Acknowledgements

We would like to thank M. K. Hutchinson, R. Horner, D. Love, and B. Draper for their efforts in data preparation and display, and G. V. Haines and G. D. Mead for valuable discussion and review of the manuscript.

BARRACLOUGH, D. R., HARWOOD, J. M., LEATON, B. R., and MALIN, S. R. C. 1975. A model of the geomagnetic field at epoch 1975. Geophysical Journal of the Royal Astronomical Society, **43**, pp. 645–659.

BERRY, M. J. 1973. Structure of the crust and upper mantle in Canada. Tectonophysics, **20**, pp. 183–201.

BERRY, M. J., and BARR, K. G. 1971. A seismic refraction profile across the polar continental shield of the Queen Elizabeth Islands. Canadian Journal of Earth Sciences, **8**, pp. 360–374.

BHATTACHARYYA, B. K. 1977. Reduction and treatment of magnetic anomalies of crustal origin in satellite data. Journal of Geophysical Research, **82**, pp. 3379–3390.

CAIN, J. C. 1976. Introductory remarks. Abstract. EOS, Transactions of the American Geophysical Union, **57**, p. 907.

CAIN, J. C., DAVIS, W. M., and REGAN, R. D. 1974. An $N = 22$ model of the geomagnetic field. Abstract. EOS, Transactions of the American Geophysical Union, **56**, p. 1108.

CHANDRA, N. N., and CUMMING, G. L. 1972. Seismic refraction studies in western Canada. Canadian Journal of Earth Sciences, **9**, pp. 1099–1109.

CHURKIN, M. 1973. Geologic concepts of Arctic Ocean Basin. *In* Arctic geology. *Edited by* M. G. Pitcher. American Association of Petroleum Geology, Memoir 19, pp. 485–499.

COLES, R. L. 1979. Some comparisons among geomagnetic field models, observatory data and airborne magnetometer data: implications for broad scale anomaly studies over Canada. Journal of Geomagnetism and Geoelectricity, **31**, pp. 459–478.

COLES, R. L., and HAINES, G. V. 1979. Long-wavelength magnetic anomalies over Canada, using polynomial and upward continuation techniques. Journal of Geomagnetism and Geoelectricity, **31**, pp. 545–566.

COLES, R. L., HAINES, G. V., and HANNAFORD, W. 1976. Large

scale magnetic anomalies over western Canada and the Arctic: a discussion. Canadian Journal of Earth Sciences, **13**, pp. 790–802.

COLES, R. L., HANNAFORD, W., and HAINES, G. V. 1978. Magnetic anomalies and the evolution of the Arctic. *In* Arctic geophysical review. *Edited by* J. F. Sweeney. Publication of the Earth Physics Branch, Energy, Mines and Resources, Ottawa, Ont., **45**, pp. 51–66.

DELAURIER, J. M. 1978. The Alpha ridge is not a spreading centre. *In* Arctic geophysical review. *Edited by* J. F. Sweeney. Publication of the Earth Physics Branch, Energy, Mines and Resources, Ottawa, Ont., **45**, pp. 87–90.

EARDLEY, A. J. 1971. History of geologic thought on the origin of the Arctic Basin. *In* Geology of the Arctic. *Edited by* G. O. Raesh. University of Toronto Press, Toronto, Ont., pp. 223–249.

FORSYTH, D. A., MAIR, J. A., and FRASER, I. 1979. Crustal structure of the central Sverdrup basin. Canadian Journal of Earth Sciences, **16**, pp. 1581–1598.

HAINES, G. V., and HANNAFORD, W. 1972. Magnetic anomaly maps of British Columbia and the adjacent Pacific Ocean. Publication of the Earth Physics Branch, Energy, Mines and Resources, Ottawa, Ont., **42**, pp. 211–228.

——— 1974. A three-component aeromagnetic survey of the Canadian Arctic. Publication of the Earth Physics Branch, Energy, Mines and Resources, Ottawa, Ont., **44**, pp. 209–234.

——— 1976. A three-component aeromagnetic survey of Saskatchewan, Alberta, Yukon and the District of Mackenzie. Earth Physics Branch, Geomagnetic Series No. 8, Ottawa, Ont. 34 p.

HAINES, G. V., HANNAFORD, W., and RIDDIHOUGH, R. P. 1971. Magnetic anomalies over British Columbia and the adjacent Pacific Ocean. Canadian Journal of Earth Sciences, **8**, pp. 387–391.

HALL, D. H. 1974. Long-wavelength aeromagnetic anomalies and deep crustal magnetization in Manitoba and northwestern Ontario, Canada. Journal of Geophysics, **40**, pp. 403–430.

HALL, J. K. 1973. Geophysical evidence for ancient sea floor spreading from Alpha Cordillera and Mendeleyev Ridge. *In* Arctic geology. *Edited by* M. G. Pitcher. American Association of Petroleum Geology, Memoir 19, Tulsa, OK.

HANNAFORD, W., and HAINES, G. V. 1974. A three-component aeromagnetic survey of British Columbia and the adjacent Pacific Ocean. Publication of the Earth Physics Branch, Energy, Mines and Resources, Ottawa, Ont. **44**, pp. 323–379.

HERRON, E. M., DEWEY, J. F., and PITMAN, W. C., III. 1974. Plate tectonics model for the evolution of the Arctic. Geology, **2**, pp. 377–380.

International Association of Geomagnetism and Aeronomy (IAGA) DIVISION 1 STUDY GROUP 1976. International geomagnetic reference field 1975. EOS, Transactions of the American Geophysical Union, **57**, pp. 120–121.

KING, E. R., ZIETZ, I., and ALLDREDGE, L. R. 1966. Magnetic data on the structure of the central Arctic region. Geological Society of America Bulletin, **77**, pp. 619–646.

KRUTIKHOVSKAYA, Z. A., and PASHKEVICH, I. K. 1977. Magnetic model for the Earth's crust under the Ukrainian shield. Canadian Journal of Earth Sciences, **14**, pp. 2718–2728.

LANGEL, R. A. 1973. A study of high latitude magnetic disturbance. Technical Note BN-767, Institute for Fluid Dynamics and Applied Mathematics, University of Maryland, College Park, MD.

——— 1974. Near-Earth magnetic disturbance in total field at high latitudes 1. Summary of data from OGO 2, 4, and 6. Journal of Geophysical Research, **79**, pp. 2363–2371.

MAYHEW, M. A. 1978. A computer program for reduction of Pogo satellite magnetic anomaly data to common elevation and to the pole. Contract Report, NASA Contract NAS 5-41625-B.

——— 1979. Inversion of satellite magnetic anomaly data. Journal of Geophysics, **45**, pp. 119–128.

——— In preparation. Satellite-derived equivalent magnetization of the United States.

MEAD, G. D. 1979. An evaluation of recent internal field models. *In* Quantitative modeling of magnetospheric processes. *Edited by* W. P. Olson. Geophysics Monograph, **21**, pp. 110–117.

OVERTON, A. 1970. Seismic refraction surveys, western Queen Elizabeth Islands and polar continental margin. Canadian Journal of Earth Sciences, **7**, pp. 346–363.

PAKISER, L. C., and ZIETZ, I. 1965. Transcontinental crustal and upper mantle structure. Review of Geophysics, **3**, pp. 505–520.

PEDDIE, N. W., and FABIANO, E. B. 1976. A model of the geomagnetic field for 1975. Journal of Geophysical Research, **81**, pp. 2539–2542.

REGAN, R. D., and MARSH, B. D. In preparation. The Bangui anomaly: its geological origin.

REGAN, R. D., CAIN, J. C., and DAVIS, W. M. 1975. A global magnetic anomaly map. Journal of Geophysical Research, **80**, pp. 794–802.

RIDDIHOUGH, R. P., HAINES, G. V., and HANNAFORD, W. 1973. Regional magnetic anomalies of the Canadian Arctic. Canadian Journal of Earth Sciences, **10**, pp. 147–163.

SANDER, G. W., and OVERTON, A. 1965. Deep seismic refraction investigations in the Canadian Arctic archipelago. Geophysics, **30**, pp. 87–96.

SHUEY, R. T., SCHELLINGER, D. R., JOHNSON, E. H., and ALLEY, L. G. 1973. Aeromagnetics and the transition between the Colorado Plateau and the Basin Range province. Geology, **1**, pp. 107–110.

SWEENEY, J. F., COLES, R. L., DELAURIER, J. M., FORSYTH, D. A., IRVING, E., JUDGE, A., SOBCZAK, L. W., and WETMILLER, R. J. 1978. Arctic geophysical review—a summary. Publication of the Earth Physics Branch, Energy, Mines and Resources, Ottawa, Ont., **45**, pp. 101–108.

TAILLEUR, I. L. 1973. Probable rift origin of Canada Basin, Arctic Ocean. *In* Arctic geology. *Edited by* M. G. Pitcher. American Association of Petroleum Geology, Memoir 19, pp. 526–535.

TAYLOR, P. T. 1978. Low-level aeromagnetic data across the western Arctic basin. Abstract. EOS, Transactions of the American Geophysical Union, **59**, p. 268.

VOGT, P. R., and AVERY, O. E. 1974. Tectonic history of the Arctic basins: partial solutions and unsolved mysteries. *In* Marine geology and oceanography of the Arctic seas. *Edited by* Y. Hermann. Springer-Verlag, New York, NY, pp. 83–117.

VOGT, P. R., and OSTENSO, N. A. 1970. Magnetic and gravity profiles across the Alpha Cordillera and their relations to arctic sea floor spreading. Journal of Geophysical Research, **75**, pp. 4925–4937.

VOGT, P. R., TAYLOR, P. T., KOVACS, L. C., and JOHNSON, G. L. 1979. Detailed aeromagnetic investigation of the Arctic basin. Journal of Geophysical Research, **84**, pp. 1071–1089.

ZIETZ, I., KING, E. R., GEDDES, W., and LIDIAK, E. G. 1966. Crustal study of a continental strip from the Atlantic Ocean to the Rocky Mountains. Geological Society of America Bulletin, **77**, pp. 1427–1448.

Appendix

The spherical harmonic analysis used to represent the Earth's main field in this study is designated Pogo(02/72). The data set utilized in the derivation

TABLE A1. Pogo (02/72) coefficients, epoch 1960

n	m	g_n^m	h_n^m	$\dot{g}_n^m$	$\dot{h}_n^m$	n	m	g_n^m	h_n^m	$\dot{g}_n^m$	$\dot{h}_n^m$
1	0	−30456.2	0.0	23.47	0.0	9	8	10.3	4.7	−1.09	−1.09
1	1	−2180.3	5819.0	12.67	−8.84	9	9	−6.5	8.6	1.45	−1.06
2	0	−1546.2	0.0	−23.09	0.0	10	0	−2.1	0.0	0.05	0.0
2	1	2996.2	−1994.0	0.53	−4.20	10	1	−1.7	3.5	−0.14	−0.17
2	2	1605.2	203.2	−2.19	−17.71	10	2	1.5	0.3	0.05	0.07
3	0	1304.8	0.0	−2.29	0.0	10	3	−4.1	0.3	−0.05	0.17
3	1	−1982.6	−443.9	−11.86	8.18	10	4	−3.4	4.8	0.22	0.14
3	2	1305.6	222.6	−2.08	3.02	10	5	9.3	−2.7	−0.42	−0.14
3	3	886.7	−156.7	−5.50	−2.99	10	6	5.7	2.2	−0.12	−0.20
4	0	961.4	0.0	−1.11	0.0	10	7	2.8	−5.4	−0.33	0.38
4	1	811.7	136.7	−1.15	2.96	10	8	0.6	8.7	−0.04	−0.67
4	2	496.7	−276.6	−2.69	0.96	10	9	0.9	−7.0	0.39	0.91
4	3	−381.7	16.2	−1.05	0.54	10	10	4.0	−9.3	−0.48	0.63
4	4	264.5	−259.9	−2.66	−1.39	11	0	2.4	0.0	0.01	0.0
5	0	−222.7	0.0	0.89	0.0	11	1	−0.2	1.3	−0.09	0.01
5	1	358.9	11.7	0.30	0.98	11	2	−1.9	2.6	0.00	0.04
5	2	242.9	118.4	1.52	1.75	11	3	5.0	−1.8	−0.17	−0.00
5	3	−28.1	−111.4	−0.97	−2.99	11	4	−2.4	−4.2	0.20	−0.19
5	4	−140.6	−101.2	−2.37	0.84	11	5	−1.2	1.5	0.18	0.14
5	5	−95.2	119.1	4.86	−3.81	11	6	−4.0	−3.9	0.47	0.54
6	0	46.0	0.0	−0.02	0.0	11	7	3.7	−1.0	−0.28	−0.05
6	1	59.1	−9.0	0.32	−0.21	11	8	−0.0	−3.0	0.33	0.44
6	2	−0.1	−106.8	1.36	−0.46	11	9	−0.7	−5.3	−0.26	0.37
6	3	−243.2	61.5	2.83	1.28	11	10	−3.6	−3.8	0.80	0.36
6	4	−3.3	−26.5	0.58	−1.42	11	11	5.4	−8.7	−0.28	1.28
6	5	−0.1	−20.3	0.11	1.59	12	0	−0.5	0.0	−0.15	0.0
6	6	−102.1	−4.4	−1.01	0.30	12	1	0.3	1.1	−0.03	−0.08
7	0	71.1	0.0	−0.15	0.0	12	2	0.4	0.1	−0.13	0.05
7	1	−51.6	−52.9	−0.29	−1.68	12	3	0.2	1.9	−0.02	0.03
7	2	3.9	−27.3	−0.32	0.18	12	4	1.6	0.3	−0.15	−0.10
7	3	12.3	−7.2	0.28	0.11	12	5	0.4	−0.6	0.02	0.04
7	4	−39.9	1.4	1.85	1.01	12	6	0.1	0.4	−0.11	−0.02
7	5	0.9	17.6	−0.46	0.36	12	7	−2.3	−1.3	0.20	0.13
7	6	−4.0	−35.1	2.25	1.80	12	8	0.7	−1.3	−0.04	0.25
7	7	39.7	−47.5	−5.78	4.11	12	9	0.3	2.7	−0.13	−0.30
8	0	8.9	0.0	0.36	0.0	12	10	−0.5	−0.6	0.06	−0.07
8	1	3.9	11.1	0.24	−0.35	12	11	−4.4	4.8	0.44	−0.55
8	2	−4.6	−12.7	0.41	−0.20	12	12	−5.4	−4.6	0.80	0.40
8	3	−11.0	8.8	−0.01	−0.48	13	0	1.1	0.0	−0.10	0.0
8	4	−0.3	−15.4	−0.51	−0.34	13	1	0.7	1.8	−0.15	−0.23
8	5	6.2	8.1	0.04	−0.36	13	2	0.7	0.7	−0.00	−0.05
8	6	−5.5	19.6	0.34	0.14	13	3	−0.6	0.6	0.00	0.06
8	7	12.3	6.1	−0.01	−1.44	13	4	1.0	−0.3	−0.09	0.00
8	8	−6.8	−35.1	1.49	2.05	13	5	0.7	−0.7	−0.03	0.08
9	0	11.4	0.0	−0.31	0.0	13	6	0.9	0.9	−0.13	−0.19
9	1	7.8	−22.0	0.12	−0.08	13	7	−1.0	−0.2	0.10	0.09
9	2	3.4	14.7	−0.26	−0.01	13	8	0.8	0.1	−0.16	−0.10
9	3	−12.3	2.1	0.01	0.42	13	9	2.2	0.3	−0.20	0.06
9	4	17.0	1.2	−0.73	−0.51	13	10	3.5	3.6	−0.49	−0.45
9	5	1.2	−1.7	−0.22	−0.25	13	11	−1.5	6.9	0.17	−0.79
9	6	8.1	18.5	−1.15	−1.30	13	12	−8.5	−6.2	0.88	0.63
9	7	−9.1	18.2	1.70	−0.90	13	13	3.3	−11.4	−0.15	1.14

NOTE: Units are nT and nT/year.

of this field model is identical to that used for the Pogo(08/71) field model (Langel 1973, 1974) except that no data from 1970 were used in the derivation of Pogo(02/72). The fitting procedure used 47 485 data points that were fit with the coefficients given in Table A1 to a root mean square residual of 6.2 nT. The distribution of residuals is given in Table A2, and pertinent statistics relative to data from the three satellites in Table A3.

The model generation assumed a spheroidal Earth with mean radius of 6371.0 km, equatorial radius of 6378.16 km, and a flattening factor of 1/298.25.

Because it was not designed as a predictive

TABLE A2. Distribution of residuals

Range (nT)	−60 to −50	−50 to −40	−40 to −30	−30 to −20	−20 to −10	−10 to 0	0 to 10	10 to 20	20 to 30	30 to 40
Number of points	2	4	25	216	2562	19 113	23 692	1831	28	2

TABLE A3. Statistics for OGO 2, OGO 4, and OGO 6

	Number of points	RMS (nT)	Mean (nT)	Standard deviation about mean (nT)
OGO 2	12 773	5.17	0.263	5.16
OGO 4	18 431	6.80	0.088	6.80
OGO 6	16 281	6.25	−0.063	6.21

model, Pogo(02/72) does not include data from observatories to aid in determination of the secular variation. It is, however, suitable for some uses at times past 1971. Mead (1979) has recently evaluated four field models for the epoch 1973–1976, well past the time span of the data utilized to create the models. The models evaluated were Pogo(08/71), IGS/75 (Barraclough *et al.* 1975), AWC/75 (Peddie and Fabiano 1976), and IGRF 1975 (IAGA 1976). He concluded that the first three were all about equally accurate and much superior to IGRF 1975. Both AWC/75 and IGS/75 are slightly better than Pogo(08/71). An extension of Mead's result shows that Pogo(02/72) is of comparable accuracy to Pogo(08/71) for the interval 1973–1976.

Reprinted from

Canadian Journal of Earth Sciences

Réimpression du

Journal canadien des sciences de la terre

Comparisons of magnetic anomalies of lithospheric origin measured by satellite and airborne magnetometers over western Canada

R. A. LANGEL, R. L. COLES, AND M. A. MAYHEW

Volume 17 • Number 7 • 1980

Pages 876–887

National Research Council Canada

Conseil national de recherches Canada

Comparisons of magnetic anomalies of lithospheric origin measured by satellite and airborne magnetometers over western Canada[1]

R. A. LANGEL
Geophysics Branch, National Aeronautics and Space Administration, Goddard Space Flight Center, Greenbelt, MD 20771, U.S.A.
R. L. COLES
Earth Physics Branch, Department of Energy, Mines and Resources, Ottawa, Ont., Canada K1A 0Y3
AND
M. A. MAYHEW
Business and Technological Systems, Inc., Seabrook, MD 20801, U.S.A.

Received October 11, 1979
Revision accepted March 7, 1980

Crustal magnetic anomaly data from the Orbiting Geophysical Observatories 2, 4, and 6 (Pogo) satellites are compared with upward-continued aeromagnetic data between 50–85°N latitude and 220–260°E longitude. Agreement is good, both in anomaly location and in amplitude, giving confidence that it is possible to proceed with the derivation and interpretation of satellite anomaly maps in all parts of the globe. The data contain a magnetic high over the Alpha ridge suggesting continental composition and a magnetic low over the southern Canada basin and northern Canadian Arctic Islands (Sverdrup basin). The low in the Sverdrup basin corresponds to a region of high heat flow, suggesting a shallow Curie isotherm. A ridge of high field, with two distinct peaks in amplitude, is found over the northern portion of the platform deposits and a relative high is located in the central portion of the Churchill Province. No features are present to indicate a magnetic boundary between Slave and Bear Provinces, but a trend change is evident between Slave and Churchill Provinces. South of 60° latitude a broad magnetic low is located over very thick (40–50 km) crust, interpreted to be a region of low magnetization.

On compare les données recueillies par les satellites OGO 2, 4 et 6 (Pogo) sur les anomalies magnétiques dans la croûte avec un prolongement vers le haut des données aéromagnétiques situées entre les latitudes 50–85°N et les longitudes 220–260°E. L'accord est bon à la fois pour la localisation des anomalies et leur amplitude, ce qui permet d'être optimiste quant à la possibilité de procéder à la confection et à l'interprétation de cartes d'anomalies magnétiques par satellite dans toutes les parties du globe. Les données contiennent un pic magnétique sur la crête Alpha suggérant une composition continentale et une dépression magnétique sur le bassin du sud du Canada et dans les îles de l'Arctique canadien au nord (le bassin de Sverdrup). La dépression dans le bassin de Sverdrup correspond à une région de flux thermique élevé ce qui laisse supposer une isotherme de Curie à faible profondeur. Une crête de champ intense avec deux pics distincts dans l'amplitude se retrouve dans la partie nord des dépôts de plate-forme et un sommet relatif est localisé dans la portion centrale de la province de Churchill. Il n'y a rien qui indique une limite magnétique entre les provinces de l'Esclave et de l'Ours, il y a un changement évident entre les provinces de Churchill et de l'Esclave. Au sud de la latitude 60°N, on observe une vaste dépression magnétique située sur une croûte très épaisse (40–50 km) et qu'on interprète comme une région de faible aimantation.

Can. J. Earth Sci., 17, 876–887 (1980)

[Traduit par le journal]

Introduction

In recent years it has been realized that crustal magnetic anomalies exist which are of longer wavelengths than those investigated by exploration geophysicists and that these longer wavelength (greater than 50 km) anomalies are indicative of geologic and tectonic features in the deep crust (Pakiser and Zietz 1965; Zietz *et al.* 1966; Shuey *et al.* 1973; Hall 1974; Krutikhovskaya and Pashkevich 1977).

With the publication of the paper by Regan *et al.* (1975) it was demonstrated that long wavelength lithospheric anomalies could be mapped successfully from satellites. That map showed a global distribution of anomalies of about 500–3000 km scale size which were never before mapped and whose very existence was in most cases discovered for the first time. Although this map was distorted by variations in altitude over the data set and by contamination from magnetospheric fields, Regan *et al.* were able to demonstrate that the probable source of the anomalies is indeed the lithosphere.

[1]Contribution from the Earth Physics Branch No. 854.

0008-4077/80/070876-12$01.00/0

TABLE 1. Some characteristics of the Pogo orbits

Satellite	Launch date	Inclination	Perigee (km)	Apogee (km)
OGO 2 (1965 81A)	October 14, 1965	87.3°	410	1510
OGO 4 (1967 73A)	July 28, 1967	86.0°	410	910
OGO 6 (1969 51A)	June 5, 1969	82.0°	400	1100

Subsequently, Regan and Marsh (in preparation) have collected ancillary data and derived a quantitative model of an anomaly located in central Africa. Analysis techniques for this type of data are rapidly becoming available (Bhattacharyya 1977; Mayhew 1978, 1979).

While analysis of data at lower latitudes has proceeded (Regan and Marsh, in preparation; Mayhew 1979), nothing has been published dealing with anomalies measured by satellite at the higher latitudes. The reason for this is that at low latitudes the external (magnetospheric/ionospheric) fields are mainly of longer wavelength than the anomalies being mapped, and can be readily filtered from the data, thus isolating the anomaly fields. This remains true as long as data within about 3 h of local noon are not utilized. At high latitudes, however, ionospheric currents occur at all local times and are very often present even during magnetically quiet periods of time. Further, these currents result in fields of the same spatial scale as the anomalies of interest, thus complicating the problem of isolating the anomaly fields. This paper is a report on an attempt to isolate the anomaly fields at satellite altitude for such high latitudes, and in particular over that part of Canada between 50–85°N latitude and 220–260°E longitude. To gauge the success of this attempt, the resulting anomaly map is compared to aeromagnetic data upward continued to satellite altitude, 500 km.

The Satellite Data

A survey of the near-Earth magnetic field was carried out by the Polar Orbiting Geophysical Observatories (OGO 2, 4, and 6), also known as the Pogo satellites (Langel 1973, 1974). Some characteristics of the Pogo orbits are given in Table 1. Orbiting Geophysical Observatory 2 acquired data from launch until October 2, 1967; OGO 4 from launch until January 19, 1969; and OGO 6 from launch until August 29, 1970 and then sporadically until June 1971. Each satellite completed about 15 revolutions each day. Orbiting Geophysical Observatory 2 and OGO 4 acquired a data point every 0.5 s and OGO 6 every 0.288 s.

The measured magnetic field, $\boldsymbol{B}$, is the vector sum of magnetic fields from several sources. These are the main (core) field of the Earth, $\boldsymbol{M}$, the variable field due to ionospheric and magnetospheric currents, $\boldsymbol{D}$, and the field originating in the lithosphere of the Earth, $\boldsymbol{A}$. In this study the main field is represented by a spherical harmonic model, $\boldsymbol{M}_c$, of degree and order 13, designated Pogo(02/72) and described in the Appendix. It should be noted that this model is intended primarily as a representation of the main field of the Earth for the time span of the Pogo data. The degree and order were chosen on the basis of studies by Phillips (J. Phillips, personal communication, 1978), Cain *et al.* (1974), and Cain (1976), which indicate that a 13th degree and order representation is sufficient to represent the main field without unduly distorting the anomaly field. Any such choice is, of course, a compromise and no exact separation is possible.

Orbiting Geophysical Observatories 2, 4, and 6 measured the magnitude but not the direction of the field $\boldsymbol{B}$. The quantity analyzed is thus the residual field

$$\Delta B = |\boldsymbol{B}| - |\boldsymbol{M}_c|$$

This residual field contains contributions from: (1) any inaccuracy in modeling the core field $\boldsymbol{M}$ with $\boldsymbol{M}_c$, (2) the external field, $\boldsymbol{D}$, and (3) the lithospheric field, $\boldsymbol{A}$. Contributions from $\boldsymbol{D}$ are minimized by elimination of all data in which the residual field was considered to be dominantly due to $\boldsymbol{D}$. This elimination was accomplished on a pass by pass basis in two steps. (A pass is defined as a continuous set of data beginning when the satellite goes above 50° latitude and ending when it again goes below 50° on the other side of the pole.) Firstly, if the magnitude of the residual field, ΔB, exceeds 20 nT (nanotesla) at any place in the pass, the entire pass is rejected. Secondly, the remaining passes are visually intercompared to attempt to distinguish the time invariant features, the lithospheric field $|\boldsymbol{A}|$, from the time varying external field $|\boldsymbol{D}|$, and passes with significant contribution from the latter are not used in the anomaly map. A total of 271 "quiet" passes remained and were used in deriving the anomaly map. After performing these operations the internal agreement of passes which are nearly coincident geographically is substantial, which indicates the presence and reality of the crustal

anomalies. However, significant differences of wavelength more than 2000–3000 km still remain between coincident passes. This is similar to the results of Mayhew (1979) over the continental United States. His solution was to remove a polynomial function separately from each individual pass. Only passes with several thousand kilometres of data were used. This function is determined by a least squares fit to that pass. The procedure of Mayhew was followed with the data presented here except that Mayhew chose a quadratic function whereas we have chosen a linear function. The function chosen is a matter of subjective judgement. The difference between the linear and quadratic functions for these data is not substantial. We are, of course, left with an anomaly field with arbitrary zero. After the data selection and trend removal, individual residual field data points were averaged in an equal-area grid superimposed over an equal-area map of the area of interest. The grid is square and the distance along each side is equivalent to 3° of latitude. Figure 1 shows the density distribution of the data used in the averages. The resulting averaged residual anomaly map, contoured at 2 nT intervals, is shown in Fig. 2*a*. Results in the southwest portion of the map, between 220–240° longitude and 50–60°N latitude, are to be regarded with caution because of the sparseness of data as shown in Fig. 1. The residuals plotted in Fig. 2*a* are not at a common altitude but are at the altitudes determined in each block over which the data were averaged. The average altitude varies from 440–560 km, with mean near 520 km. A map reduced to common altitude is discussed later in the paper.

The anomalies range from a maximum of 14 nT at about 85° latitude to a minimum of −11 nT at 50° latitude and 239° longitude.

The Airborne Magnetometer Data

The airborne magnetic field data considered here have been acquired by the Earth Physics Branch of the Department of Energy, Mines and Resources, Ottawa, since 1969 in a series of airborne vector magnetometer surveys, each survey covering 2×10^6 to 4×10^6 km^2 at a typical altitude of 3.5 km above sea level, with excursions giving a range of 2.5–6.0 km. The instrumentation and survey details have been variously described by Haines and Hannaford (1972, 1974, 1976) and Hannaford and Haines (1974). Discussions of the data have been given by Haines *et al.* (1971), Riddihough *et al.* (1973), Coles *et al.* (1976), and Coles and Haines (1979).

The data were obtained in three separate surveys

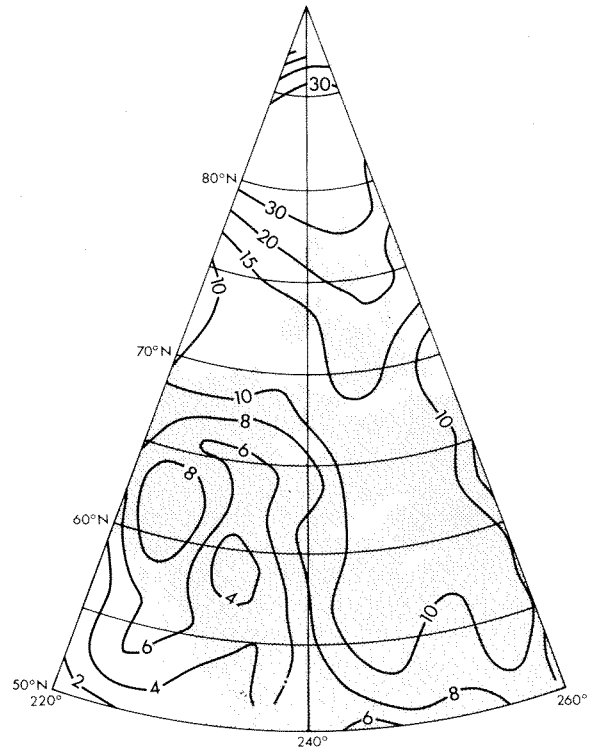

FIG. 1. Density of distribution of Pogo data, as number of points in averages.

flown at approximately 2 year intervals. In order to remove level differences due to secular change, a reference field has been removed. Coles (1979) has shown that the best available reference field models for this region and for this interval of time are based on the Pogo data. The model chosen was the Pogo(02/72) model, i.e., the same reference field used for the satellite data. Coles also demonstrated a way of correcting for inadequacies in the secular change terms of the reference model in its application to the airborne data. The residual data values are, in effect, adjusted to a single epoch. At each magnetic observatory in or near the survey region, the change in average quiet day field level from the epoch of the survey to the updated epoch is compared with the change in value of the field model between the two epochs. This comparison leads to a low-degree polynomial correction surface to be applied to the data residuals. The airborne data residuals were upward continued to 500 km in order to compare them with the satellite data. A more detailed discussion of this procedure is given by Coles and Haines (1979).

At high geomagnetic latitudes, differences between scalar and vertical component regional anomaly fields are minor (Langel 1974). The vertical

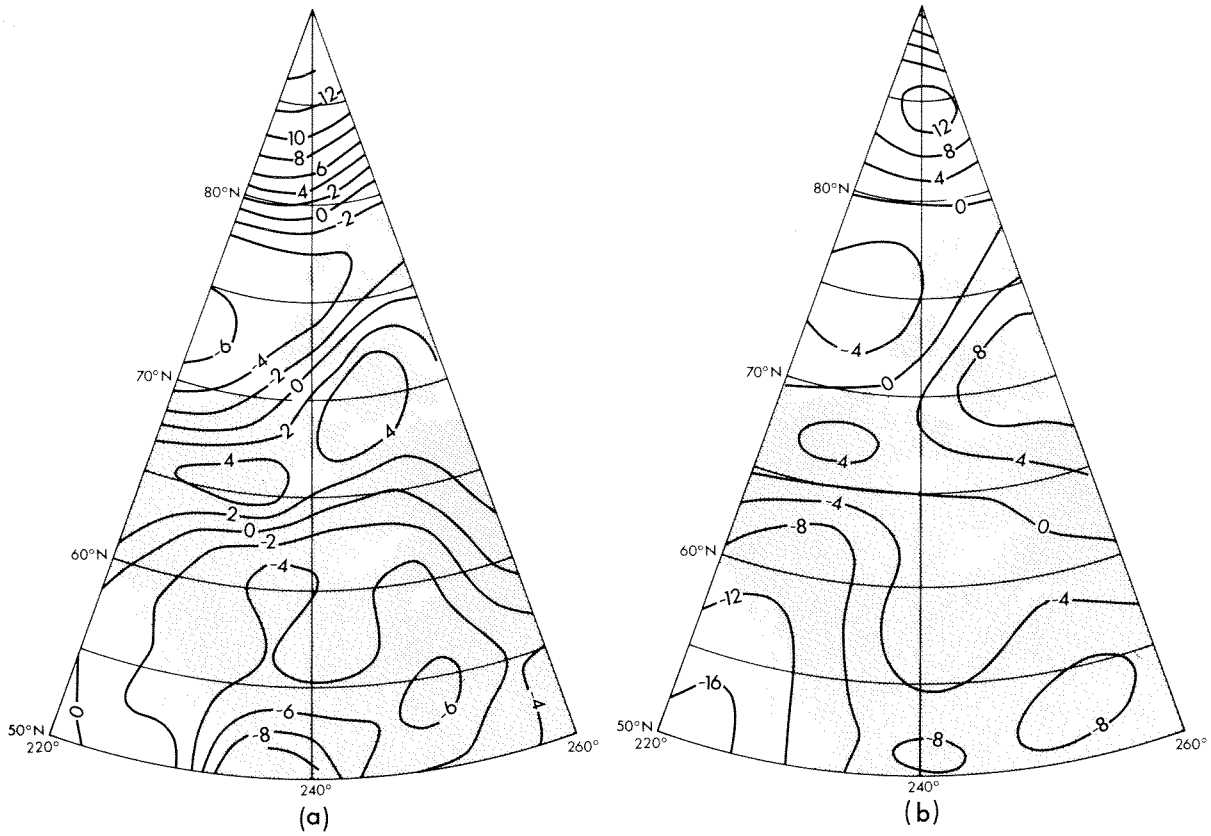

FIG. 2. Comparison of (*a*) averaged scalar magnetic anomalies from Pogo data with (*b*) upward-continued aeromagnetic vertical component anomaly data (500 km altitude).

component airborne data were used for the upward continuation because the data coverage is more complete than the scalar data coverage, and because the scalar field is not strictly harmonic. The input data to the upward continuation were in the form of averages of vertical component residuals along flight tracks over 5 min of time (about 35 km distance). The data points are shown in Fig. 3, and Fig. 4 is a contoured map prepared from the 5 min averaged data.

The data averages were each associated with an area determined by the spacing (35 km) multiplied by the mean flight-line spacing in the region of each data average. Although the original data were only along flight lines, the approximation is sufficient for the present purposes. No corrections for variations in flight altitude have been incorporated.

The basic equation for upward continuation from a sphere can be approximately represented, for the vertical component Z_p at point P, by

$$Z_p = \frac{R^2 - R_0^2}{4\Pi R} \sum \frac{Z_i}{\rho_i^3} \Delta S_i$$

where the summation is over all data points i, each associated with an area ΔS_i and field value Z_i. R is the geocentric distance to the point P, R_0 is the radius of the Earth, and ρ_i is the distance from P to the point i. The data values, Z_i, are residuals relative to the reference field. The residual field beyond the data area is assumed to be zero and, therefore, has no contribution to the summation. This is an assumption, of course, which limits the accuracy of the upward continuation. Coles and Haines (1979) discuss this point in more detail; however, the actual total contribution from distant points beyond the data area is small (less than about 2 nT for most parts of the area), since the integral of the residual field over a large region tends to zero.

The data (5600 points) have been upward continued to 100, 300, and 500 km (Figs. 5, 2*b*). As the altitude increases, the anomalies become smoother and reduced in amplitude. Broad features, however, persist through the series of figures.

Comparison of the Anomaly Maps

There is good agreement between the satellite

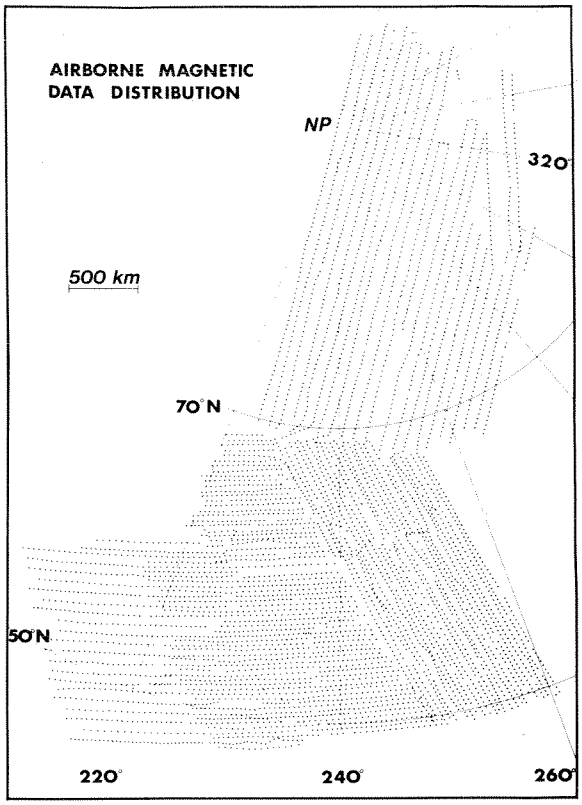

FIG. 3. Relative distribution of aeromagnetic data.

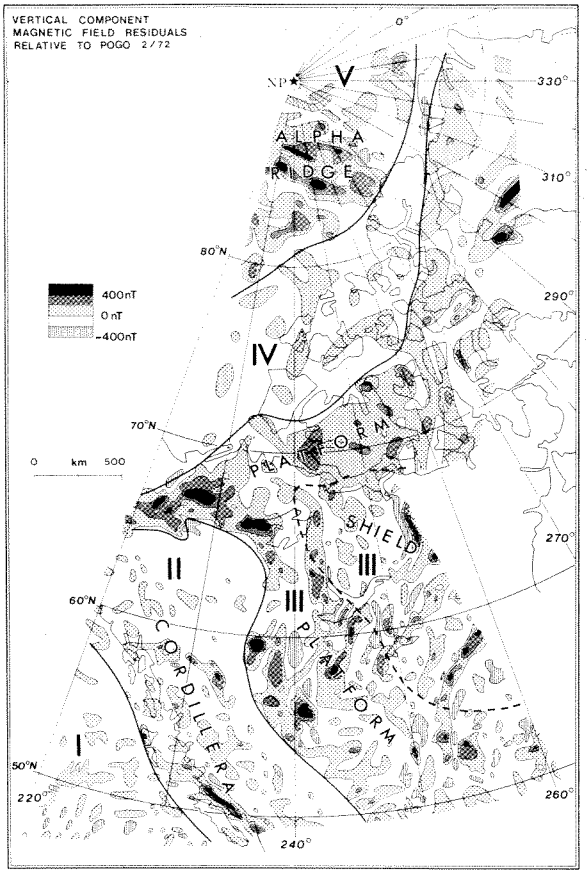

FIG. 4. Residuals of aeromagnetic data at an altitude of 3 km. Roman numerals designate regions of differing characteristics as described in the text.

and airborne data in their common spectral region. The agreement is excellent in the north, with a high anomaly north of 80°N, a low region between about 70 and 80°N, and a north-easterly trending ridge of high field centered near 65–67°N in the west and extending to about 70°N in the east. A south-trending, relatively positive area extends between 55 and 62°N at a longitude of about 240°. In the southwest the agreement is not as good, with a large gradient evident in the airborne-derived map. Nevertheless, the indications are of a relatively low field over the southwestern Cordillera region in Canada. The agreement in anomaly amplitudes is also very good, except in the southwest corner. This comparison gives a confirmation over a sub-continental size region of the reality of the anomalies derived from satellite data. This is particularly important for this region of the Earth where contaminating fields from high latitude currents are strong and it indicates that we have been successful in separating the anomaly fields from fields due to those currents.

The reason for the discrepancy in the southwest between the two maps is not clear. The method of upward continuation is not a major factor since different analyses of the original data also indicate a similar discrepancy (Coles and Haines 1979). The Pogo anomaly map is determined relative to a model also derived from Pogo data, so one would not expect trends of 10–20 nT to be present in that map. Either the available satellite data are consistently high in this region (the density of satellite passes is very low here), or the airborne data (one particular survey) are consistently low.

Effect of Model Removed

Any bias in the field model utilized to estimate the core field may be reflected as an error in anomaly maps derived by this method. This would be the case, for example, if the higher order terms of the model utilized were negatively correlated with the anomalies derived. Obviously, some error is introduced simply because the spectra of core and crustal fields overlap so that it is not possible to do a clean separation. We believe that, if anything, our results are biased by removing too much long

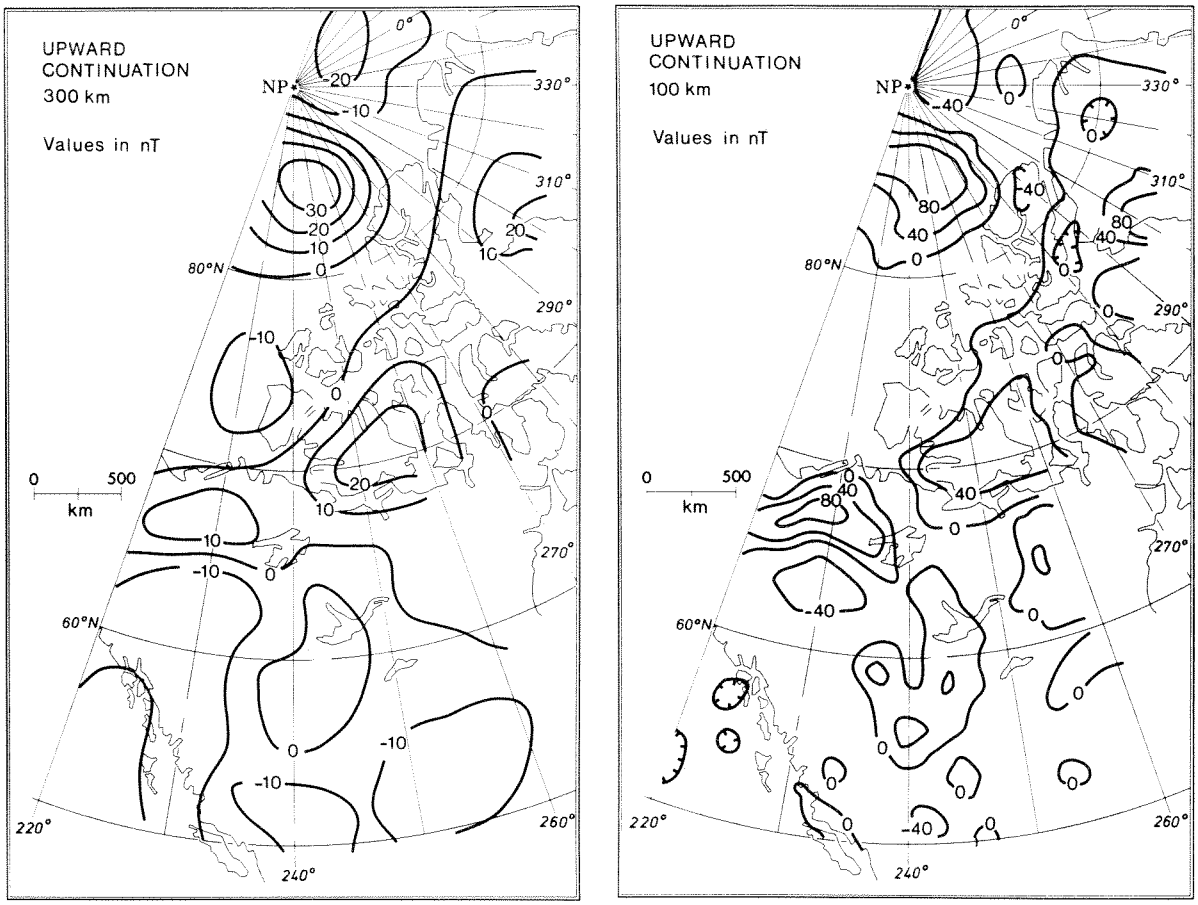

FIG. 5. Upward continuation of aeromagnetic data.

wavelength field rather than too little, because of the pass by pass linear trend removal.

We have two indications that field model biases are not significantly contaminating our results. Firstly, Coles *et al.* (1976, Fig. 2) subtracted the vertical component of the International Geomagnetic Reference Field (IGRF) from the vertical component of the Pogo(02/72) model (erroneously designated Pogo(6/71) in their paper). This difference plot shows *no* correlation with the derived anomaly maps. Secondly, we have recomputed the satellite anomaly map utilizing the Pogo(06/74) field model (Cain *et al.* 1974) which is of degree and order 22. This map is presented here as Fig. 6. Comparison with Fig. 2*a* shows that the greatest differences are in the southwest corner of the map—already noted to be suspect. All other features remain relatively unchanged except for subtle longer wavelength effects. We believe this indicates that any biases due to the degree of the field models used are negligible.

Geologic Implications

It is not our intention to present a detailed interpretation of the magnetic anomaly maps shown here. Interpretations of the aeromagnetic data have already been published (Haines *et al.* 1971; Riddihough *et al.* 1973; Coles *et al.* 1976). In this section we wish to contrast the different viewpoints offered by the aeromagnetic and satellite magnetic data and to illustrate the use of the satellite data in making geologic inferences.

Examination of Fig. 4 shows changes in the character of the anomaly patterns from region to region, often delineating geologic boundaries. Such changes are clearly apparent between the Cordillera and the platform, i.e., between regions II and III and between the platform of region III and the thick sediments, both onshore and offshore, of region IV. The character changes most evident are (1) changes from high magnetic relief to low magnetic relief and (2) changes in the trends of the anomalies. Because most of the high relief features are positive

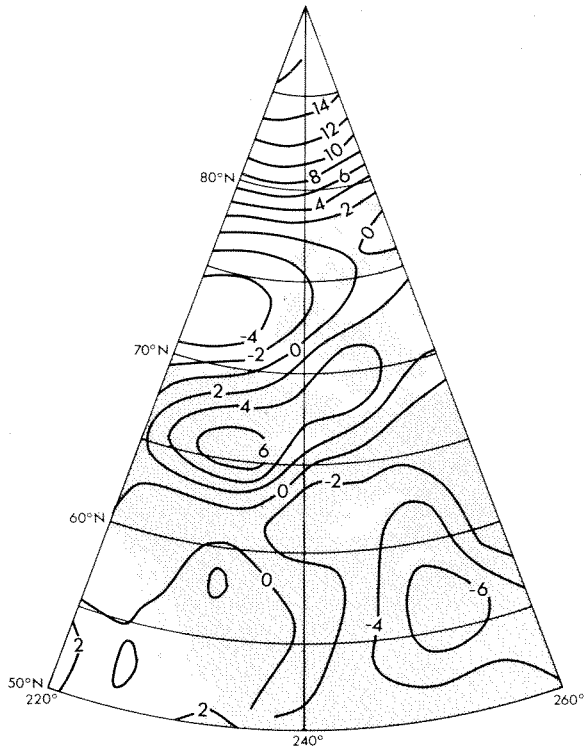

FIG. 6. Averaged magnetic anomaly map from Pogo data, using a 22nd degree spherical harmonic model to remove the core field.

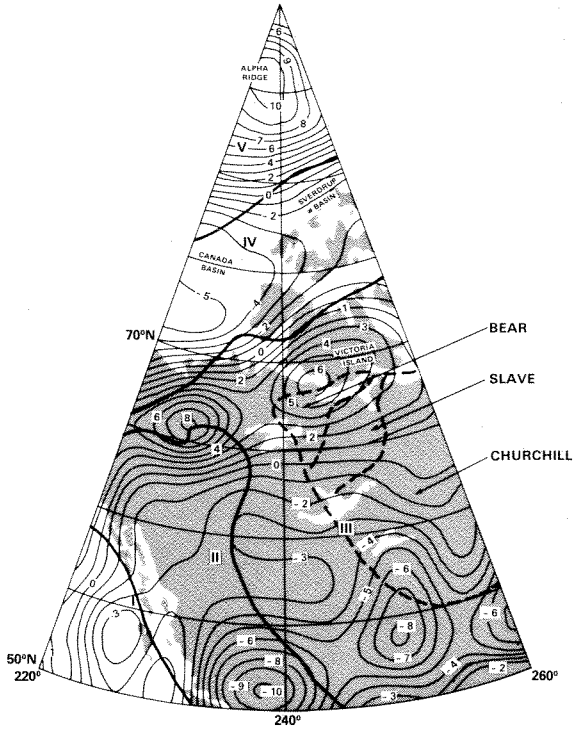

FIG. 7. Reduction of Pogo anomaly map to an altitude of 500 km using an equivalent source representation (reference field is Pogo(02/72)). The contour interval is 1 nT.

there is also an apparent contrast between regions of predominantly positive and predominantly negative fields. Figure 7 shows the satellite field, now reduced to common altitude using an equivalent source representation (Mayhew 1978, 1979). In contrast to Fig. 4, the satellite map shows only the contrasts between the predominantly positive and negative regions. The aeromagnetic data clearly contain all of the information in the satellite data and more and are able to delineate boundaries more definitively. However, the satellite map (or an upward-continued aeromagnetic map) gives a clearer picture of broad trends and can serve as a guide in discerning those same trends in the lower altitude data. In the following paragraphs we will discuss the various "regions" delineated by the satellite anomalies (Fig. 7) compared with those delineated by the aeromagnetic data (Fig. 4) and known geologic provinces.

At the very north of the map the satellite data show a prominent high of about 12 nT magnitude. This is centered on the Alpha ridge of the Arctic Basin. The airborne survey also shows a broad positive in this region but is punctuated by a complex series of intense positive anomalies nearly parallel to the trend of the ridge. These extend both north and south of the ridge and are all contained within the area of positive field as seen by Pogo. This region has also been surveyed by Vogt *et al.* (1979) who concluded that the principal magnetic anomalies in this region are topographic effects in a normally magnetized basement with high magnetization intensity (20–30 A/m). The broader picture afforded by the satellite data supports the existence of a region of highly magnetized crust and partially outlines its extent. Unfortunately, the satellite data do not extend above 87° latitude so the northern portion of this region is not mapped. The upward-continued aeromagnetic data indicate that it terminates at about 88° latitude.

The Alpha ridge has been variously interpreted as a subduction zone (Herron *et al.* 1974), as an extinct center of sea-floor spreading (Churkin 1973; Vogt and Ostenso 1970; Hall 1973; Tailleur 1973; Vogt and Avery 1974), or as subsided continental crust (Eardley 1961; King *et al.* 1966; Taylor 1978). DeLaurier (1978) rejects the hypotheses of a subduction zone or a center of sea-floor spreading on the basis of a comparison of the measured relief with the relief expected from a cooling model, because of a lack of seismic activity, and because active accretion is inconsistent with the known

marine fossils and sediment thickness. Vogt *et al.* (1979) also examine these questions and conclude that on the basis of the airborne magnetic data it is not possible to rule out any of the three hypotheses. In addition to the arguments noted above against a spreading center or subduction zone, they claim that the depth of the Alpha ridge argues against it being a subsided shield.

Taylor (1978) suggests that the Alpha ridge is an aseismic ridge similar to the Lord Howe Rise, which is continental in nature, in the southwest Pacific. In fact, the satellite data show a similar positive anomaly over the Lord Howe Rise (Regan *et al.* 1975). Coles *et al.* (1978) and Sweeney *et al.* (1978) note that the positive long-wavelength anomaly over the Alpha ridge is consistent with a region of crust of continental composition since most of the major long-wavelength positive anomalies detected by satellites are associated with continental crust, both in shield areas and in regions such as Broken Ridge in the Indian Ocean (Regan *et al.* 1975).

To the south of the Alpha ridge and its environs the satellite map shows a broad negative over the southern Canada Basin and the northern Canadian Arctic Islands. The aeromagnetic data in this region are remarkably free from shorter wavelength anomalies. Geologically, this is a region of deep (3–12 km) sediments (Sweeney *et al.* 1978) resulting in a greater depth to basement which may account for the lack of shorter wavelength anomalies in the aeromagnetic data (Riddihough *et al.* 1973). The southern 0 nT contour of this region is close to the edge of the craton but both bathymetric (Sweeney *et al.* 1978) and seismic (Sweeney *et al.* 1978; Berry and Barr 1971; Sander and Overton 1965; Overton 1970; Berry 1973) data show that the transition from continental to oceanic crust, the Canada Basin, takes place well within the region of negative anomaly. Comparison of Fig. 7 with the bathymetry (Sweeney *et al.* 1978) indicates that over much of its length the −4 nT contour nearly coincides with the continental slope. Thus, the central low of the negative anomaly is located over oceanic crust. The eastward extension of this magnetic low is over the Sverdrup basin, where refraction data (Sander and Overton 1965; Overton 1970; Forsyth *et al.* 1979) indicate sediments reaching 12 km. Forsyth *et al.* note that "Based on heat flow measurements taken in bore-holes throughout the Sverdrup Basin, A. S. Judge has estimated that maximum temperatures are 600 to 650°C at 20 km and 850 to 900°C at 30 km (personal communication)." Judge noted higher than average heat flow values for the central Sverdrup basin. Thus, the magnetite Curie isotherm is well up into a thickly sedimented crust in this region which could account for the relative negative magnetic anomaly. The cause of the negative anomaly over the Canada Basin is unknown. Future refinement of the satellite data over the rest of the Arctic will be required to see if the negative anomaly is coextensive with the entire Amerasian Basin.

An elongated region of high magnetic field (Fig. 7) is located near 65° latitude at 220°E longitude in the west and extends to 71° latitude at 260°E longitude. This "high" occurs over the northern portion of the platform deposits on the Precambrian craton and can be resolved into two maxima. In the east the positive anomaly extends southward over the northern parts of the exposed shield. Considering the two highs over the platform deposits, comparison with Fig. 4 shows positive anomalies in the aeromagnetic data in these regions but of significantly different character. In the east, over Victoria Island, there is no concentration of short-wavelength anomalies, whereas in the west, the broad positive background is punctuated by narrow regions of intense positive short-wavelength anomalies. This region of large amplitude anomalies extends around the top of region II (Fig. 4) and has been interpreted to indicate that the crystalline continental basement extends far to the west of the exposed and known buried shield (Coles *et al.* 1976). This regional difference seems to be reflected in the heat flow data (although a good thermal model is not yet available and the available data are sparse) in that the available heat flow values near the western field maximum are considerably higher than those near the eastern maximum. This difference in heat flow between two magnetic highs of nearly equal amplitude indicates that the long-wavelength anomalies, at least to the east of the Cordillera, do not correlate well with heat flow and, therefore, are not indicative of variations in the depth to the Curie isotherm. For comparison, in the United States good heat flow vs. long-wavelength anomaly correlation is evident in the tectonically active region west of the Cordillera (Mayhew, in preparation), whereas in the more stable region to the east of the Cordillera the extremely sparse heat flow data do not seem to correlate with the long-wavelength magnetic anomalies.

Just to the south of the double maximum the contour lines are relatively featureless with a northeasterly trend. In particular, no features are present marking the boundary between Bear and Slave Provinces. Below 67° latitude a trend change is evident between Slave and Churchill Provinces and, near the eastern border of the map, a relative

high extends through the central portion of the Churchill Province. This relative high is not clearly defined in the aeromagnetic data, which do not extend as far east as the satellite data.

South of about 60–63° the satellite anomaly map is everywhere negative, highly negative in some regions. The low altitude data of Fig. 4 show that large portions of this area are relatively free of large amplitude short-wavelength anomalies. A relative negative anomalous region can be caused by one or a combination of three things: very low rock magnetization, a shallow Curie isotherm, or a high reversed remanent magnetization. The latter is extremely unlikely for a geographic region of this size; reversed magnetizations for regions this size are neither expected nor found in practice. Although sparse, the existing heat flow data are at or below normal values, with no indication of a shallow Curie isotherm. Thus the crust in this region, which is 40–50 km thick (Chandra and Cumming 1972; Berry 1973), most likely has very low average rock magnetization over most of its area. The satellite data show a relative high at about 57–60° latitude and 238–241° longitude. This is reflected in the low latitude aeromagnetic data (Fig. 4) as a cluster of magnetic highs east of the Cordillera, and in fact the Cordillera is outlined by their western boundary. Most of this region of "highs" is underlain by sedimentary cratonic cover rocks, reaching several kilometres thickness in the west. Some deep drill holes exist to the east of the Cordillera within both the area of short-wavelength intense positive anomalies and the area further southeast, free of such anomalies. The magnetizations of basement rocks from the bottoms of the drill holes have been measured (R. A. Burwash, personal communication, 1974; R. L. Coles, unpublished data, 1975). Although sparse, the magnetization values outside the area of short-wavelength positive anomalies are lower on average than what appears to be typical for shield areas, whereas within the area of short-wavelength "highs," much of the crystalline basement is highly magnetic.

Summary

Aeromagnetic and satellite magnetic data have been presented and compared for western Canada. Such a comparison at these geomagnetic latitudes is important because both data types are affected by fields from external (ionospheric and magnetospheric) sources. Such external fields are particularly troublesome to the satellite data where, even after careful data selection, external fields are undoubtedly present on most data passes. The close agreement between the two data types indicates that it is possible to extract the anomaly "signal" from the satellite data and that the anomalies so defined are indeed crustal in origin. We believe it is now possible to proceed in confidence with the derivation and interpretation of satellite anomaly maps in all parts of the globe.

Both averaging of satellite data and upward continuation of aeromagnetic data serve to filter out details in the field. For aeromagnetic data this is not a problem since one can compare with results for lower altitudes. Derivation of an equivalent source representation of the satellite data preserves most of the information content of the data, as is apparent from comparison of Fig. 7 and Fig. 2*a*. Broad interpretative comparison of the equivalent source field with known geologic and geophysical data has indicated that it is indeed indicative of important features in the crust and can aid in the solution of such problems as the nature and origin of the Alpha ridge and the nature of the crystalline basement underlying sedimentary cover.

Acknowledgements

We would like to thank M. K. Hutchinson, R. Horner, D. Love, and B. Draper for their efforts in data preparation and display, and G. V. Haines and G. D. Mead for valuable discussion and review of the manuscript.

BARRACLOUGH, D. R., HARWOOD, J. M., LEATON, B. R., and MALIN, S. R. C. 1975. A model of the geomagnetic field at epoch 1975. Geophysical Journal of the Royal Astronomical Society, **43**, pp. 645–659.

BERRY, M. J. 1973. Structure of the crust and upper mantle in Canada. Tectonophysics, **20**, pp. 183–201.

BERRY, M. J., and BARR, K. G. 1971. A seismic refraction profile across the polar continental shield of the Queen Elizabeth Islands. Canadian Journal of Earth Sciences, **8**, pp. 360–374.

BHATTACHARYYA, B. K. 1977. Reduction and treatment of magnetic anomalies of crustal origin in satellite data. Journal of Geophysical Research, **82**, pp. 3379–3390.

CAIN, J. C. 1976. Introductory remarks. Abstract. EOS, Transactions of the American Geophysical Union, **57**, p. 907.

CAIN, J. C., DAVIS, W. M., and REGAN, R. D. 1974. An $N = 22$ model of the geomagnetic field. Abstract. EOS, Transactions of the American Geophysical Union, **56**, p. 1108.

CHANDRA, N. N., and CUMMING, G. L. 1972. Seismic refraction studies in western Canada. Canadian Journal of Earth Sciences, **9**, pp. 1099–1109.

CHURKIN, M. 1973. Geologic concepts of Arctic Ocean Basin. *In* Arctic geology. *Edited by* M. G. Pitcher. American Association of Petroleum Geology, Memoir 19, pp. 485–499.

COLES, R. L. 1979. Some comparisons among geomagnetic field models, observatory data and airborne magnetometer data: implications for broad scale anomaly studies over Canada. Journal of Geomagnetism and Geoelectricity, **31**, pp. 459–478.

COLES, R. L., and HAINES, G. V. 1979. Long-wavelength magnetic anomalies over Canada, using polynomial and upward continuation techniques. Journal of Geomagnetism and Geoelectricity, **31**, pp. 545–566.

COLES, R. L., HAINES, G. V., and HANNAFORD, W. 1976. Large

scale magnetic anomalies over western Canada and the Arctic: a discussion. Canadian Journal of Earth Sciences, **13**, pp. 790–802.

COLES, R. L., HANNAFORD, W., and HAINES, G. V. 1978. Magnetic anomalies and the evolution of the Arctic. *In* Arctic geophysical review. *Edited by* J. F. Sweeney. Publication of the Earth Physics Branch, Energy, Mines and Resources, Ottawa, Ont., **45**, pp. 51–66.

DELAURIER, J. M. 1978. The Alpha ridge is not a spreading centre. *In* Arctic geophysical review. *Edited by* J. F. Sweeney. Publication of the Earth Physics Branch, Energy, Mines and Resources, Ottawa, Ont., **45**, pp. 87–90.

EARDLEY, A. J. 1971. History of geologic thought on the origin of the Arctic Basin. *In* Geology of the Arctic. *Edited by* G. O. Raesh. University of Toronto Press, Toronto, Ont., pp. 223–249.

FORSYTH, D. A., MAIR, J. A., and FRASER, I. 1979. Crustal structure of the central Sverdrup basin. Canadian Journal of Earth Sciences, **16**, pp. 1581–1598.

HAINES, G. V., and HANNAFORD, W. 1972. Magnetic anomaly maps of British Columbia and the adjacent Pacific Ocean. Publication of the Earth Physics Branch, Energy, Mines and Resources, Ottawa, Ont., **42**, pp. 211–228.

——— 1974. A three-component aeromagnetic survey of the Canadian Arctic. Publication of the Earth Physics Branch, Energy, Mines and Resources, Ottawa, Ont., **44**, pp. 209–234.

——— 1976. A three-component aeromagnetic survey of Saskatchewan, Alberta, Yukon and the District of Mackenzie. Earth Physics Branch, Geomagnetic Series No. 8, Ottawa, Ont. 34 p.

HAINES, G. V., HANNAFORD, W., and RIDDIHOUGH, R. P. 1971. Magnetic anomalies over British Columbia and the adjacent Pacific Ocean. Canadian Journal of Earth Sciences, **8**, pp. 387–391.

HALL, D. H. 1974. Long-wavelength aeromagnetic anomalies and deep crustal magnetization in Manitoba and northwestern Ontario, Canada. Journal of Geophysics, **40**, pp. 403–430.

HALL, J. K. 1973. Geophysical evidence for ancient sea floor spreading from Alpha Cordillera and Mendeleyev Ridge. *In* Arctic geology. *Edited by* M. G. Pitcher. American Association of Petroleum Geology, Memoir 19, Tulsa, OK.

HANNAFORD, W., and HAINES, G. V. 1974. A three-component aeromagnetic survey of British Columbia and the adjacent Pacific Ocean. Publication of the Earth Physics Branch, Energy, Mines and Resources, Ottawa, Ont. **44**, pp. 323–379.

HERRON, E. M., DEWEY, J. F., and PITMAN, W. C., III. 1974. Plate tectonics model for the evolution of the Arctic. Geology, **2**, pp. 377–380.

International Association of Geomagnetism and Aeronomy (IAGA) DIVISION I STUDY GROUP 1976. International geomagnetic reference field 1975. EOS, Transactions of the American Geophysical Union, **57**, pp. 120–121.

KING, E. R., ZIETZ, I., and ALLDREDGE, L. R. 1966. Magnetic data on the structure of the central Arctic region. Geological Society of America Bulletin, **77**, pp. 619–646.

KRUTIKHOVSKAYA, Z. A., and PASHKEVICH, I. K. 1977. Magnetic model for the Earth's crust under the Ukrainian shield. Canadian Journal of Earth Sciences, **14**, pp. 2718–2728.

LANGEL, R. A. 1973. A study of high latitude magnetic disturbance. Technical Note BN-767, Institute for Fluid Dynamics and Applied Mathematics, University of Maryland, College Park, MD.

——— 1974. Near-Earth magnetic disturbance in total field at high latitudes 1. Summary of data from OGO 2, 4, and 6. Journal of Geophysical Research, **79**, pp. 2363–2371.

MAYHEW, M. A. 1978. A computer program for reduction of Pogo satellite magnetic anomaly data to common elevation and to the pole. Contract Report, NASA Contract NAS 5-41625-B.

——— 1979. Inversion of satellite magnetic anomaly data. Journal of Geophysics, **45**, pp. 119–128.

——— In preparation. Satellite-derived equivalent magnetization of the United States.

MEAD, G. D. 1979. An evaluation of recent internal field models. *In* Quantitative modeling of magnetospheric processes. *Edited by* W. P. Olson. Geophysics Monograph, **21**, pp. 110–117.

OVERTON, A. 1970. Seismic refraction surveys, western Queen Elizabeth Islands and polar continental margin. Canadian Journal of Earth Sciences, **7**, pp. 346–363.

PAKISER, L. C., and ZIETZ, I. 1965. Transcontinental crustal and upper mantle structure. Review of Geophysics, **3**, pp. 505–520.

PEDDIE, N. W., and FABIANO, E. B. 1976. A model of the geomagnetic field for 1975. Journal of Geophysical Research, **81**, pp. 2539–2542.

REGAN, R. D., and MARSH, B. D. In preparation. The Bangui anomaly: its geological origin.

REGAN, R. D., CAIN, J. C., and DAVIS, W. M. 1975. A global magnetic anomaly map. Journal of Geophysical Research, **80**, pp. 794–802.

RIDDIHOUGH, R. P., HAINES, G. V., and HANNAFORD, W. 1973. Regional magnetic anomalies of the Canadian Arctic. Canadian Journal of Earth Sciences, **10**, pp. 147–163.

SANDER, G. W., and OVERTON, A. 1965. Deep seismic refraction investigations in the Canadian Arctic archipelago. Geophysics, **30**, pp. 87–96.

SHUEY, R. T., SCHELLINGER, D. R., JOHNSON, E. H., and ALLEY, L. G. 1973. Aeromagnetics and the transition between the Colorado Plateau and the Basin Range province. Geology, **1**, pp. 107–110.

SWEENEY, J. F., COLES, R. L., DELAURIER, J. M., FORSYTH, D. A., IRVING, E., JUDGE, A., SOBCZAK, L. W., and WETMILLER, R. J. 1978. Arctic geophysical review—a summary. Publication of the Earth Physics Branch, Energy, Mines and Resources, Ottawa, Ont., **45**, pp. 101–108.

TAILLEUR, I. L. 1973. Probable rift origin of Canada Basin, Arctic Ocean. *In* Arctic geology. *Edited by* M. G. Pitcher. American Association of Petroleum Geology, Memoir 19, pp. 526–535.

TAYLOR, P. T. 1978. Low-level aeromagnetic data across the western Arctic basin. Abstract. EOS, Transactions of the American Geophysical Union, **59**, p. 268.

VOGT, P. R., and AVERY, O. E. 1974. Tectonic history of the Arctic basins: partial solutions and unsolved mysteries. *In* Marine geology and oceanography of the Arctic seas. *Edited by* Y. Hermann. Springer-Verlag, New York, NY, pp. 83–117.

VOGT, P. R., and OSTENSO, N. A. 1970. Magnetic and gravity profiles across the Alpha Cordillera and their relations to arctic sea floor spreading. Journal of Geophysical Research, **75**, pp. 4925–4937.

VOGT, P. R., TAYLOR, P. T., KOVACS, L. C., and JOHNSON, G. L. 1979. Detailed aeromagnetic investigation of the Arctic basin. Journal of Geophysical Research, **84**, pp. 1071–1089.

ZIETZ, I., KING, E. R., GEDDES, W., and LIDIAK, E. G. 1966. Crustal study of a continental strip from the Atlantic Ocean to the Rocky Mountains. Geological Society of America Bulletin, **77**, pp. 1427–1448.

Appendix

The spherical harmonic analysis used to represent the Earth's main field in this study is designated Pogo(02/72). The data set utilized in the derivation

TABLE A1. Pogo (02/72) coefficients, epoch 1960

n	m	g_n^m	h_n^m	$\dot{g}_n^m$	$\dot{h}_n^m$	n	m	g_n^m	h_n^m	$\dot{g}_n^m$	$\dot{h}_n^m$
1	0	−30456.2	0.0	23.47	0.0	9	8	10.3	4.7	−1.09	−1.09
1	1	−2180.3	5819.0	12.67	−8.84	9	9	−6.5	8.6	1.45	−1.06
2	0	−1546.2	0.0	−23.09	0.0	10	0	−2.1	0.0	0.05	0.0
2	1	2996.2	−1994.0	0.53	−4.20	10	1	−1.7	3.5	−0.14	−0.17
2	2	1605.2	203.2	−2.19	−17.71	10	2	1.5	0.3	0.05	0.07
3	0	1304.8	0.0	−2.29	0.0	10	3	−4.1	0.3	−0.05	0.17
3	1	−1982.6	−443.9	−11.86	8.18	10	4	−3.4	4.8	0.22	0.14
3	2	1305.6	222.6	−2.08	3.02	10	5	9.3	−2.7	−0.42	−0.14
3	3	886.7	−156.7	−5.50	−2.99	10	6	5.7	2.2	−0.12	−0.20
4	0	961.4	0.0	−1.11	0.0	10	7	2.8	−5.4	−0.33	0.38
4	1	811.7	136.7	−1.15	2.96	10	8	0.6	8.7	−0.04	−0.67
4	2	496.7	−276.6	−2.69	0.96	10	9	0.9	−7.0	0.39	0.91
4	3	−381.7	16.2	−1.05	0.54	10	10	4.0	−9.3	−0.48	0.63
4	4	264.5	−259.9	−2.66	−1.39	11	0	2.4	0.0	0.01	0.0
5	0	−222.7	0.0	0.89	0.0	11	1	−0.2	1.3	−0.09	0.01
5	1	358.9	11.7	0.30	0.98	11	2	−1.9	2.6	0.00	0.04
5	2	242.9	118.4	1.52	1.75	11	3	5.0	−1.8	−0.17	−0.00
5	3	−28.1	−111.4	−0.97	−2.99	11	4	−2.4	−4.2	0.20	−0.19
5	4	−140.6	−101.2	−2.37	0.84	11	5	−1.2	1.5	0.18	0.14
5	5	−95.2	119.1	4.86	−3.81	11	6	−4.0	−3.9	0.47	0.54
6	0	46.0	0.0	−0.02	0.0	11	7	3.7	−1.0	−0.28	−0.05
6	1	59.1	−9.0	0.32	−0.21	11	8	−0.0	−3.0	0.33	0.44
6	2	−0.1	−106.8	1.36	−0.46	11	9	−0.7	−5.3	−0.26	0.37
6	3	−243.2	61.5	2.83	1.28	11	10	−3.6	−3.8	0.80	0.36
6	4	−3.3	−26.5	0.58	−1.42	11	11	5.4	−8.7	−0.28	1.28
6	5	−0.1	−20.3	0.11	1.59	12	0	−0.5	0.0	−0.15	0.0
6	6	−102.1	−4.4	−1.01	0.30	12	1	0.3	1.1	−0.03	−0.08
7	0	71.1	0.0	−0.15	0.0	12	2	0.4	0.1	−0.13	0.05
7	1	−51.6	−52.9	−0.29	−1.68	12	3	0.2	1.9	−0.02	0.03
7	2	3.9	−27.3	−0.32	0.18	12	4	1.6	0.3	−0.15	−0.10
7	3	12.3	−7.2	0.28	0.11	12	5	0.4	−0.6	0.02	0.04
7	4	−39.9	1.4	1.85	1.01	12	6	0.1	0.4	−0.11	−0.02
7	5	0.9	17.6	−0.46	0.36	12	7	−2.3	−1.3	0.20	0.13
7	6	−4.0	−35.1	2.25	1.80	12	8	0.7	−1.3	−0.04	0.25
7	7	39.7	−47.5	−5.78	4.11	12	9	0.3	2.7	−0.13	−0.30
8	0	8.9	0.0	0.36	0.0	12	10	−0.5	−0.6	0.06	−0.07
8	1	3.9	11.1	0.24	−0.35	12	11	−4.4	4.8	0.44	−0.55
8	2	−4.6	−12.7	0.41	−0.20	12	12	−5.4	−4.6	0.80	0.40
8	3	−11.0	8.8	−0.01	−0.48	13	0	1.1	0.0	−0.10	0.0
8	4	−0.3	−15.4	−0.51	−0.34	13	1	0.7	1.8	−0.15	−0.23
8	5	6.2	8.1	0.04	−0.36	13	2	0.7	0.7	−0.00	−0.05
8	6	−5.5	19.6	0.34	0.14	13	3	−0.6	0.6	0.00	0.06
8	7	12.3	6.1	−0.01	−1.44	13	4	1.0	−0.3	−0.09	0.00
8	8	−6.8	−35.1	1.49	2.05	13	5	0.7	−0.7	−0.03	0.08
9	0	11.4	0.0	−0.31	0.0	13	6	0.9	0.9	−0.13	−0.19
9	1	7.8	−22.0	0.12	−0.08	13	7	−1.0	−0.2	0.10	0.09
9	2	3.4	14.7	−0.26	−0.01	13	8	0.8	0.1	−0.16	−0.10
9	3	−12.3	2.1	0.01	0.42	13	9	2.2	0.3	−0.20	0.06
9	4	17.0	1.2	−0.73	−0.51	13	10	3.5	3.6	−0.49	−0.45
9	5	1.2	−1.7	−0.22	−0.25	13	11	−1.5	6.9	0.17	−0.79
9	6	8.1	18.5	−1.15	−1.30	13	12	−8.5	−6.2	0.88	0.63
9	7	−9.1	18.2	1.70	−0.90	13	13	3.3	−11.4	−0.15	1.14

NOTE: Units are nT and nT/year.

of this field model is identical to that used for the Pogo(08/71) field model (Langel 1973, 1974) except that no data from 1970 were used in the derivation of Pogo(02/72). The fitting procedure used 47 485 data points that were fit with the coefficients given in Table A1 to a root mean square residual of 6.2 nT. The distribution of residuals is given in Table A2, and pertinent statistics relative to data from the three satellites in Table A3.

The model generation assumed a spheroidal Earth with mean radius of 6371.0 km, equatorial radius of 6378.16 km, and a flattening factor of 1/298.25.

Because it was not designed as a predictive

TABLE A2. Distribution of residuals

Range (nT)	−60 to −50	−50 to −40	−40 to −30	−30 to −20	−20 to −10	−10 to 0	0 to 10	10 to 20	20 to 30	30 to 40
Number of points	2	4	25	216	2562	19 113	23 692	1831	28	2

TABLE A3. Statistics for OGO 2, OGO 4, and OGO 6

	Number of points	RMS (nT)	Mean (nT)	Standard deviation about mean (nT)
OGO 2	12 773	5.17	0.263	5.16
OGO 4	18 431	6.80	0.088	6.80
OGO 6	16 281	6.25	−0.063	6.21

model, Pogo(02/72) does not include data from observatories to aid in determination of the secular variation. It is, however, suitable for some uses at times past 1971. Mead (1979) has recently evaluated four field models for the epoch 1973–1976, well past the time span of the data utilized to create the models. The models evaluated were Pogo(08/71), IGS/75 (Barraclough *et al.* 1975), AWC/75 (Peddie and Fabiano 1976), and IGRF 1975 (IAGA 1976). He concluded that the first three were all about equally accurate and much superior to IGRF 1975. Both AWC/75 and IGS/75 are slightly better than Pogo(08/71). An extension of Mead's result shows that Pogo(02/72) is of comparable accuracy to Pogo(08/71) for the interval 1973–1976.

Reprinted from

Canadian Journal of Earth Sciences

Réimpression du

Journal canadien des sciences de la terre

Comparisons of magnetic anomalies of lithospheric origin measured by satellite and airborne magnetometers over western Canada

R. A. LANGEL, R. L. COLES, AND M. A. MAYHEW

Volume 17 • Number 7 • 1980

Pages 876–887

National Research Council Canada

Conseil national de recherches Canada

Comparisons of magnetic anomalies of lithospheric origin measured by satellite and airborne magnetometers over western Canada[1]

R. A. LANGEL

Geophysics Branch, National Aeronautics and Space Administration, Goddard Space Flight Center, Greenbelt, MD 20771, U.S.A.

R. L. COLES

Earth Physics Branch, Department of Energy, Mines and Resources, Ottawa, Ont., Canada K1A 0Y3

AND

M. A. MAYHEW

Business and Technological Systems, Inc., Seabrook, MD 20801, U.S.A.

Received October 11, 1979

Revision accepted March 7, 1980

Crustal magnetic anomaly data from the Orbiting Geophysical Observatories 2, 4, and 6 (Pogo) satellites are compared with upward-continued aeromagnetic data between 50–85°N latitude and 220–260°E longitude. Agreement is good, both in anomaly location and in amplitude, giving confidence that it is possible to proceed with the derivation and interpretation of satellite anomaly maps in all parts of the globe. The data contain a magnetic high over the Alpha ridge suggesting continental composition and a magnetic low over the southern Canada basin and northern Canadian Arctic Islands (Sverdrup basin). The low in the Sverdrup basin corresponds to a region of high heat flow, suggesting a shallow Curie isotherm. A ridge of high field, with two distinct peaks in amplitude, is found over the northern portion of the platform deposits and a relative high is located in the central portion of the Churchill Province. No features are present to indicate a magnetic boundary between Slave and Bear Provinces, but a trend change is evident between Slave and Churchill Provinces. South of 60° latitude a broad magnetic low is located over very thick (40–50 km) crust, interpreted to be a region of low magnetization.

On compare les données recueillies par les satellites OGO 2, 4 et 6 (Pogo) sur les anomalies magnétiques dans la croûte avec un prolongement vers le haut des données aéromagnétiques situées entre les latitudes 50–85°N et les longitudes 220–260°E. L'accord est bon à la fois pour la localisation des anomalies et leur amplitude, ce qui permet d'être optimiste quant à la possibilité de procéder à la confection et à l'interprétation de cartes d'anomalies magnétiques par satellite dans toutes les parties du globe. Les données contiennent un pic magnétique sur la crête Alpha suggérant une composition continentale et une dépression magnétique sur le bassin du sud du Canada et dans les îles de l'Arctique canadien au nord (le bassin de Sverdrup). La dépression dans le bassin de Sverdrup correspond à une région de flux thermique élevé ce qui laisse supposer une isotherme de Curie à faible profondeur. Une crête de champ intense avec deux pics distincts dans l'amplitude se retrouve dans la partie nord des dépôts de plate-forme et un sommet relatif est localisé dans la portion centrale de la province de Churchill. Il n'y a rien qui indique une limite magnétique entre les provinces de l'Esclave et de l'Ours, il y a un changement évident entre les provinces de Churchill et de l'Esclave. Au sud de la latitude 60°N, on observe une vaste dépression magnétique située sur une croûte très épaisse (40–50 km) et qu'on interprète comme une région de faible aimantation.

[Traduit par le journal]

Can. J. Earth Sci., **17**, 876–887 (1980)

Introduction

In recent years it has been realized that crustal magnetic anomalies exist which are of longer wavelengths than those investigated by exploration geophysicists and that these longer wavelength (greater than 50 km) anomalies are indicative of geologic and tectonic features in the deep crust (Pakiser and Zietz 1965; Zietz *et al.* 1966; Shuey *et al.* 1973; Hall 1974; Krutikhovskaya and Pashkevich 1977).

With the publication of the paper by Regan *et al.* (1975) it was demonstrated that long wavelength lithospheric anomalies could be mapped successfully from satellites. That map showed a global distribution of anomalies of about 500–3000 km scale size which were never before mapped and whose very existence was in most cases discovered for the first time. Although this map was distorted by variations in altitude over the data set and by contamination from magnetospheric fields, Regan *et al.* were able to demonstrate that the probable source of the anomalies is indeed the lithosphere.

[1]Contribution from the Earth Physics Branch No. 854.

0008-4077/80/070876-12$01.00/0

TABLE 1. Some characteristics of the Pogo orbits

Satellite	Launch date	Inclination	Perigee (km)	Apogee (km)
OGO 2 (1965 81A)	October 14, 1965	87.3°	410	1510
OGO 4 (1967 73A)	July 28, 1967	86.0°	410	910
OGO 6 (1969 51A)	June 5, 1969	82.0°	400	1100

Subsequently, Regan and Marsh (in preparation) have collected ancillary data and derived a quantitative model of an anomaly located in central Africa. Analysis techniques for this type of data are rapidly becoming available (Bhattacharyya 1977; Mayhew 1978, 1979).

While analysis of data at lower latitudes has proceeded (Regan and Marsh, in preparation; Mayhew 1979), nothing has been published dealing with anomalies measured by satellite at the higher latitudes. The reason for this is that at low latitudes the external (magnetospheric/ionospheric) fields are mainly of longer wavelength than the anomalies being mapped, and can be readily filtered from the data, thus isolating the anomaly fields. This remains true as long as data within about 3 h of local noon are not utilized. At high latitudes, however, ionospheric currents occur at all local times and are very often present even during magnetically quiet periods of time. Further, these currents result in fields of the same spatial scale as the anomalies of interest, thus complicating the problem of isolating the anomaly fields. This paper is a report on an attempt to isolate the anomaly fields at satellite altitude for such high latitudes, and in particular over that part of Canada between 50–85°N latitude and 220–260°E longitude. To gauge the success of this attempt, the resulting anomaly map is compared to aeromagnetic data upward continued to satellite altitude, 500 km.

The Satellite Data

A survey of the near-Earth magnetic field was carried out by the Polar Orbiting Geophysical Observatories (OGO 2, 4, and 6), also known as the Pogo satellites (Langel 1973, 1974). Some characteristics of the Pogo orbits are given in Table 1. Orbiting Geophysical Observatory 2 acquired data from launch until October 2, 1967; OGO 4 from launch until January 19, 1969; and OGO 6 from launch until August 29, 1970 and then sporadically until June 1971. Each satellite completed about 15 revolutions each day. Orbiting Geophysical Observatory 2 and OGO 4 acquired a data point every 0.5 s and OGO 6 every 0.288 s.

The measured magnetic field, $\boldsymbol{B}$, is the vector sum of magnetic fields from several sources. These are the main (core) field of the Earth, $\boldsymbol{M}$, the variable field due to ionospheric and magnetospheric currents, $\boldsymbol{D}$, and the field originating in the lithosphere of the Earth, $\boldsymbol{A}$. In this study the main field is represented by a spherical harmonic model, $\boldsymbol{M}_c$, of degree and order 13, designated Pogo(02/72) and described in the Appendix. It should be noted that this model is intended primarily as a representation of the main field of the Earth for the time span of the Pogo data. The degree and order were chosen on the basis of studies by Phillips (J. Phillips, personal communication, 1978), Cain *et al.* (1974), and Cain (1976), which indicate that a 13th degree and order representation is sufficient to represent the main field without unduly distorting the anomaly field. Any such choice is, of course, a compromise and no exact separation is possible.

Orbiting Geophysical Observatories 2, 4, and 6 measured the magnitude but not the direction of the field $\boldsymbol{B}$. The quantity analyzed is thus the residual field

$$\Delta B = |\boldsymbol{B}| - |\boldsymbol{M}_c|$$

This residual field contains contributions from: (1) any inaccuracy in modeling the core field $\boldsymbol{M}$ with $\boldsymbol{M}_c$, (2) the external field, $\boldsymbol{D}$, and (3) the lithospheric field, $\boldsymbol{A}$. Contributions from $\boldsymbol{D}$ are minimized by elimination of all data in which the residual field was considered to be dominantly due to $\boldsymbol{D}$. This elimination was accomplished on a pass by pass basis in two steps. (A pass is defined as a continuous set of data beginning when the satellite goes above 50° latitude and ending when it again goes below 50° on the other side of the pole.) Firstly, if the magnitude of the residual field, ΔB, exceeds 20 nT (nanotesla) at any place in the pass, the entire pass is rejected. Secondly, the remaining passes are visually intercompared to attempt to distinguish the time invariant features, the lithospheric field $|\boldsymbol{A}|$, from the time varying external field $|\boldsymbol{D}|$, and passes with significant contribution from the latter are not used in the anomaly map. A total of 271 "quiet" passes remained and were used in deriving the anomaly map. After performing these operations the internal agreement of passes which are nearly coincident geographically is substantial, which indicates the presence and reality of the crustal

anomalies. However, significant differences of wavelength more than 2000–3000 km still remain between coincident passes. This is similar to the results of Mayhew (1979) over the continental United States. His solution was to remove a polynomial function separately from each individual pass. Only passes with several thousand kilometres of data were used. This function is determined by a least squares fit to that pass. The procedure of Mayhew was followed with the data presented here except that Mayhew chose a quadratic function whereas we have chosen a linear function. The function chosen is a matter of subjective judgement. The difference between the linear and quadratic functions for these data is not substantial. We are, of course, left with an anomaly field with arbitrary zero. After the data selection and trend removal, individual residual field data points were averaged in an equal-area grid superimposed over an equal-area map of the area of interest. The grid is square and the distance along each side is equivalent to 3° of latitude. Figure 1 shows the density distribution of the data used in the averages. The resulting averaged residual anomaly map, contoured at 2 nT intervals, is shown in Fig. 2*a*. Results in the southwest portion of the map, between 220–240° longitude and 50–60°N latitude, are to be regarded with caution because of the sparseness of data as shown in Fig. 1. The residuals plotted in Fig. 2*a* are not at a common altitude but are at the altitudes determined in each block over which the data were averaged. The average altitude varies from 440–560 km, with mean near 520 km. A map reduced to common altitude is discussed later in the paper.

The anomalies range from a maximum of 14 nT at about 85° latitude to a minimum of −11 nT at 50° latitude and 239° longitude.

The Airborne Magnetometer Data

The airborne magnetic field data considered here have been acquired by the Earth Physics Branch of the Department of Energy, Mines and Resources, Ottawa, since 1969 in a series of airborne vector magnetometer surveys, each survey covering 2×10^6 to 4×10^6 km^2 at a typical altitude of 3.5 km above sea level, with excursions giving a range of 2.5–6.0 km. The instrumentation and survey details have been variously described by Haines and Hannaford (1972, 1974, 1976) and Hannaford and Haines (1974). Discussions of the data have been given by Haines *et al.* (1971), Riddihough *et al.* (1973), Coles *et al.* (1976), and Coles and Haines (1979).

The data were obtained in three separate surveys

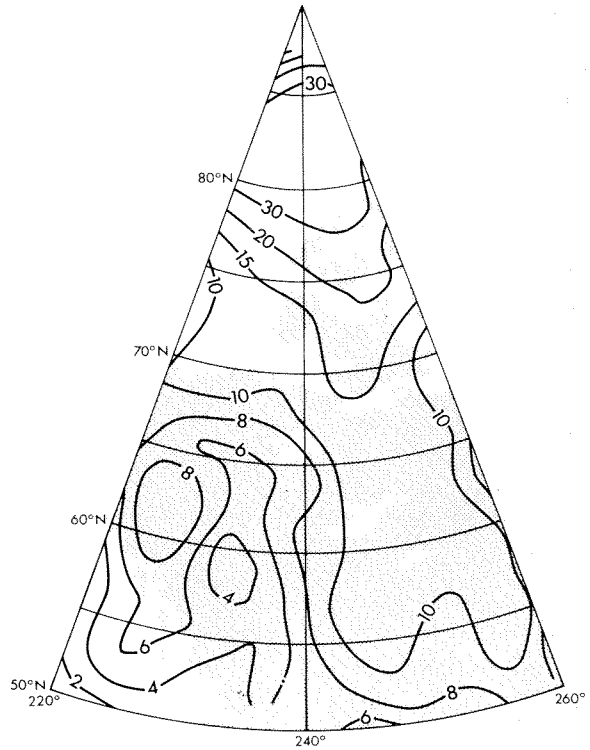

FIG. 1. Density of distribution of Pogo data, as number of points in averages.

flown at approximately 2 year intervals. In order to remove level differences due to secular change, a reference field has been removed. Coles (1979) has shown that the best available reference field models for this region and for this interval of time are based on the Pogo data. The model chosen was the Pogo(02/72) model, i.e., the same reference field used for the satellite data. Coles also demonstrated a way of correcting for inadequacies in the secular change terms of the reference model in its application to the airborne data. The residual data values are, in effect, adjusted to a single epoch. At each magnetic observatory in or near the survey region, the change in average quiet day field level from the epoch of the survey to the updated epoch is compared with the change in value of the field model between the two epochs. This comparison leads to a low-degree polynomial correction surface to be applied to the data residuals. The airborne data residuals were upward continued to 500 km in order to compare them with the satellite data. A more detailed discussion of this procedure is given by Coles and Haines (1979).

At high geomagnetic latitudes, differences between scalar and vertical component regional anomaly fields are minor (Langel 1974). The vertical

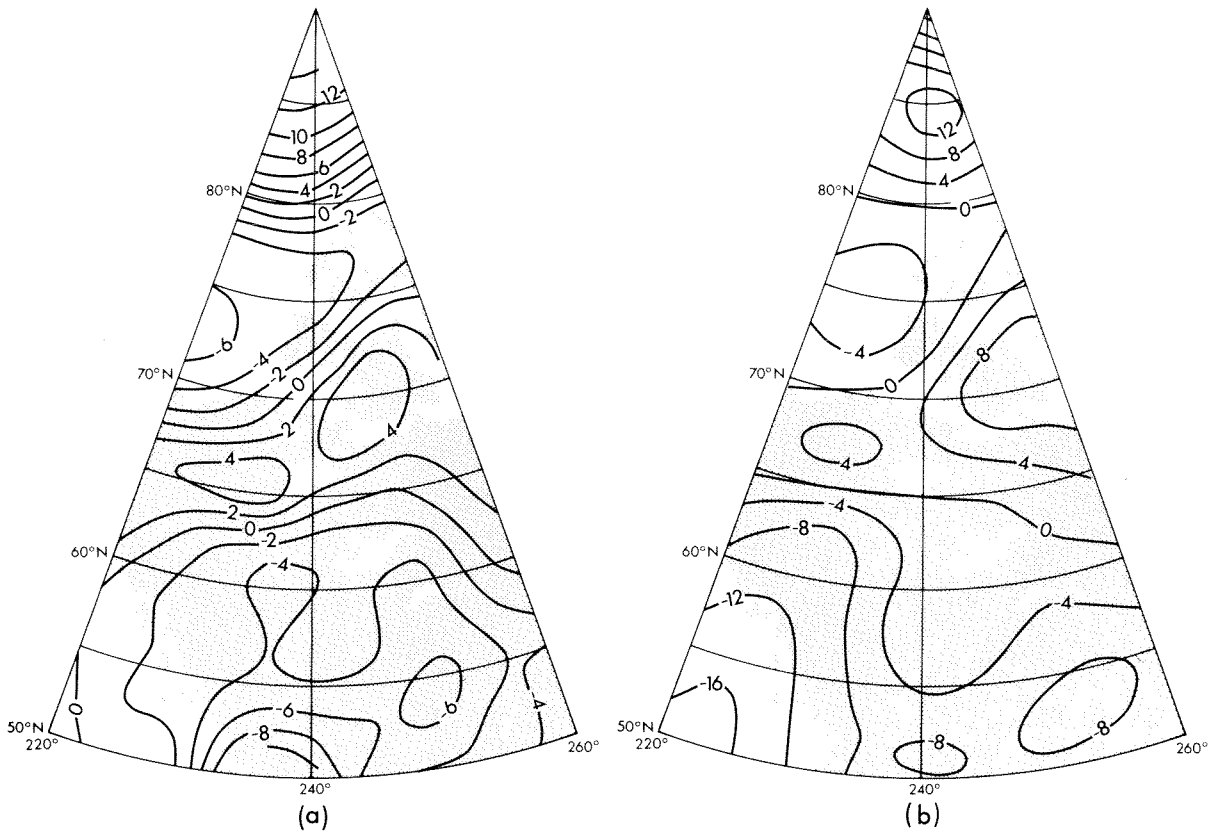

FIG. 2. Comparison of (*a*) averaged scalar magnetic anomalies from Pogo data with (*b*) upward-continued aeromagnetic vertical component anomaly data (500 km altitude).

component airborne data were used for the upward continuation because the data coverage is more complete than the scalar data coverage, and because the scalar field is not strictly harmonic. The input data to the upward continuation were in the form of averages of vertical component residuals along flight tracks over 5 min of time (about 35 km distance). The data points are shown in Fig. 3, and Fig. 4 is a contoured map prepared from the 5 min averaged data.

The data averages were each associated with an area determined by the spacing (35 km) multiplied by the mean flight-line spacing in the region of each data average. Although the original data were only along flight lines, the approximation is sufficient for the present purposes. No corrections for variations in flight altitude have been incorporated.

The basic equation for upward continuation from a sphere can be approximately represented, for the vertical component Z_p at point P, by

$$Z_p = \frac{R^2 - R_0^2}{4\Pi R} \sum \frac{Z_i}{\rho_i^3} \Delta S_i$$

where the summation is over all data points i, each associated with an area ΔS_i and field value Z_i. R is the geocentric distance to the point P, R_0 is the radius of the Earth, and ρ_i is the distance from P to the point i. The data values, Z_i, are residuals relative to the reference field. The residual field beyond the data area is assumed to be zero and, therefore, has no contribution to the summation. This is an assumption, of course, which limits the accuracy of the upward continuation. Coles and Haines (1979) discuss this point in more detail; however, the actual total contribution from distant points beyond the data area is small (less than about 2 nT for most parts of the area), since the integral of the residual field over a large region tends to zero.

The data (5600 points) have been upward continued to 100, 300, and 500 km (Figs. 5, 2*b*). As the altitude increases, the anomalies become smoother and reduced in amplitude. Broad features, however, persist through the series of figures.

Comparison of the Anomaly Maps

There is good agreement between the satellite

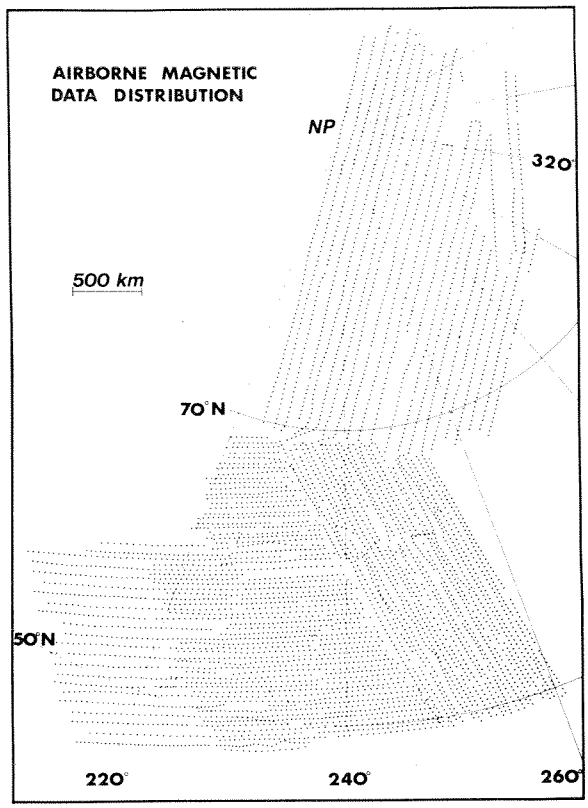

FIG. 3. Relative distribution of aeromagnetic data.

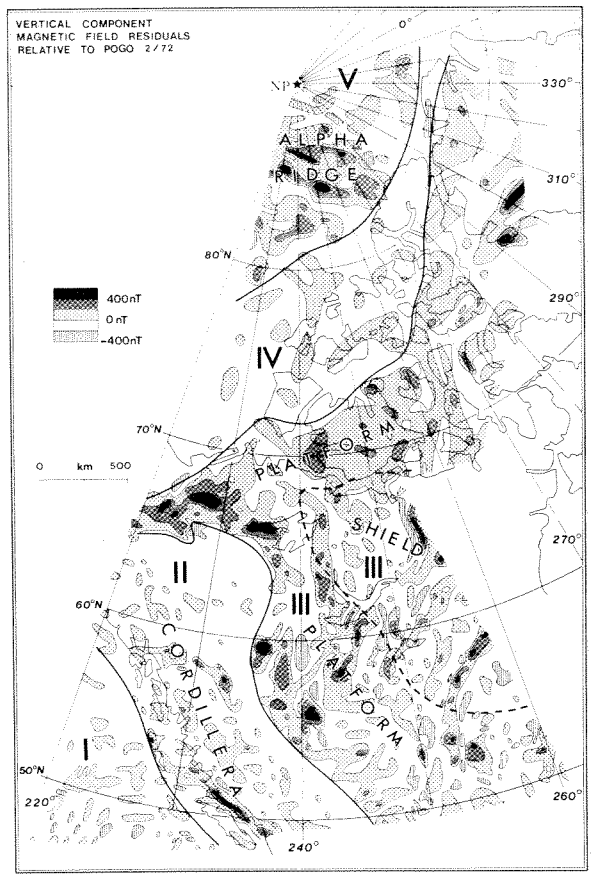

FIG. 4. Residuals of aeromagnetic data at an altitude of 3 km. Roman numerals designate regions of differing characteristics as described in the text.

and airborne data in their common spectral region. The agreement is excellent in the north, with a high anomaly north of 80°N, a low region between about 70 and 80°N, and a north-easterly trending ridge of high field centered near 65–67°N in the west and extending to about 70°N in the east. A south-trending, relatively positive area extends between 55 and 62°N at a longitude of about 240°. In the southwest the agreement is not as good, with a large gradient evident in the airborne-derived map. Nevertheless, the indications are of a relatively low field over the southwestern Cordillera region in Canada. The agreement in anomaly amplitudes is also very good, except in the southwest corner. This comparison gives a confirmation over a sub-continental size region of the reality of the anomalies derived from satellite data. This is particularly important for this region of the Earth where contaminating fields from high latitude currents are strong and it indicates that we have been successful in separating the anomaly fields from fields due to those currents.

The reason for the discrepancy in the southwest between the two maps is not clear. The method of upward continuation is not a major factor since different analyses of the original data also indicate a similar discrepancy (Coles and Haines 1979). The Pogo anomaly map is determined relative to a model also derived from Pogo data, so one would not expect trends of 10–20 nT to be present in that map. Either the available satellite data are consistently high in this region (the density of satellite passes is very low here), or the airborne data (one particular survey) are consistently low.

Effect of Model Removed

Any bias in the field model utilized to estimate the core field may be reflected as an error in anomaly maps derived by this method. This would be the case, for example, if the higher order terms of the model utilized were negatively correlated with the anomalies derived. Obviously, some error is introduced simply because the spectra of core and crustal fields overlap so that it is not possible to do a clean separation. We believe that, if anything, our results are biased by removing too much long

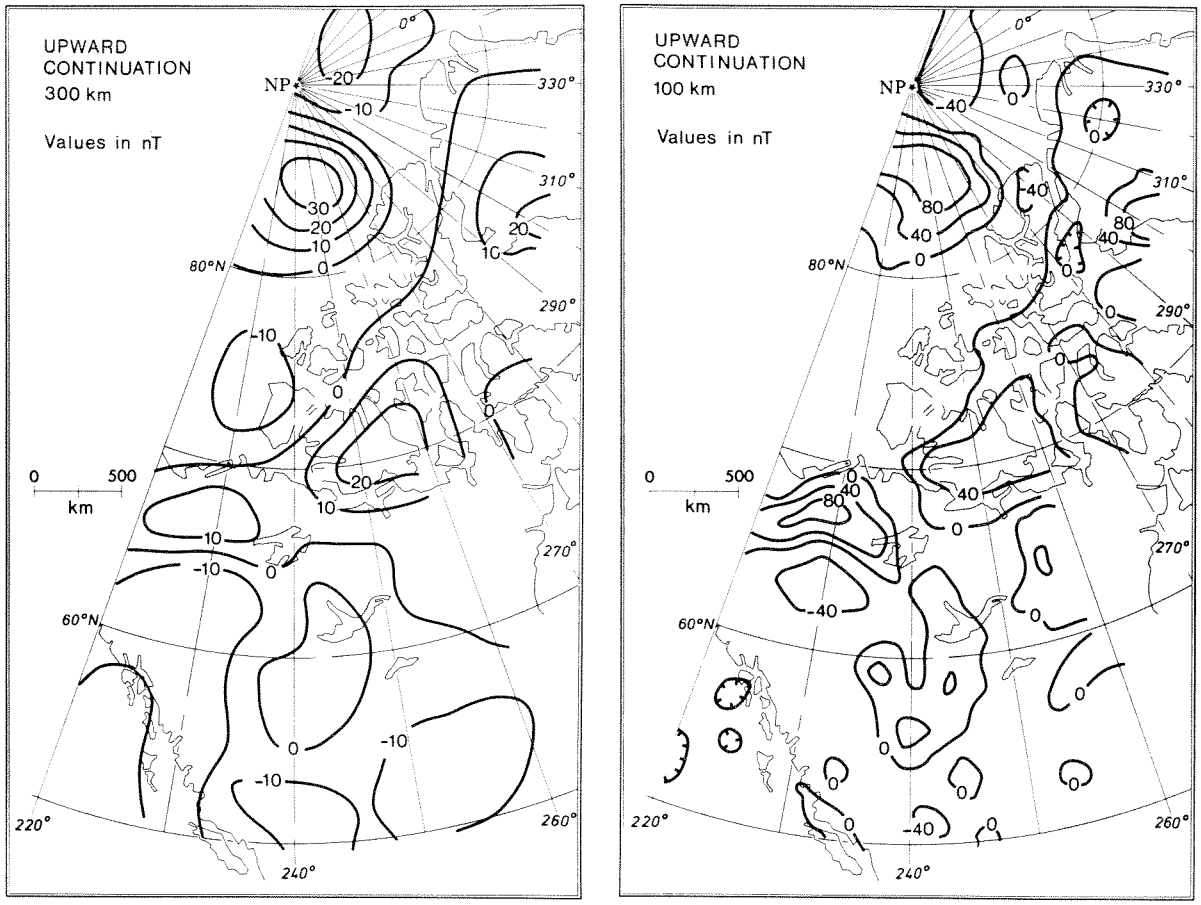

FIG. 5. Upward continuation of aeromagnetic data.

wavelength field rather than too little, because of the pass by pass linear trend removal.

We have two indications that field model biases are not significantly contaminating our results. Firstly, Coles *et al.* (1976, Fig. 2) subtracted the vertical component of the International Geomagnetic Reference Field (IGRF) from the vertical component of the Pogo(02/72) model (erroneously designated Pogo(6/71) in their paper). This difference plot shows *no* correlation with the derived anomaly maps. Secondly, we have recomputed the satellite anomaly map utilizing the Pogo(06/74) field model (Cain *et al.* 1974) which is of degree and order 22. This map is presented here as Fig. 6. Comparison with Fig. 2*a* shows that the greatest differences are in the southwest corner of the map—already noted to be suspect. All other features remain relatively unchanged except for subtle longer wavelength effects. We believe this indicates that any biases due to the degree of the field models used are negligible.

Geologic Implications

It is not our intention to present a detailed interpretation of the magnetic anomaly maps shown here. Interpretations of the aeromagnetic data have already been published (Haines *et al.* 1971; Riddihough *et al.* 1973; Coles *et al.* 1976). In this section we wish to contrast the different viewpoints offered by the aeromagnetic and satellite magnetic data and to illustrate the use of the satellite data in making geologic inferences.

Examination of Fig. 4 shows changes in the character of the anomaly patterns from region to region, often delineating geologic boundaries. Such changes are clearly apparent between the Cordillera and the platform, i.e., between regions II and III and between the platform of region III and the thick sediments, both onshore and offshore, of region IV. The character changes most evident are (1) changes from high magnetic relief to low magnetic relief and (2) changes in the trends of the anomalies. Because most of the high relief features are positive

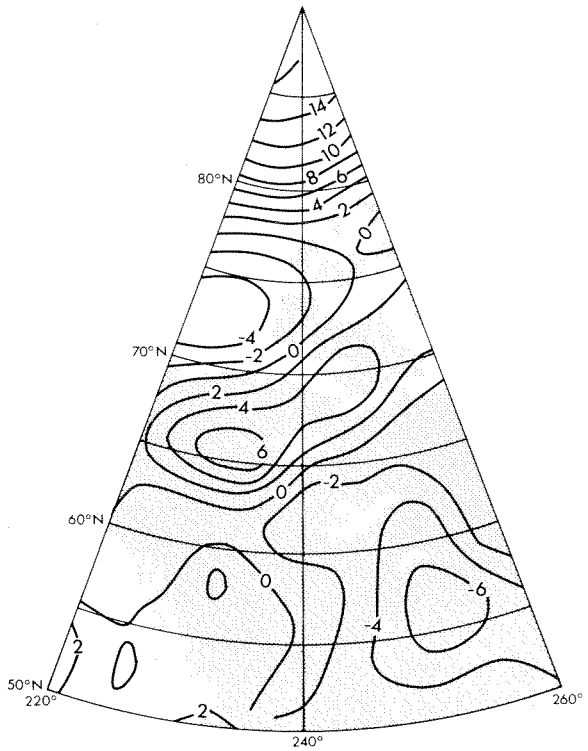

FIG. 6. Averaged magnetic anomaly map from Pogo data, using a 22nd degree spherical harmonic model to remove the core field.

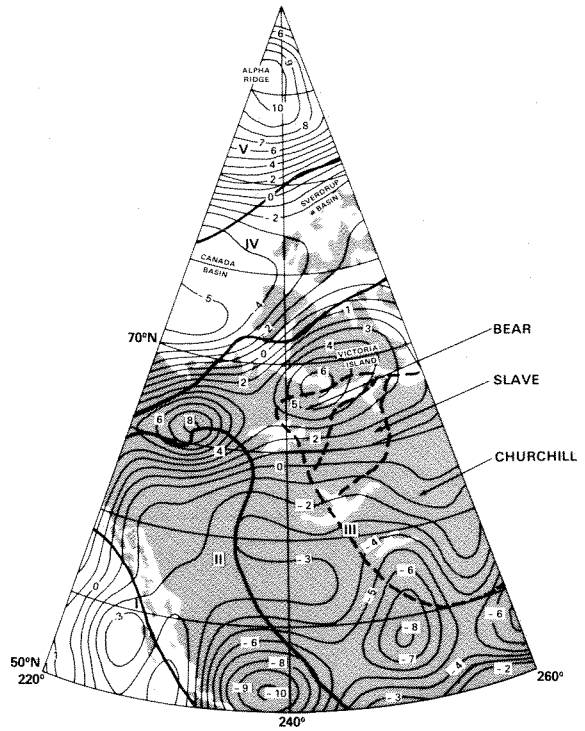

FIG. 7. Reduction of Pogo anomaly map to an altitude of 500 km using an equivalent source representation (reference field is Pogo(02/72)). The contour interval is 1 nT.

there is also an apparent contrast between regions of predominantly positive and predominantly negative fields. Figure 7 shows the satellite field, now reduced to common altitude using an equivalent source representation (Mayhew 1978, 1979). In contrast to Fig. 4, the satellite map shows only the contrasts between the predominantly positive and negative regions. The aeromagnetic data clearly contain all of the information in the satellite data and more and are able to delineate boundaries more definitively. However, the satellite map (or an upward-continued aeromagnetic map) gives a clearer picture of broad trends and can serve as a guide in discerning those same trends in the lower altitude data. In the following paragraphs we will discuss the various "regions" delineated by the satellite anomalies (Fig. 7) compared with those delineated by the aeromagnetic data (Fig. 4) and known geologic provinces.

At the very north of the map the satellite data show a prominent high of about 12 nT magnitude. This is centered on the Alpha ridge of the Arctic Basin. The airborne survey also shows a broad positive in this region but is punctuated by a complex series of intense positive anomalies nearly parallel to the trend of the ridge. These extend both north and south of the ridge and are all contained within the area of positive field as seen by Pogo. This region has also been surveyed by Vogt *et al.* (1979) who concluded that the principal magnetic anomalies in this region are topographic effects in a normally magnetized basement with high magnetization intensity (20–30 A/m). The broader picture afforded by the satellite data supports the existence of a region of highly magnetized crust and partially outlines its extent. Unfortunately, the satellite data do not extend above 87° latitude so the northern portion of this region is not mapped. The upward-continued aeromagnetic data indicate that it terminates at about 88° latitude.

The Alpha ridge has been variously interpreted as a subduction zone (Herron *et al.* 1974), as an extinct center of sea-floor spreading (Churkin 1973; Vogt and Ostenso 1970; Hall 1973; Tailleur 1973; Vogt and Avery 1974), or as subsided continental crust (Eardley 1961; King *et al.* 1966; Taylor 1978). DeLaurier (1978) rejects the hypotheses of a subduction zone or a center of sea-floor spreading on the basis of a comparison of the measured relief with the relief expected from a cooling model, because of a lack of seismic activity, and because active accretion is inconsistent with the known

marine fossils and sediment thickness. Vogt *et al.* (1979) also examine these questions and conclude that on the basis of the airborne magnetic data it is not possible to rule out any of the three hypotheses. In addition to the arguments noted above against a spreading center or subduction zone, they claim that the depth of the Alpha ridge argues against it being a subsided shield.

Taylor (1978) suggests that the Alpha ridge is an aseismic ridge similar to the Lord Howe Rise, which is continental in nature, in the southwest Pacific. In fact, the satellite data show a similar positive anomaly over the Lord Howe Rise (Regan *et al.* 1975). Coles *et al.* (1978) and Sweeney *et al.* (1978) note that the positive long-wavelength anomaly over the Alpha ridge is consistent with a region of crust of continental composition since most of the major long-wavelength positive anomalies detected by satellites are associated with continental crust, both in shield areas and in regions such as Broken Ridge in the Indian Ocean (Regan *et al.* 1975).

To the south of the Alpha ridge and its environs the satellite map shows a broad negative over the southern Canada Basin and the northern Canadian Arctic Islands. The aeromagnetic data in this region are remarkably free from shorter wavelength anomalies. Geologically, this is a region of deep (3–12 km) sediments (Sweeney *et al.* 1978) resulting in a greater depth to basement which may account for the lack of shorter wavelength anomalies in the aeromagnetic data (Riddihough *et al.* 1973). The southern 0 nT contour of this region is close to the edge of the craton but both bathymetric (Sweeney *et al.* 1978) and seismic (Sweeney *et al.* 1978; Berry and Barr 1971; Sander and Overton 1965; Overton 1970; Berry 1973) data show that the transition from continental to oceanic crust, the Canada Basin, takes place well within the region of negative anomaly. Comparison of Fig. 7 with the bathymetry (Sweeney *et al.* 1978) indicates that over much of its length the −4 nT contour nearly coincides with the continental slope. Thus, the central low of the negative anomaly is located over oceanic crust. The eastward extension of this magnetic low is over the Sverdrup basin, where refraction data (Sander and Overton 1965; Overton 1970; Forsyth *et al.* 1979) indicate sediments reaching 12 km. Forsyth *et al.* note that "Based on heat flow measurements taken in bore-holes throughout the Sverdrup Basin, A. S. Judge has estimated that maximum temperatures are 600 to 650°C at 20 km and 850 to 900°C at 30 km (personal communication)." Judge noted higher than average heat flow values for the central Sverdrup basin. Thus, the magnetite Curie isotherm is well up into a thickly sedimented crust in this region which could account for the relative negative magnetic anomaly. The cause of the negative anomaly over the Canada Basin is unknown. Future refinement of the satellite data over the rest of the Arctic will be required to see if the negative anomaly is coextensive with the entire Amerasian Basin.

An elongated region of high magnetic field (Fig. 7) is located near 65° latitude at 220°E longitude in the west and extends to 71° latitude at 260°E longitude. This "high" occurs over the northern portion of the platform deposits on the Precambrian craton and can be resolved into two maxima. In the east the positive anomaly extends southward over the northern parts of the exposed shield. Considering the two highs over the platform deposits, comparison with Fig. 4 shows positive anomalies in the aeromagnetic data in these regions but of significantly different character. In the east, over Victoria Island, there is no concentration of short-wavelength anomalies, whereas in the west, the broad positive background is punctuated by narrow regions of intense positive short-wavelength anomalies. This region of large amplitude anomalies extends around the top of region II (Fig. 4) and has been interpreted to indicate that the crystalline continental basement extends far to the west of the exposed and known buried shield (Coles *et al.* 1976). This regional difference seems to be reflected in the heat flow data (although a good thermal model is not yet available and the available data are sparse) in that the available heat flow values near the western field maximum are considerably higher than those near the eastern maximum. This difference in heat flow between two magnetic highs of nearly equal amplitude indicates that the long-wavelength anomalies, at least to the east of the Cordillera, do not correlate well with heat flow and, therefore, are not indicative of variations in the depth to the Curie isotherm. For comparison, in the United States good heat flow vs. long-wavelength anomaly correlation is evident in the tectonically active region west of the Cordillera (Mayhew, in preparation), whereas in the more stable region to the east of the Cordillera the extremely sparse heat flow data do not seem to correlate with the long-wavelength magnetic anomalies.

Just to the south of the double maximum the contour lines are relatively featureless with a northeasterly trend. In particular, no features are present marking the boundary between Bear and Slave Provinces. Below 67° latitude a trend change is evident between Slave and Churchill Provinces and, near the eastern border of the map, a relative

high extends through the central portion of the Churchill Province. This relative high is not clearly defined in the aeromagnetic data, which do not extend as far east as the satellite data.

South of about 60–63° the satellite anomaly map is everywhere negative, highly negative in some regions. The low altitude data of Fig. 4 show that large portions of this area are relatively free of large amplitude short-wavelength anomalies. A relative negative anomalous region can be caused by one or a combination of three things: very low rock magnetization, a shallow Curie isotherm, or a high reversed remanent magnetization. The latter is extremely unlikely for a geographic region of this size; reversed magnetizations for regions this size are neither expected nor found in practice. Although sparse, the existing heat flow data are at or below normal values, with no indication of a shallow Curie isotherm. Thus the crust in this region, which is 40–50 km thick (Chandra and Cumming 1972; Berry 1973), most likely has very low average rock magnetization over most of its area. The satellite data show a relative high at about 57–60° latitude and 238–241° longitude. This is reflected in the low latitude aeromagnetic data (Fig. 4) as a cluster of magnetic highs east of the Cordillera, and in fact the Cordillera is outlined by their western boundary. Most of this region of "highs" is underlain by sedimentary cratonic cover rocks, reaching several kilometres thickness in the west. Some deep drill holes exist to the east of the Cordillera within both the area of short-wavelength intense positive anomalies and the area further southeast, free of such anomalies. The magnetizations of basement rocks from the bottoms of the drill holes have been measured (R. A. Burwash, personal communication, 1974; R. L. Coles, unpublished data, 1975). Although sparse, the magnetization values outside the area of short-wavelength positive anomalies are lower on average than what appears to be typical for shield areas, whereas within the area of short-wavelength "highs," much of the crystalline basement is highly magnetic.

Summary

Aeromagnetic and satellite magnetic data have been presented and compared for western Canada. Such a comparison at these geomagnetic latitudes is important because both data types are affected by fields from external (ionospheric and magnetospheric) sources. Such external fields are particularly troublesome to the satellite data where, even after careful data selection, external fields are undoubtedly present on most data passes. The close agreement between the two data types indicates that it is possible to extract the anomaly "signal" from the satellite data and that the anomalies so defined are indeed crustal in origin. We believe it is now possible to proceed in confidence with the derivation and interpretation of satellite anomaly maps in all parts of the globe.

Both averaging of satellite data and upward continuation of aeromagnetic data serve to filter out details in the field. For aeromagnetic data this is not a problem since one can compare with results for lower altitudes. Derivation of an equivalent source representation of the satellite data preserves most of the information content of the data, as is apparent from comparison of Fig. 7 and Fig. 2*a*. Broad interpretative comparison of the equivalent source field with known geologic and geophysical data has indicated that it is indeed indicative of important features in the crust and can aid in the solution of such problems as the nature and origin of the Alpha ridge and the nature of the crystalline basement underlying sedimentary cover.

Acknowledgements

We would like to thank M. K. Hutchinson, R. Horner, D. Love, and B. Draper for their efforts in data preparation and display, and G. V. Haines and G. D. Mead for valuable discussion and review of the manuscript.

BARRACLOUGH, D. R., HARWOOD, J. M., LEATON, B. R., and MALIN, S. R. C. 1975. A model of the geomagnetic field at epoch 1975. Geophysical Journal of the Royal Astronomical Society, **43**, pp. 645–659.

BERRY, M. J. 1973. Structure of the crust and upper mantle in Canada. Tectonophysics, **20**, pp. 183–201.

BERRY, M. J., and BARR, K. G. 1971. A seismic refraction profile across the polar continental shield of the Queen Elizabeth Islands. Canadian Journal of Earth Sciences, **8**, pp. 360–374.

BHATTACHARYYA, B. K. 1977. Reduction and treatment of magnetic anomalies of crustal origin in satellite data. Journal of Geophysical Research, **82**, pp. 3379–3390.

CAIN, J. C. 1976. Introductory remarks. Abstract. EOS, Transactions of the American Geophysical Union, **57**, p. 907.

CAIN, J. C., DAVIS, W. M., and REGAN, R. D. 1974. An $N = 22$ model of the geomagnetic field. Abstract. EOS, Transactions of the American Geophysical Union, **56**, p. 1108.

CHANDRA, N. N., and CUMMING, G. L. 1972. Seismic refraction studies in western Canada. Canadian Journal of Earth Sciences, **9**, pp. 1099–1109.

CHURKIN, M. 1973. Geologic concepts of Arctic Ocean Basin. *In* Arctic geology. *Edited by* M. G. Pitcher. American Association of Petroleum Geology, Memoir 19, pp. 485–499.

COLES, R. L. 1979. Some comparisons among geomagnetic field models, observatory data and airborne magnetometer data: implications for broad scale anomaly studies over Canada. Journal of Geomagnetism and Geoelectricity, **31**, pp. 459–478.

COLES, R. L., and HAINES, G. V. 1979. Long-wavelength magnetic anomalies over Canada, using polynomial and upward continuation techniques. Journal of Geomagnetism and Geoelectricity, **31**, pp. 545–566.

COLES, R. L., HAINES, G. V., and HANNAFORD, W. 1976. Large

scale magnetic anomalies over western Canada and the Arctic: a discussion. Canadian Journal of Earth Sciences, **13**, pp. 790–802.

COLES, R. L., HANNAFORD, W., and HAINES, G. V. 1978. Magnetic anomalies and the evolution of the Arctic. *In* Arctic geophysical review. *Edited by* J. F. Sweeney. Publication of the Earth Physics Branch, Energy, Mines and Resources, Ottawa, Ont., **45**, pp. 51–66.

DELAURIER, J. M. 1978. The Alpha ridge is not a spreading centre. *In* Arctic geophysical review. *Edited by* J. F. Sweeney. Publication of the Earth Physics Branch, Energy, Mines and Resources, Ottawa, Ont., **45**, pp. 87–90.

EARDLEY, A. J. 1971. History of geologic thought on the origin of the Arctic Basin. *In* Geology of the Arctic. *Edited by* G. O. Raesh. University of Toronto Press, Toronto, Ont., pp. 223–249.

FORSYTH, D. A., MAIR, J. A., and FRASER, I. 1979. Crustal structure of the central Sverdrup basin. Canadian Journal of Earth Sciences, **16**, pp. 1581–1598.

HAINES, G. V., and HANNAFORD, W. 1972. Magnetic anomaly maps of British Columbia and the adjacent Pacific Ocean. Publication of the Earth Physics Branch, Energy, Mines and Resources, Ottawa, Ont., **42**, pp. 211–228.

——— 1974. A three-component aeromagnetic survey of the Canadian Arctic. Publication of the Earth Physics Branch, Energy, Mines and Resources, Ottawa, Ont., **44**, pp. 209–234.

——— 1976. A three-component aeromagnetic survey of Saskatchewan, Alberta, Yukon and the District of Mackenzie. Earth Physics Branch, Geomagnetic Series No. 8, Ottawa, Ont. 34 p.

HAINES, G. V., HANNAFORD, W., and RIDDIHOUGH, R. P. 1971. Magnetic anomalies over British Columbia and the adjacent Pacific Ocean. Canadian Journal of Earth Sciences, **8**, pp. 387–391.

HALL, D. H. 1974. Long-wavelength aeromagnetic anomalies and deep crustal magnetization in Manitoba and northwestern Ontario, Canada. Journal of Geophysics, **40**, pp. 403–430.

HALL, J. K. 1973. Geophysical evidence for ancient sea floor spreading from Alpha Cordillera and Mendeleyev Ridge. *In* Arctic geology. *Edited by* M. G. Pitcher. American Association of Petroleum Geology, Memoir 19, Tulsa, OK.

HANNAFORD, W., and HAINES, G. V. 1974. A three-component aeromagnetic survey of British Columbia and the adjacent Pacific Ocean. Publication of the Earth Physics Branch, Energy, Mines and Resources, Ottawa, Ont. **44**, pp. 323–379.

HERRON, E. M., DEWEY, J. F., and PITMAN, W. C., III. 1974. Plate tectonics model for the evolution of the Arctic. Geology, **2**, pp. 377–380.

International Association of Geomagnetism and Aeronomy (IAGA) DIVISION I STUDY GROUP 1976. International geomagnetic reference field 1975. EOS, Transactions of the American Geophysical Union, **57**, pp. 120–121.

KING, E. R., ZIETZ, I., and ALLDREDGE, L. R. 1966. Magnetic data on the structure of the central Arctic region. Geological Society of America Bulletin, **77**, pp. 619–646.

KRUTIKHOVSKAYA, Z. A., and PASHKEVICH, I. K. 1977. Magnetic model for the Earth's crust under the Ukrainian shield. Canadian Journal of Earth Sciences, **14**, pp. 2718–2728.

LANGEL, R. A. 1973. A study of high latitude magnetic disturbance. Technical Note BN-767, Institute for Fluid Dynamics and Applied Mathematics, University of Maryland, College Park, MD.

——— 1974. Near-Earth magnetic disturbance in total field at high latitudes 1. Summary of data from OGO 2, 4, and 6. Journal of Geophysical Research, **79**, pp. 2363–2371.

MAYHEW, M. A. 1978. A computer program for reduction of Pogo satellite magnetic anomaly data to common elevation and to the pole. Contract Report, NASA Contract NAS 5-41625-B.

——— 1979. Inversion of satellite magnetic anomaly data. Journal of Geophysics, **45**, pp. 119–128.

——— In preparation. Satellite-derived equivalent magnetization of the United States.

MEAD, G. D. 1979. An evaluation of recent internal field models. *In* Quantitative modeling of magnetospheric processes. *Edited by* W. P. Olson. Geophysics Monograph, **21**, pp. 110–117.

OVERTON, A. 1970. Seismic refraction surveys, western Queen Elizabeth Islands and polar continental margin. Canadian Journal of Earth Sciences, **7**, pp. 346–363.

PAKISER, L. C., and ZIETZ, I. 1965. Transcontinental crustal and upper mantle structure. Review of Geophysics, **3**, pp. 505–520.

PEDDIE, N. W., and FABIANO, E. B. 1976. A model of the geomagnetic field for 1975. Journal of Geophysical Research, **81**, pp. 2539–2542.

REGAN, R. D., and MARSH, B. D. In preparation. The Bangui anomaly: its geological origin.

REGAN, R. D., CAIN, J. C., and DAVIS, W. M. 1975. A global magnetic anomaly map. Journal of Geophysical Research, **80**, pp. 794–802.

RIDDIHOUGH, R. P., HAINES, G. V., and HANNAFORD, W. 1973. Regional magnetic anomalies of the Canadian Arctic. Canadian Journal of Earth Sciences, **10**, pp. 147–163.

SANDER, G. W., and OVERTON, A. 1965. Deep seismic refraction investigations in the Canadian Arctic archipelago. Geophysics, **30**, pp. 87–96.

SHUEY, R. T., SCHELLINGER, D. R., JOHNSON, E. H., and ALLEY, L. G. 1973. Aeromagnetics and the transition between the Colorado Plateau and the Basin Range province. Geology, **1**, pp. 107–110.

SWEENEY, J. F., COLES, R. L., DELAURIER, J. M., FORSYTH, D. A., IRVING, E., JUDGE, A., SOBCZAK, L. W., and WETMILLER, R. J. 1978. Arctic geophysical review—a summary. Publication of the Earth Physics Branch, Energy, Mines and Resources, Ottawa, Ont., **45**, pp. 101–108.

TAILLEUR, I. L. 1973. Probable rift origin of Canada Basin, Arctic Ocean. *In* Arctic geology. *Edited by* M. G. Pitcher. American Association of Petroleum Geology, Memoir 19, pp. 526–535.

TAYLOR, P. T. 1978. Low-level aeromagnetic data across the western Arctic basin. Abstract. EOS, Transactions of the American Geophysical Union, **59**, p. 268.

VOGT, P. R., and AVERY, O. E. 1974. Tectonic history of the Arctic basins: partial solutions and unsolved mysteries. *In* Marine geology and oceanography of the Arctic seas. *Edited by* Y. Hermann. Springer-Verlag, New York, NY, pp. 83–117.

VOGT, P. R., and OSTENSO, N. A. 1970. Magnetic and gravity profiles across the Alpha Cordillera and their relations to arctic sea floor spreading. Journal of Geophysical Research, **75**, pp. 4925–4937.

VOGT, P. R., TAYLOR, P. T., KOVACS, L. C., and JOHNSON, G. L. 1979. Detailed aeromagnetic investigation of the Arctic basin. Journal of Geophysical Research, **84**, pp. 1071–1089.

ZIETZ, I., KING, E. R., GEDDES, W., and LIDIAK, E. G. 1966. Crustal study of a continental strip from the Atlantic Ocean to the Rocky Mountains. Geological Society of America Bulletin, **77**, pp. 1427–1448.

Appendix

The spherical harmonic analysis used to represent the Earth's main field in this study is designated Pogo(02/72). The data set utilized in the derivation

TABLE A1. Pogo (02/72) coefficients, epoch 1960

n	m	g_n^m	h_n^m	$\dot{g}_n^m$	$\dot{h}_n^m$	n	m	g_n^m	h_n^m	$\dot{g}_n^m$	$\dot{h}_n^m$
1	0	−30456.2	0.0	23.47	0.0	9	8	10.3	4.7	−1.09	−1.09
1	1	−2180.3	5819.0	12.67	−8.84	9	9	−6.5	8.6	1.45	−1.06
2	0	−1546.2	0.0	−23.09	0.0	10	0	−2.1	0.0	0.05	0.0
2	1	2996.2	−1994.0	0.53	−4.20	10	1	−1.7	3.5	−0.14	−0.17
2	2	1605.2	203.2	−2.19	−17.71	10	2	1.5	0.3	0.05	0.07
3	0	1304.8	0.0	−2.29	0.0	10	3	−4.1	0.3	−0.05	0.17
3	1	−1982.6	−443.9	−11.86	8.18	10	4	−3.4	4.8	0.22	0.14
3	2	1305.6	222.6	−2.08	3.02	10	5	9.3	−2.7	−0.42	−0.14
3	3	886.7	−156.7	−5.50	−2.99	10	6	5.7	2.2	−0.12	−0.20
4	0	961.4	0.0	−1.11	0.0	10	7	2.8	−5.4	−0.33	0.38
4	1	811.7	136.7	−1.15	2.96	10	8	0.6	8.7	−0.04	−0.67
4	2	496.7	−276.6	−2.69	0.96	10	9	0.9	−7.0	0.39	0.91
4	3	−381.7	16.2	−1.05	0.54	10	10	4.0	−9.3	−0.48	0.63
4	4	264.5	−259.9	−2.66	−1.39	11	0	2.4	0.0	0.01	0.0
5	0	−222.7	0.0	0.89	0.0	11	1	−0.2	1.3	−0.09	0.01
5	1	358.9	11.7	0.30	0.98	11	2	−1.9	2.6	0.00	0.04
5	2	242.9	118.4	1.52	1.75	11	3	5.0	−1.8	−0.17	−0.00
5	3	−28.1	−111.4	−0.97	−2.99	11	4	−2.4	−4.2	0.20	−0.19
5	4	−140.6	−101.2	−2.37	0.84	11	5	−1.2	1.5	0.18	0.14
5	5	−95.2	119.1	4.86	−3.81	11	6	−4.0	−3.9	0.47	0.54
6	0	46.0	0.0	−0.02	0.0	11	7	3.7	−1.0	−0.28	−0.05
6	1	59.1	−9.0	0.32	−0.21	11	8	−0.0	−3.0	0.33	0.44
6	2	−0.1	−106.8	1.36	−0.46	11	9	−0.7	−5.3	−0.26	0.37
6	3	−243.2	61.5	2.83	1.28	11	10	−3.6	−3.8	0.80	0.36
6	4	−3.3	−26.5	0.58	−1.42	11	11	5.4	−8.7	−0.28	1.28
6	5	−0.1	−20.3	0.11	1.59	12	0	−0.5	0.0	−0.15	0.0
6	6	−102.1	−4.4	−1.01	0.30	12	1	0.3	1.1	−0.03	−0.08
7	0	71.1	0.0	−0.15	0.0	12	2	0.4	0.1	−0.13	0.05
7	1	−51.6	−52.9	−0.29	−1.68	12	3	0.2	1.9	−0.02	0.03
7	2	3.9	−27.3	−0.32	0.18	12	4	1.6	0.3	−0.15	−0.10
7	3	12.3	−7.2	0.28	0.11	12	5	0.4	−0.6	0.02	0.04
7	4	−39.9	1.4	1.85	1.01	12	6	0.1	0.4	−0.11	−0.02
7	5	0.9	17.6	−0.46	0.36	12	7	−2.3	−1.3	0.20	0.13
7	6	−4.0	−35.1	2.25	1.80	12	8	0.7	−1.3	−0.04	0.25
7	7	39.7	−47.5	−5.78	4.11	12	9	0.3	2.7	−0.13	−0.30
8	0	8.9	0.0	0.36	0.0	12	10	−0.5	−0.6	0.06	−0.07
8	1	3.9	11.1	0.24	−0.35	12	11	−4.4	4.8	0.44	−0.55
8	2	−4.6	−12.7	0.41	−0.20	12	12	−5.4	−4.6	0.80	0.40
8	3	−11.0	8.8	−0.01	−0.48	13	0	1.1	0.0	−0.10	0.0
8	4	−0.3	−15.4	−0.51	−0.34	13	1	0.7	1.8	−0.15	−0.23
8	5	6.2	8.1	0.04	−0.36	13	2	0.7	0.7	−0.00	−0.05
8	6	−5.5	19.6	0.34	0.14	13	3	−0.6	0.6	0.00	0.06
8	7	12.3	6.1	−0.01	−1.44	13	4	1.0	−0.3	−0.09	0.00
8	8	−6.8	−35.1	1.49	2.05	13	5	0.7	−0.7	−0.03	0.08
9	0	11.4	0.0	−0.31	0.0	13	6	0.9	0.9	−0.13	−0.19
9	1	7.8	−22.0	0.12	−0.08	13	7	−1.0	−0.2	0.10	0.09
9	2	3.4	14.7	−0.26	−0.01	13	8	0.8	0.1	−0.16	−0.10
9	3	−12.3	2.1	0.01	0.42	13	9	2.2	0.3	−0.20	0.06
9	4	17.0	1.2	−0.73	−0.51	13	10	3.5	3.6	−0.49	−0.45
9	5	1.2	−1.7	−0.22	−0.25	13	11	−1.5	6.9	0.17	−0.79
9	6	8.1	18.5	−1.15	−1.30	13	12	−8.5	−6.2	0.88	0.63
9	7	−9.1	18.2	1.70	−0.90	13	13	3.3	−11.4	−0.15	1.14

NOTE: Units are nT and nT/year.

of this field model is identical to that used for the Pogo(08/71) field model (Langel 1973, 1974) except that no data from 1970 were used in the derivation of Pogo(02/72). The fitting procedure used 47 485 data points that were fit with the coefficients given in Table A1 to a root mean square residual of 6.2 nT. The distribution of residuals is given in Table A2, and pertinent statistics relative to data from the three satellites in Table A3.

The model generation assumed a spheroidal Earth with mean radius of 6371.0 km, equatorial radius of 6378.16 km, and a flattening factor of 1/298.25.

Because it was not designed as a predictive

TABLE A2. Distribution of residuals

Range (nT)	−60 to −50	−50 to −40	−40 to −30	−30 to −20	−20 to −10	−10 to 0	0 to 10	10 to 20	20 to 30	30 to 40
Number of points	2	4	25	216	2562	19 113	23 692	1831	28	2

TABLE A3. Statistics for OGO 2, OGO 4, and OGO 6

	Number of points	RMS (nT)	Mean (nT)	Standard deviation about mean (nT)
OGO 2	12 773	5.17	0.263	5.16
OGO 4	18 431	6.80	0.088	6.80
OGO 6	16 281	6.25	−0.063	6.21

model, Pogo(02/72) does not include data from observatories to aid in determination of the secular variation. It is, however, suitable for some uses at times past 1971. Mead (1979) has recently evaluated four field models for the epoch 1973–1976, well past the time span of the data utilized to create the models. The models evaluated were Pogo(08/71), IGS/75 (Barraclough *et al.* 1975), AWC/75 (Peddie and Fabiano 1976), and IGRF 1975 (IAGA 1976). He concluded that the first three were all about equally accurate and much superior to IGRF 1975. Both AWC/75 and IGS/75 are slightly better than Pogo(08/71). An extension of Mead's result shows that Pogo(02/72) is of comparable accuracy to Pogo(08/71) for the interval 1973–1976.

Reprinted from

Canadian Journal of Earth Sciences

Réimpression du

Journal canadien des sciences de la terre

Comparisons of magnetic anomalies of lithospheric origin measured by satellite and airborne magnetometers over western Canada

R. A. LANGEL, R. L. COLES, AND M. A. MAYHEW

Volume 17 • Number 7 • 1980

Pages 876–887

National Research Council Canada

Conseil national de recherches Canada

Comparisons of magnetic anomalies of lithospheric origin measured by satellite and airborne magnetometers over western Canada[1]

R. A. LANGEL
Geophysics Branch, National Aeronautics and Space Administration, Goddard Space Flight Center, Greenbelt, MD 20771, U.S.A.
R. L. COLES
Earth Physics Branch, Department of Energy, Mines and Resources, Ottawa, Ont., Canada K1A 0Y3
AND
M. A. MAYHEW
Business and Technological Systems, Inc., Seabrook, MD 20801, U.S.A.

Received October 11, 1979
Revision accepted March 7, 1980

Crustal magnetic anomaly data from the Orbiting Geophysical Observatories 2, 4, and 6 (Pogo) satellites are compared with upward-continued aeromagnetic data between 50–85°N latitude and 220–260°E longitude. Agreement is good, both in anomaly location and in amplitude, giving confidence that it is possible to proceed with the derivation and interpretation of satellite anomaly maps in all parts of the globe. The data contain a magnetic high over the Alpha ridge suggesting continental composition and a magnetic low over the southern Canada basin and northern Canadian Arctic Islands (Sverdrup basin). The low in the Sverdrup basin corresponds to a region of high heat flow, suggesting a shallow Curie isotherm. A ridge of high field, with two distinct peaks in amplitude, is found over the northern portion of the platform deposits and a relative high is located in the central portion of the Churchill Province. No features are present to indicate a magnetic boundary between Slave and Bear Provinces, but a trend change is evident between Slave and Churchill Provinces. South of 60° latitude a broad magnetic low is located over very thick (40–50 km) crust, interpreted to be a region of low magnetization.

On compare les données recueillies par les satellites OGO 2, 4 et 6 (Pogo) sur les anomalies magnétiques dans la croûte avec un prolongement vers le haut des données aéromagnétiques situées entre les latitudes 50–85°N et les longitudes 220–260°E. L'accord est bon à la fois pour la localisation des anomalies et leur amplitude, ce qui permet d'être optimiste quant à la possibilité de procéder à la confection et à l'interprétation de cartes d'anomalies magnétiques par satellite dans toutes les parties du globe. Les données contiennent un pic magnétique sur la crête Alpha suggérant une composition continentale et une dépression magnétique sur le bassin du sud du Canada et dans les îles de l'Arctique canadien au nord (le bassin de Sverdrup). La dépression dans le bassin de Sverdrup correspond à une région de flux thermique élevé ce qui laisse supposer une isotherme de Curie à faible profondeur. Une crête de champ intense avec deux pics distincts dans l'amplitude se retrouve dans la partie nord des dépôts de plate-forme et un sommet relatif est localisé dans la portion centrale de la province de Churchill. Il n'y a rien qui indique une limite magnétique entre les provinces de l'Esclave et de l'Ours, il y a un changement évident entre les provinces de Churchill et de l'Esclave. Au sud de la latitude 60°N, on observe une vaste dépression magnétique située sur une croûte très épaisse (40–50 km) et qu'on interprète comme une région de faible aimantation.

[Traduit par le journal]

Can. J. Earth Sci., **17**, 876–887 (1980)

Introduction

In recent years it has been realized that crustal magnetic anomalies exist which are of longer wavelengths than those investigated by exploration geophysicists and that these longer wavelength (greater than 50 km) anomalies are indicative of geologic and tectonic features in the deep crust (Pakiser and Zietz 1965; Zietz *et al.* 1966; Shuey *et al.* 1973; Hall 1974; Krutikhovskaya and Pashkevich 1977).

With the publication of the paper by Regan *et al.* (1975) it was demonstrated that long wavelength lithospheric anomalies could be mapped successfully from satellites. That map showed a global distribution of anomalies of about 500–3000 km scale size which were never before mapped and whose very existence was in most cases discovered for the first time. Although this map was distorted by variations in altitude over the data set and by contamination from magnetospheric fields, Regan *et al.* were able to demonstrate that the probable source of the anomalies is indeed the lithosphere.

[1]Contribution from the Earth Physics Branch No. 854.

0008-4077/80/070876-12$01.00/0

TABLE 1. Some characteristics of the Pogo orbits

Satellite	Launch date	Inclination	Perigee (km)	Apogee (km)
OGO 2 (1965 81A)	October 14, 1965	87.3°	410	1510
OGO 4 (1967 73A)	July 28, 1967	86.0°	410	910
OGO 6 (1969 51A)	June 5, 1969	82.0°	400	1100

Subsequently, Regan and Marsh (in preparation) have collected ancillary data and derived a quantitative model of an anomaly located in central Africa. Analysis techniques for this type of data are rapidly becoming available (Bhattacharyya 1977; Mayhew 1978, 1979).

While analysis of data at lower latitudes has proceeded (Regan and Marsh, in preparation; Mayhew 1979), nothing has been published dealing with anomalies measured by satellite at the higher latitudes. The reason for this is that at low latitudes the external (magnetospheric/ionospheric) fields are mainly of longer wavelength than the anomalies being mapped, and can be readily filtered from the data, thus isolating the anomaly fields. This remains true as long as data within about 3 h of local noon are not utilized. At high latitudes, however, ionospheric currents occur at all local times and are very often present even during magnetically quiet periods of time. Further, these currents result in fields of the same spatial scale as the anomalies of interest, thus complicating the problem of isolating the anomaly fields. This paper is a report on an attempt to isolate the anomaly fields at satellite altitude for such high latitudes, and in particular over that part of Canada between 50–85°N latitude and 220–260°E longitude. To gauge the success of this attempt, the resulting anomaly map is compared to aeromagnetic data upward continued to satellite altitude, 500 km.

The Satellite Data

A survey of the near-Earth magnetic field was carried out by the Polar Orbiting Geophysical Observatories (OGO 2, 4, and 6), also known as the Pogo satellites (Langel 1973, 1974). Some characteristics of the Pogo orbits are given in Table 1. Orbiting Geophysical Observatory 2 acquired data from launch until October 2, 1967; OGO 4 from launch until January 19, 1969; and OGO 6 from launch until August 29, 1970 and then sporadically until June 1971. Each satellite completed about 15 revolutions each day. Orbiting Geophysical Observatory 2 and OGO 4 acquired a data point every 0.5 s and OGO 6 every 0.288 s.

The measured magnetic field, $\boldsymbol{B}$, is the vector sum of magnetic fields from several sources. These are the main (core) field of the Earth, $\boldsymbol{M}$, the variable field due to ionospheric and magnetospheric currents, $\boldsymbol{D}$, and the field originating in the lithosphere of the Earth, $\boldsymbol{A}$. In this study the main field is represented by a spherical harmonic model, $\boldsymbol{M}_c$, of degree and order 13, designated Pogo(02/72) and described in the Appendix. It should be noted that this model is intended primarily as a representation of the main field of the Earth for the time span of the Pogo data. The degree and order were chosen on the basis of studies by Phillips (J. Phillips, personal communication, 1978), Cain *et al.* (1974), and Cain (1976), which indicate that a 13th degree and order representation is sufficient to represent the main field without unduly distorting the anomaly field. Any such choice is, of course, a compromise and no exact separation is possible.

Orbiting Geophysical Observatories 2, 4, and 6 measured the magnitude but not the direction of the field $\boldsymbol{B}$. The quantity analyzed is thus the residual field

$$\Delta B = |\boldsymbol{B}| - |\boldsymbol{M}_c|$$

This residual field contains contributions from: (1) any inaccuracy in modeling the core field $\boldsymbol{M}$ with $\boldsymbol{M}_c$, (2) the external field, $\boldsymbol{D}$, and (3) the lithospheric field, $\boldsymbol{A}$. Contributions from $\boldsymbol{D}$ are minimized by elimination of all data in which the residual field was considered to be dominantly due to $\boldsymbol{D}$. This elimination was accomplished on a pass by pass basis in two steps. (A pass is defined as a continuous set of data beginning when the satellite goes above 50° latitude and ending when it again goes below 50° on the other side of the pole.) Firstly, if the magnitude of the residual field, ΔB, exceeds 20 nT (nanotesla) at any place in the pass, the entire pass is rejected. Secondly, the remaining passes are visually intercompared to attempt to distinguish the time invariant features, the lithospheric field $|\boldsymbol{A}|$, from the time varying external field $|\boldsymbol{D}|$, and passes with significant contribution from the latter are not used in the anomaly map. A total of 271 "quiet" passes remained and were used in deriving the anomaly map. After performing these operations the internal agreement of passes which are nearly coincident geographically is substantial, which indicates the presence and reality of the crustal

anomalies. However, significant differences of wavelength more than 2000–3000 km still remain between coincident passes. This is similar to the results of Mayhew (1979) over the continental United States. His solution was to remove a polynomial function separately from each individual pass. Only passes with several thousand kilometres of data were used. This function is determined by a least squares fit to that pass. The procedure of Mayhew was followed with the data presented here except that Mayhew chose a quadratic function whereas we have chosen a linear function. The function chosen is a matter of subjective judgement. The difference between the linear and quadratic functions for these data is not substantial. We are, of course, left with an anomaly field with arbitrary zero. After the data selection and trend removal, individual residual field data points were averaged in an equal-area grid superimposed over an equal-area map of the area of interest. The grid is square and the distance along each side is equivalent to 3° of latitude. Figure 1 shows the density distribution of the data used in the averages. The resulting averaged residual anomaly map, contoured at 2 nT intervals, is shown in Fig. 2*a*. Results in the southwest portion of the map, between 220–240° longitude and 50–60°N latitude, are to be regarded with caution because of the sparseness of data as shown in Fig. 1. The residuals plotted in Fig. 2*a* are not at a common altitude but are at the altitudes determined in each block over which the data were averaged. The average altitude varies from 440–560 km, with mean near 520 km. A map reduced to common altitude is discussed later in the paper.

The anomalies range from a maximum of 14 nT at about 85° latitude to a minimum of −11 nT at 50° latitude and 239° longitude.

The Airborne Magnetometer Data

The airborne magnetic field data considered here have been acquired by the Earth Physics Branch of the Department of Energy, Mines and Resources, Ottawa, since 1969 in a series of airborne vector magnetometer surveys, each survey covering 2×10^6 to 4×10^6 km^2 at a typical altitude of 3.5 km above sea level, with excursions giving a range of 2.5–6.0 km. The instrumentation and survey details have been variously described by Haines and Hannaford (1972, 1974, 1976) and Hannaford and Haines (1974). Discussions of the data have been given by Haines *et al.* (1971), Riddihough *et al.* (1973), Coles *et al.* (1976), and Coles and Haines (1979).

The data were obtained in three separate surveys

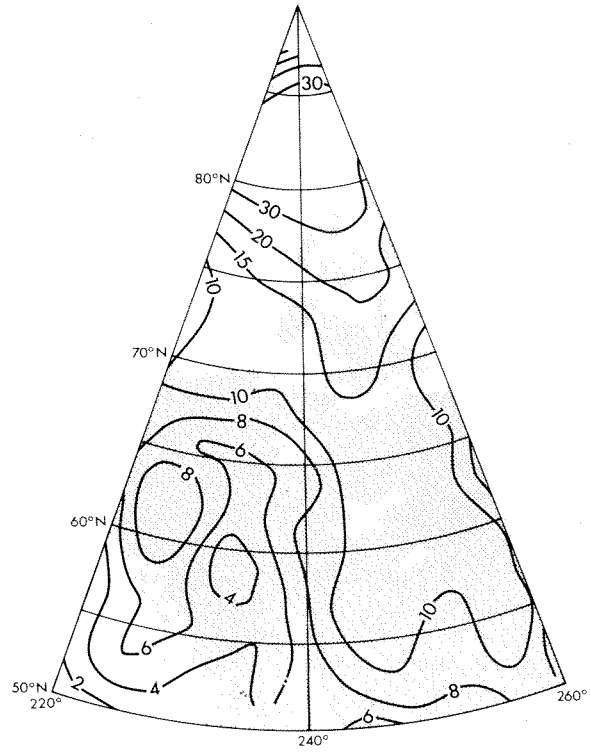

FIG. 1. Density of distribution of Pogo data, as number of points in averages.

flown at approximately 2 year intervals. In order to remove level differences due to secular change, a reference field has been removed. Coles (1979) has shown that the best available reference field models for this region and for this interval of time are based on the Pogo data. The model chosen was the Pogo(02/72) model, i.e., the same reference field used for the satellite data. Coles also demonstrated a way of correcting for inadequacies in the secular change terms of the reference model in its application to the airborne data. The residual data values are, in effect, adjusted to a single epoch. At each magnetic observatory in or near the survey region, the change in average quiet day field level from the epoch of the survey to the updated epoch is compared with the change in value of the field model between the two epochs. This comparison leads to a low-degree polynomial correction surface to be applied to the data residuals. The airborne data residuals were upward continued to 500 km in order to compare them with the satellite data. A more detailed discussion of this procedure is given by Coles and Haines (1979).

At high geomagnetic latitudes, differences between scalar and vertical component regional anomaly fields are minor (Langel 1974). The vertical

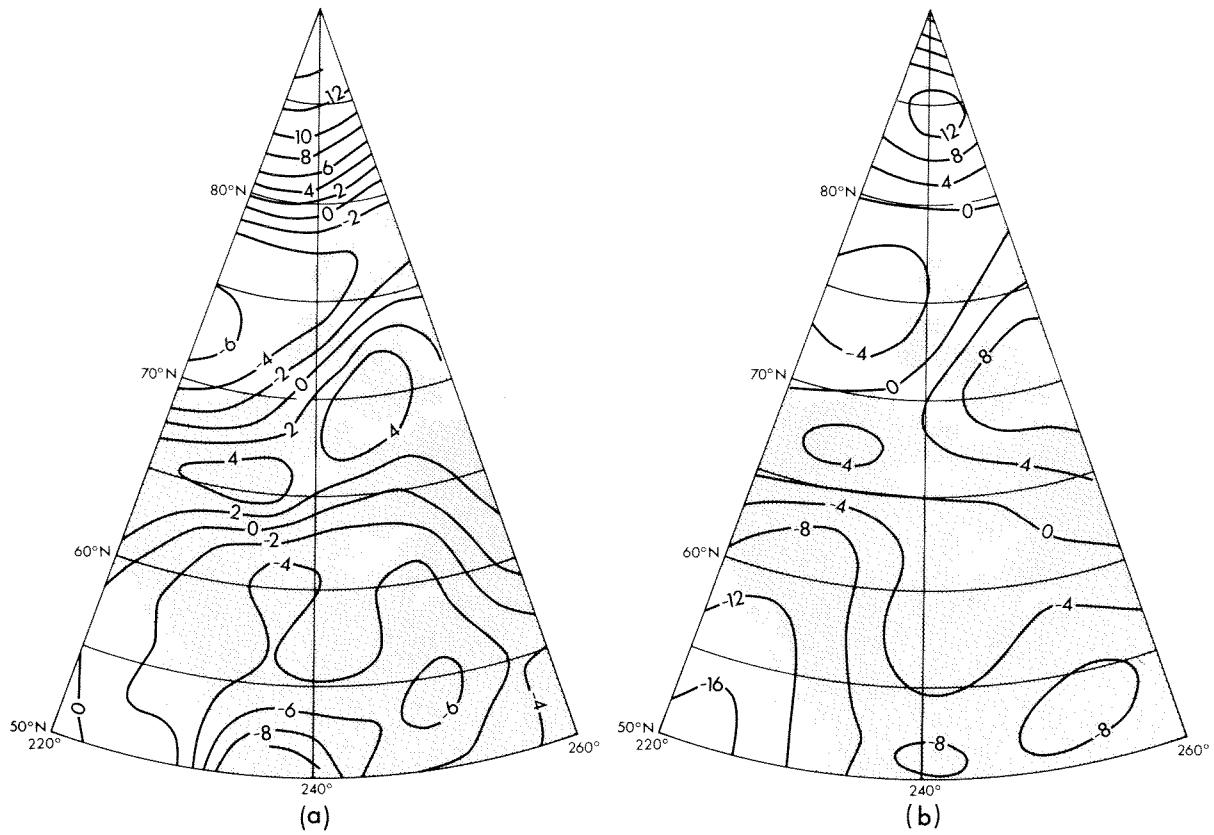

FIG. 2. Comparison of (*a*) averaged scalar magnetic anomalies from Pogo data with (*b*) upward-continued aeromagnetic vertical component anomaly data (500 km altitude).

component airborne data were used for the upward continuation because the data coverage is more complete than the scalar data coverage, and because the scalar field is not strictly harmonic. The input data to the upward continuation were in the form of averages of vertical component residuals along flight tracks over 5 min of time (about 35 km distance). The data points are shown in Fig. 3, and Fig. 4 is a contoured map prepared from the 5 min averaged data.

The data averages were each associated with an area determined by the spacing (35 km) multiplied by the mean flight-line spacing in the region of each data average. Although the original data were only along flight lines, the approximation is sufficient for the present purposes. No corrections for variations in flight altitude have been incorporated.

The basic equation for upward continuation from a sphere can be approximately represented, for the vertical component Z_p at point P, by

$$Z_p = \frac{R^2 - R_0^2}{4\pi R} \sum \frac{Z_i}{\rho_i^3} \Delta S_i$$

where the summation is over all data points i, each associated with an area ΔS_i and field value Z_i. R is the geocentric distance to the point P, R_0 is the radius of the Earth, and ρ_i is the distance from P to the point i. The data values, Z_i, are residuals relative to the reference field. The residual field beyond the data area is assumed to be zero and, therefore, has no contribution to the summation. This is an assumption, of course, which limits the accuracy of the upward continuation. Coles and Haines (1979) discuss this point in more detail; however, the actual total contribution from distant points beyond the data area is small (less than about 2 nT for most parts of the area), since the integral of the residual field over a large region tends to zero.

The data (5600 points) have been upward continued to 100, 300, and 500 km (Figs. 5, 2*b*). As the altitude increases, the anomalies become smoother and reduced in amplitude. Broad features, however, persist through the series of figures.

Comparison of the Anomaly Maps

There is good agreement between the satellite

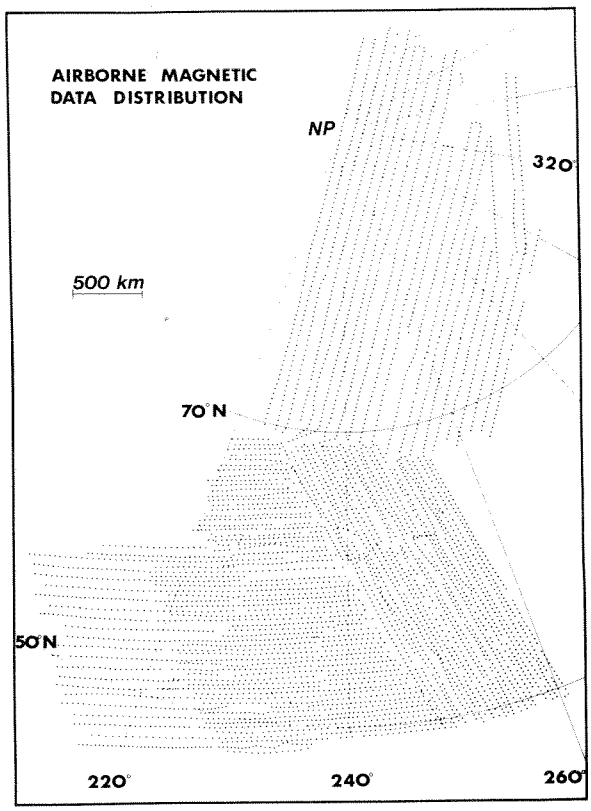

FIG. 3. Relative distribution of aeromagnetic data.

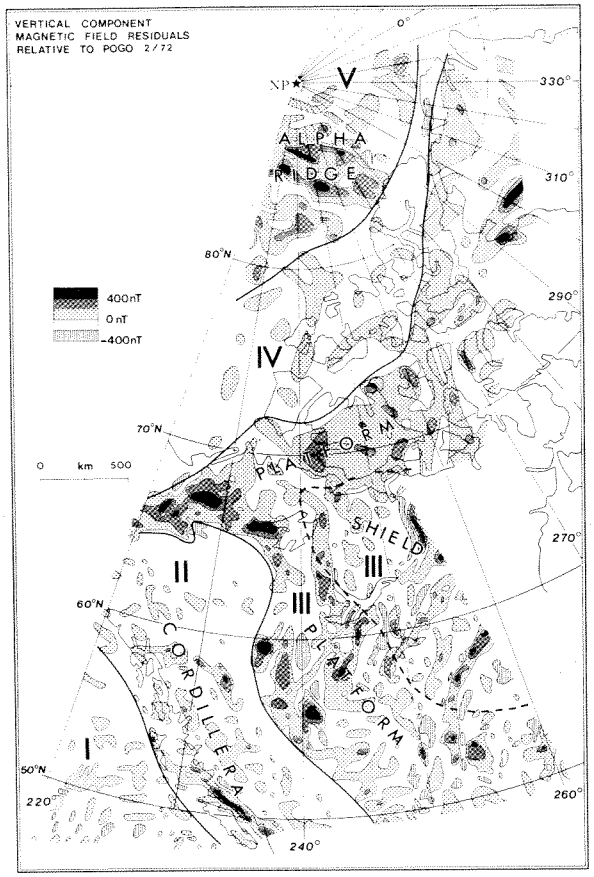

FIG. 4. Residuals of aeromagnetic data at an altitude of 3 km. Roman numerals designate regions of differing characteristics as described in the text.

and airborne data in their common spectral region. The agreement is excellent in the north, with a high anomaly north of 80°N, a low region between about 70 and 80°N, and a north-easterly trending ridge of high field centered near 65–67°N in the west and extending to about 70°N in the east. A south-trending, relatively positive area extends between 55 and 62°N at a longitude of about 240°. In the southwest the agreement is not as good, with a large gradient evident in the airborne-derived map. Nevertheless, the indications are of a relatively low field over the southwestern Cordillera region in Canada. The agreement in anomaly amplitudes is also very good, except in the southwest corner. This comparison gives a confirmation over a sub-continental size region of the reality of the anomalies derived from satellite data. This is particularly important for this region of the Earth where contaminating fields from high latitude currents are strong and it indicates that we have been successful in separating the anomaly fields from fields due to those currents.

The reason for the discrepancy in the southwest between the two maps is not clear. The method of upward continuation is not a major factor since different analyses of the original data also indicate a similar discrepancy (Coles and Haines 1979). The Pogo anomaly map is determined relative to a model also derived from Pogo data, so one would not expect trends of 10–20 nT to be present in that map. Either the available satellite data are consistently high in this region (the density of satellite passes is very low here), or the airborne data (one particular survey) are consistently low.

Effect of Model Removed

Any bias in the field model utilized to estimate the core field may be reflected as an error in anomaly maps derived by this method. This would be the case, for example, if the higher order terms of the model utilized were negatively correlated with the anomalies derived. Obviously, some error is introduced simply because the spectra of core and crustal fields overlap so that it is not possible to do a clean separation. We believe that, if anything, our results are biased by removing too much long

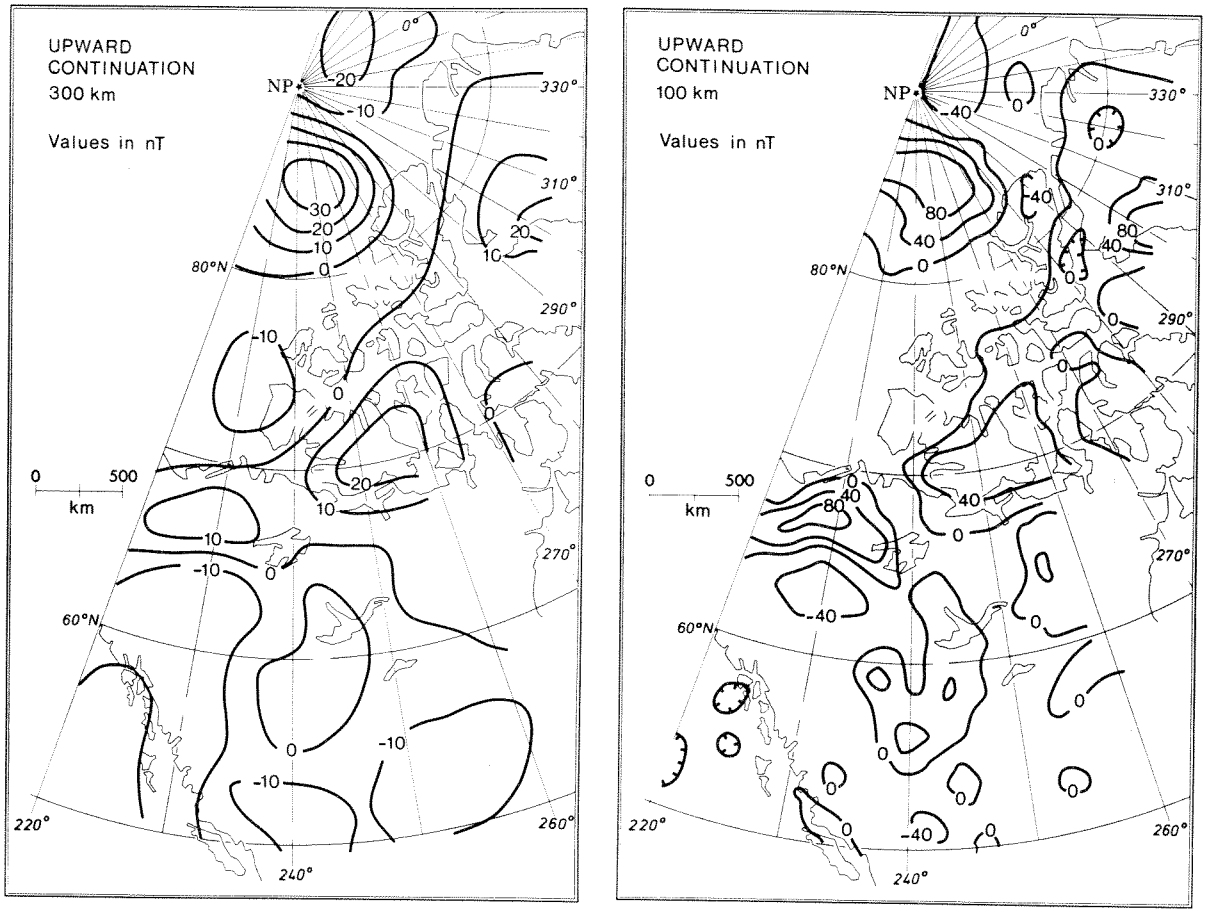

FIG. 5. Upward continuation of aeromagnetic data.

wavelength field rather than too little, because of the pass by pass linear trend removal.

We have two indications that field model biases are not significantly contaminating our results. Firstly, Coles *et al.* (1976, Fig. 2) subtracted the vertical component of the International Geomagnetic Reference Field (IGRF) from the vertical component of the Pogo(02/72) model (erroneously designated Pogo(6/71) in their paper). This difference plot shows *no* correlation with the derived anomaly maps. Secondly, we have recomputed the satellite anomaly map utilizing the Pogo(06/74) field model (Cain *et al.* 1974) which is of degree and order 22. This map is presented here as Fig. 6. Comparison with Fig. 2*a* shows that the greatest differences are in the southwest corner of the map—already noted to be suspect. All other features remain relatively unchanged except for subtle longer wavelength effects. We believe this indicates that any biases due to the degree of the field models used are negligible.

Geologic Implications

It is not our intention to present a detailed interpretation of the magnetic anomaly maps shown here. Interpretations of the aeromagnetic data have already been published (Haines *et al.* 1971; Riddihough *et al.* 1973; Coles *et al.* 1976). In this section we wish to contrast the different viewpoints offered by the aeromagnetic and satellite magnetic data and to illustrate the use of the satellite data in making geologic inferences.

Examination of Fig. 4 shows changes in the character of the anomaly patterns from region to region, often delineating geologic boundaries. Such changes are clearly apparent between the Cordillera and the platform, i.e., between regions II and III and between the platform of region III and the thick sediments, both onshore and offshore, of region IV. The character changes most evident are (1) changes from high magnetic relief to low magnetic relief and (2) changes in the trends of the anomalies. Because most of the high relief features are positive

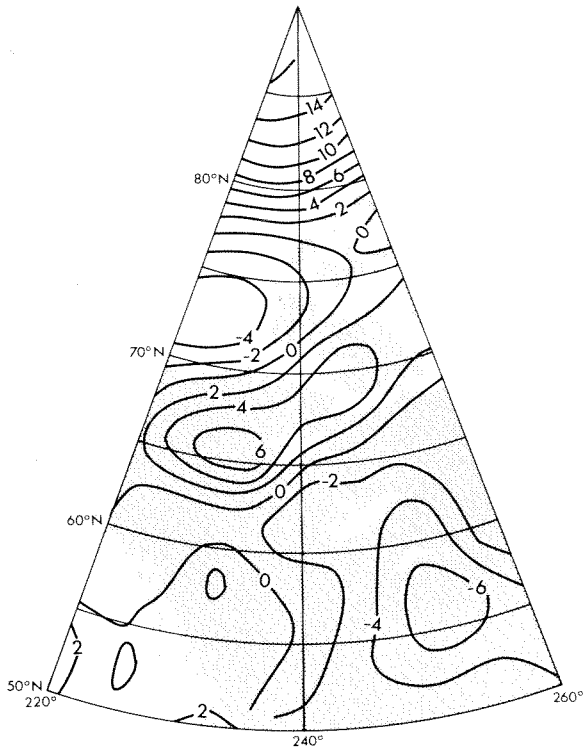

FIG. 6. Averaged magnetic anomaly map from Pogo data, using a 22nd degree spherical harmonic model to remove the core field.

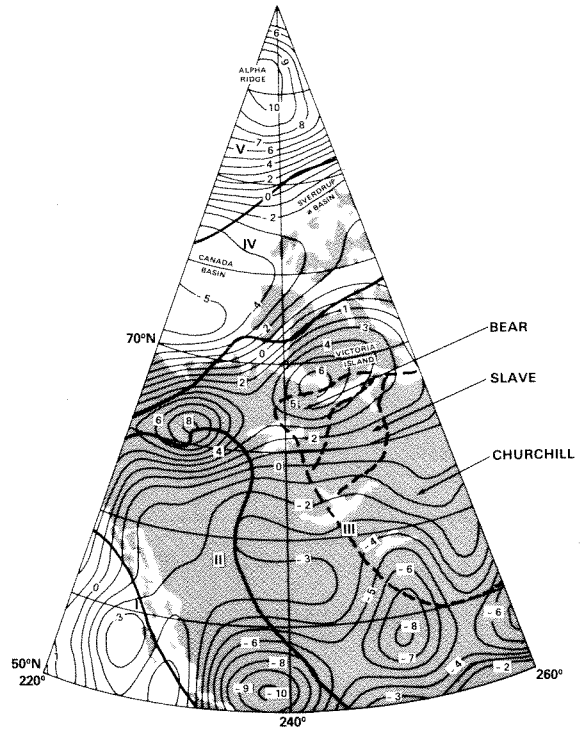

FIG. 7. Reduction of Pogo anomaly map to an altitude of 500 km using an equivalent source representation (reference field is Pogo(02/72)). The contour interval is 1 nT.

there is also an apparent contrast between regions of predominantly positive and predominantly negative fields. Figure 7 shows the satellite field, now reduced to common altitude using an equivalent source representation (Mayhew 1978, 1979). In contrast to Fig. 4, the satellite map shows only the contrasts between the predominantly positive and negative regions. The aeromagnetic data clearly contain all of the information in the satellite data and more and are able to delineate boundaries more definitively. However, the satellite map (or an upward-continued aeromagnetic map) gives a clearer picture of broad trends and can serve as a guide in discerning those same trends in the lower altitude data. In the following paragraphs we will discuss the various "regions" delineated by the satellite anomalies (Fig. 7) compared with those delineated by the aeromagnetic data (Fig. 4) and known geologic provinces.

At the very north of the map the satellite data show a prominent high of about 12 nT magnitude. This is centered on the Alpha ridge of the Arctic Basin. The airborne survey also shows a broad positive in this region but is punctuated by a complex series of intense positive anomalies nearly parallel to the trend of the ridge. These extend both north and south of the ridge and are all contained within the area of positive field as seen by Pogo. This region has also been surveyed by Vogt *et al.* (1979) who concluded that the principal magnetic anomalies in this region are topographic effects in a normally magnetized basement with high magnetization intensity (20–30 A/m). The broader picture afforded by the satellite data supports the existence of a region of highly magnetized crust and partially outlines its extent. Unfortunately, the satellite data do not extend above 87° latitude so the northern portion of this region is not mapped. The upward-continued aeromagnetic data indicate that it terminates at about 88° latitude.

The Alpha ridge has been variously interpreted as a subduction zone (Herron *et al.* 1974), as an extinct center of sea-floor spreading (Churkin 1973; Vogt and Ostenso 1970; Hall 1973; Tailleur 1973; Vogt and Avery 1974), or as subsided continental crust (Eardley 1961; King *et al.* 1966; Taylor 1978). DeLaurier (1978) rejects the hypotheses of a subduction zone or a center of sea-floor spreading on the basis of a comparison of the measured relief with the relief expected from a cooling model, because of a lack of seismic activity, and because active accretion is inconsistent with the known

marine fossils and sediment thickness. Vogt *et al.* (1979) also examine these questions and conclude that on the basis of the airborne magnetic data it is not possible to rule out any of the three hypotheses. In addition to the arguments noted above against a spreading center or subduction zone, they claim that the depth of the Alpha ridge argues against it being a subsided shield.

Taylor (1978) suggests that the Alpha ridge is an aseismic ridge similar to the Lord Howe Rise, which is continental in nature, in the southwest Pacific. In fact, the satellite data show a similar positive anomaly over the Lord Howe Rise (Regan *et al.* 1975). Coles *et al.* (1978) and Sweeney *et al.* (1978) note that the positive long-wavelength anomaly over the Alpha ridge is consistent with a region of crust of continental composition since most of the major long-wavelength positive anomalies detected by satellites are associated with continental crust, both in shield areas and in regions such as Broken Ridge in the Indian Ocean (Regan *et al.* 1975).

To the south of the Alpha ridge and its environs the satellite map shows a broad negative over the southern Canada Basin and the northern Canadian Arctic Islands. The aeromagnetic data in this region are remarkably free from shorter wavelength anomalies. Geologically, this is a region of deep (3–12 km) sediments (Sweeney *et al.* 1978) resulting in a greater depth to basement which may account for the lack of shorter wavelength anomalies in the aeromagnetic data (Riddihough *et al.* 1973). The southern 0 nT contour of this region is close to the edge of the craton but both bathymetric (Sweeney *et al.* 1978) and seismic (Sweeney *et al.* 1978; Berry and Barr 1971; Sander and Overton 1965; Overton 1970; Berry 1973) data show that the transition from continental to oceanic crust, the Canada Basin, takes place well within the region of negative anomaly. Comparison of Fig. 7 with the bathymetry (Sweeney *et al.* 1978) indicates that over much of its length the −4 nT contour nearly coincides with the continental slope. Thus, the central low of the negative anomaly is located over oceanic crust. The eastward extension of this magnetic low is over the Sverdrup basin, where refraction data (Sander and Overton 1965; Overton 1970; Forsyth *et al.* 1979) indicate sediments reaching 12 km. Forsyth *et al.* note that "Based on heat flow measurements taken in bore-holes throughout the Sverdrup Basin, A. S. Judge has estimated that maximum temperatures are 600 to 650°C at 20 km and 850 to 900°C at 30 km (personal communication)." Judge noted higher than average heat flow values for the central Sverdrup basin. Thus, the magnetite Curie isotherm is well up into a thickly sedimented crust in this region which could account for the relative negative magnetic anomaly. The cause of the negative anomaly over the Canada Basin is unknown. Future refinement of the satellite data over the rest of the Arctic will be required to see if the negative anomaly is coextensive with the entire Amerasian Basin.

An elongated region of high magnetic field (Fig. 7) is located near 65° latitude at 220°E longitude in the west and extends to 71° latitude at 260°E longitude. This "high" occurs over the northern portion of the platform deposits on the Precambrian craton and can be resolved into two maxima. In the east the positive anomaly extends southward over the northern parts of the exposed shield. Considering the two highs over the platform deposits, comparison with Fig. 4 shows positive anomalies in the aeromagnetic data in these regions but of significantly different character. In the east, over Victoria Island, there is no concentration of short-wavelength anomalies, whereas in the west, the broad positive background is punctuated by narrow regions of intense positive short-wavelength anomalies. This region of large amplitude anomalies extends around the top of region II (Fig. 4) and has been interpreted to indicate that the crystalline continental basement extends far to the west of the exposed and known buried shield (Coles *et al.* 1976). This regional difference seems to be reflected in the heat flow data (although a good thermal model is not yet available and the available data are sparse) in that the available heat flow values near the western field maximum are considerably higher than those near the eastern maximum. This difference in heat flow between two magnetic highs of nearly equal amplitude indicates that the long-wavelength anomalies, at least to the east of the Cordillera, do not correlate well with heat flow and, therefore, are not indicative of variations in the depth to the Curie isotherm. For comparison, in the United States good heat flow vs. long-wavelength anomaly correlation is evident in the tectonically active region west of the Cordillera (Mayhew, in preparation), whereas in the more stable region to the east of the Cordillera the extremely sparse heat flow data do not seem to correlate with the long-wavelength magnetic anomalies.

Just to the south of the double maximum the contour lines are relatively featureless with a northeasterly trend. In particular, no features are present marking the boundary between Bear and Slave Provinces. Below 67° latitude a trend change is evident between Slave and Churchill Provinces and, near the eastern border of the map, a relative

high extends through the central portion of the Churchill Province. This relative high is not clearly defined in the aeromagnetic data, which do not extend as far east as the satellite data.

South of about 60–63° the satellite anomaly map is everywhere negative, highly negative in some regions. The low altitude data of Fig. 4 show that large portions of this area are relatively free of large amplitude short-wavelength anomalies. A relative negative anomalous region can be caused by one or a combination of three things: very low rock magnetization, a shallow Curie isotherm, or a high reversed remanent magnetization. The latter is extremely unlikely for a geographic region of this size; reversed magnetizations for regions this size are neither expected nor found in practice. Although sparse, the existing heat flow data are at or below normal values, with no indication of a shallow Curie isotherm. Thus the crust in this region, which is 40–50 km thick (Chandra and Cumming 1972; Berry 1973), most likely has very low average rock magnetization over most of its area. The satellite data show a relative high at about 57–60° latitude and 238–241° longitude. This is reflected in the low latitude aeromagnetic data (Fig. 4) as a cluster of magnetic highs east of the Cordillera, and in fact the Cordillera is outlined by their western boundary. Most of this region of "highs" is underlain by sedimentary cratonic cover rocks, reaching several kilometres thickness in the west. Some deep drill holes exist to the east of the Cordillera within both the area of short-wavelength intense positive anomalies and the area further southeast, free of such anomalies. The magnetizations of basement rocks from the bottoms of the drill holes have been measured (R. A. Burwash, personal communication, 1974; R. L. Coles, unpublished data, 1975). Although sparse, the magnetization values outside the area of short-wavelength positive anomalies are lower on average than what appears to be typical for shield areas, whereas within the area of short-wavelength "highs," much of the crystalline basement is highly magnetic.

Summary

Aeromagnetic and satellite magnetic data have been presented and compared for western Canada. Such a comparison at these geomagnetic latitudes is important because both data types are affected by fields from external (ionospheric and magnetospheric) sources. Such external fields are particularly troublesome to the satellite data where, even after careful data selection, external fields are undoubtedly present on most data passes. The close agreement between the two data types indicates that it is possible to extract the anomaly "signal" from the satellite data and that the anomalies so defined are indeed crustal in origin. We believe it is now possible to proceed in confidence with the derivation and interpretation of satellite anomaly maps in all parts of the globe.

Both averaging of satellite data and upward continuation of aeromagnetic data serve to filter out details in the field. For aeromagnetic data this is not a problem since one can compare with results for lower altitudes. Derivation of an equivalent source representation of the satellite data preserves most of the information content of the data, as is apparent from comparison of Fig. 7 and Fig. 2*a*. Broad interpretative comparison of the equivalent source field with known geologic and geophysical data has indicated that it is indeed indicative of important features in the crust and can aid in the solution of such problems as the nature and origin of the Alpha ridge and the nature of the crystalline basement underlying sedimentary cover.

Acknowledgements

We would like to thank M. K. Hutchinson, R. Horner, D. Love, and B. Draper for their efforts in data preparation and display, and G. V. Haines and G. D. Mead for valuable discussion and review of the manuscript.

BARRACLOUGH, D. R., HARWOOD, J. M., LEATON, B. R., and MALIN, S. R. C. 1975. A model of the geomagnetic field at epoch 1975. Geophysical Journal of the Royal Astronomical Society, **43**, pp. 645–659.

BERRY, M. J. 1973. Structure of the crust and upper mantle in Canada. Tectonophysics, **20**, pp. 183–201.

BERRY, M. J., and BARR, K. G. 1971. A seismic refraction profile across the polar continental shield of the Queen Elizabeth Islands. Canadian Journal of Earth Sciences, **8**, pp. 360–374.

BHATTACHARYYA, B. K. 1977. Reduction and treatment of magnetic anomalies of crustal origin in satellite data. Journal of Geophysical Research, **82**, pp. 3379–3390.

CAIN, J. C. 1976. Introductory remarks. Abstract. EOS, Transactions of the American Geophysical Union, **57**, p. 907.

CAIN, J. C., DAVIS, W. M., and REGAN, R. D. 1974. An $N = 22$ model of the geomagnetic field. Abstract. EOS, Transactions of the American Geophysical Union, **56**, p. 1108.

CHANDRA, N. N., and CUMMING, G. L. 1972. Seismic refraction studies in western Canada. Canadian Journal of Earth Sciences, **9**, pp. 1099–1109.

CHURKIN, M. 1973. Geologic concepts of Arctic Ocean Basin. *In* Arctic geology. *Edited by* M. G. Pitcher. American Association of Petroleum Geology, Memoir 19, pp. 485–499.

COLES, R. L. 1979. Some comparisons among geomagnetic field models, observatory data and airborne magnetometer data: implications for broad scale anomaly studies over Canada. Journal of Geomagnetism and Geoelectricity, **31**, pp. 459–478.

COLES, R. L., and HAINES, G. V. 1979. Long-wavelength magnetic anomalies over Canada, using polynomial and upward continuation techniques. Journal of Geomagnetism and Geoelectricity, **31**, pp. 545–566.

COLES, R. L., HAINES, G. V., and HANNAFORD, W. 1976. Large

scale magnetic anomalies over western Canada and the Arctic: a discussion. Canadian Journal of Earth Sciences, **13**, pp. 790–802.

COLES, R. L., HANNAFORD, W., and HAINES, G. V. 1978. Magnetic anomalies and the evolution of the Arctic. *In* Arctic geophysical review. *Edited by* J. F. Sweeney. Publication of the Earth Physics Branch, Energy, Mines and Resources, Ottawa, Ont., **45**, pp. 51–66.

DELAURIER, J. M. 1978. The Alpha ridge is not a spreading centre. *In* Arctic geophysical review. *Edited by* J. F. Sweeney. Publication of the Earth Physics Branch, Energy, Mines and Resources, Ottawa, Ont., **45**, pp. 87–90.

EARDLEY, A. J. 1971. History of geologic thought on the origin of the Arctic Basin. *In* Geology of the Arctic. *Edited by* G. O. Raesh. University of Toronto Press, Toronto, Ont., pp. 223–249.

FORSYTH, D. A., MAIR, J. A., and FRASER, I. 1979. Crustal structure of the central Sverdrup basin. Canadian Journal of Earth Sciences, **16**, pp. 1581–1598.

HAINES, G. V., and HANNAFORD, W. 1972. Magnetic anomaly maps of British Columbia and the adjacent Pacific Ocean. Publication of the Earth Physics Branch, Energy, Mines and Resources, Ottawa, Ont., **42**, pp. 211–228.

——— 1974. A three-component aeromagnetic survey of the Canadian Arctic. Publication of the Earth Physics Branch, Energy, Mines and Resources, Ottawa, Ont., **44**, pp. 209–234.

——— 1976. A three-component aeromagnetic survey of Saskatchewan, Alberta, Yukon and the District of Mackenzie. Earth Physics Branch, Geomagnetic Series No. 8, Ottawa, Ont. 34 p.

HAINES, G. V., HANNAFORD, W., and RIDDIHOUGH, R. P. 1971. Magnetic anomalies over British Columbia and the adjacent Pacific Ocean. Canadian Journal of Earth Sciences, **8**, pp. 387–391.

HALL, D. H. 1974. Long-wavelength aeromagnetic anomalies and deep crustal magnetization in Manitoba and northwestern Ontario, Canada. Journal of Geophysics, **40**, pp. 403–430.

HALL, J. K. 1973. Geophysical evidence for ancient sea floor spreading from Alpha Cordillera and Mendeleyev Ridge. *In* Arctic geology. *Edited by* M. G. Pitcher. American Association of Petroleum Geology, Memoir 19, Tulsa, OK.

HANNAFORD, W., and HAINES, G. V. 1974. A three-component aeromagnetic survey of British Columbia and the adjacent Pacific Ocean. Publication of the Earth Physics Branch, Energy, Mines and Resources, Ottawa, Ont. **44**, pp. 323–379.

HERRON, E. M., DEWEY, J. F., and PITMAN, W. C., III. 1974. Plate tectonics model for the evolution of the Arctic. Geology, **2**, pp. 377–380.

International Association of Geomagnetism and Aeronomy (IAGA) DIVISION 1 STUDY GROUP 1976. International geomagnetic reference field 1975. EOS, Transactions of the American Geophysical Union, **57**, pp. 120–121.

KING, E. R., ZIETZ, I., and ALLDREDGE, L. R. 1966. Magnetic data on the structure of the central Arctic region. Geological Society of America Bulletin, **77**, pp. 619–646.

KRUTIKHOVSKAYA, Z. A., and PASHKEVICH, I. K. 1977. Magnetic model for the Earth's crust under the Ukrainian shield. Canadian Journal of Earth Sciences, **14**, pp. 2718–2728.

LANGEL, R. A. 1973. A study of high latitude magnetic disturbance. Technical Note BN-767, Institute for Fluid Dynamics and Applied Mathematics, University of Maryland, College Park, MD.

——— 1974. Near-Earth magnetic disturbance in total field at high latitudes 1. Summary of data from OGO 2, 4, and 6. Journal of Geophysical Research, **79**, pp. 2363–2371.

MAYHEW, M. A. 1978. A computer program for reduction of Pogo satellite magnetic anomaly data to common elevation and to the pole. Contract Report, NASA Contract NAS 5-41625-B.

——— 1979. Inversion of satellite magnetic anomaly data. Journal of Geophysics, **45**, pp. 119–128.

——— In preparation. Satellite-derived equivalent magnetization of the United States.

MEAD, G. D. 1979. An evaluation of recent internal field models. *In* Quantitative modeling of magnetospheric processes. *Edited by* W. P. Olson. Geophysics Monograph, **21**, pp. 110–117.

OVERTON, A. 1970. Seismic refraction surveys, western Queen Elizabeth Islands and polar continental margin. Canadian Journal of Earth Sciences, **7**, pp. 346–363.

PAKISER, L. C., and ZIETZ, I. 1965. Transcontinental crustal and upper mantle structure. Review of Geophysics, **3**, pp. 505–520.

PEDDIE, N. W., and FABIANO, E. B. 1976. A model of the geomagnetic field for 1975. Journal of Geophysical Research, **81**, pp. 2539–2542.

REGAN, R. D., and MARSH, B. D. In preparation. The Bangui anomaly: its geological origin.

REGAN, R. D., CAIN, J. C., and DAVIS, W. M. 1975. A global magnetic anomaly map. Journal of Geophysical Research, **80**, pp. 794–802.

RIDDIHOUGH, R. P., HAINES, G. V., and HANNAFORD, W. 1973. Regional magnetic anomalies of the Canadian Arctic. Canadian Journal of Earth Sciences, **10**, pp. 147–163.

SANDER, G. W., and OVERTON, A. 1965. Deep seismic refraction investigations in the Canadian Arctic archipelago. Geophysics, **30**, pp. 87–96.

SHUEY, R. T., SCHELLINGER, D. R., JOHNSON, E. H., and ALLEY, L. G. 1973. Aeromagnetics and the transition between the Colorado Plateau and the Basin Range province. Geology, **1**, pp. 107–110.

SWEENEY, J. F., COLES, R. L., DELAURIER, J. M., FORSYTH, D. A., IRVING, E., JUDGE, A., SOBCZAK, L. W., and WETMILLER, R. J. 1978. Arctic geophysical review—a summary. Publication of the Earth Physics Branch, Energy, Mines and Resources, Ottawa, Ont., **45**, pp. 101–108.

TAILLEUR, I. L. 1973. Probable rift origin of Canada Basin, Arctic Ocean. *In* Arctic geology. *Edited by* M. G. Pitcher. American Association of Petroleum Geology, Memoir 19, pp. 526–535.

TAYLOR, P. T. 1978. Low-level aeromagnetic data across the western Arctic basin. Abstract. EOS, Transactions of the American Geophysical Union, **59**, p. 268.

VOGT, P. R., and AVERY, O. E. 1974. Tectonic history of the Arctic basins: partial solutions and unsolved mysteries. *In* Marine geology and oceanography of the Arctic seas. *Edited by* Y. Hermann. Springer-Verlag, New York, NY, pp. 83–117.

VOGT, P. R., and OSTENSO, N. A. 1970. Magnetic and gravity profiles across the Alpha Cordillera and their relations to arctic sea floor spreading. Journal of Geophysical Research, **75**, pp. 4925–4937.

VOGT, P. R., TAYLOR, P. T., KOVACS, L. C., and JOHNSON, G. L. 1979. Detailed aeromagnetic investigation of the Arctic basin. Journal of Geophysical Research, **84**, pp. 1071–1089.

ZIETZ, I., KING, E. R., GEDDES, W., and LIDIAK, E. G. 1966. Crustal study of a continental strip from the Atlantic Ocean to the Rocky Mountains. Geological Society of America Bulletin, **77**, pp. 1427–1448.

Appendix

The spherical harmonic analysis used to represent the Earth's main field in this study is designated Pogo(02/72). The data set utilized in the derivation

TABLE A1. Pogo (02/72) coefficients, epoch 1960

n	m	g_n^m	h_n^m	$\dot{g}_n^m$	$\dot{h}_n^m$	n	m	g_n^m	h_n^m	$\dot{g}_n^m$	$\dot{h}_n^m$
1	0	−30456.2	0.0	23.47	0.0	9	8	10.3	4.7	−1.09	−1.09
1	1	−2180.3	5819.0	12.67	−8.84	9	9	−6.5	8.6	1.45	−1.06
2	0	−1546.2	0.0	−23.09	0.0	10	0	−2.1	0.0	0.05	0.0
2	1	2996.2	−1994.0	0.53	−4.20	10	1	−1.7	3.5	−0.14	−0.17
2	2	1605.2	203.2	−2.19	−17.71	10	2	1.5	0.3	0.05	0.07
3	0	1304.8	0.0	−2.29	0.0	10	3	−4.1	0.3	−0.05	0.17
3	1	−1982.6	−443.9	−11.86	8.18	10	4	−3.4	4.8	0.22	0.14
3	2	1305.6	222.6	−2.08	3.02	10	5	9.3	−2.7	−0.42	−0.14
3	3	886.7	−156.7	−5.50	−2.99	10	6	5.7	2.2	−0.12	−0.20
4	0	961.4	0.0	−1.11	0.0	10	7	2.8	−5.4	−0.33	0.38
4	1	811.7	136.7	−1.15	2.96	10	8	0.6	8.7	−0.04	−0.67
4	2	496.7	−276.6	−2.69	0.96	10	9	0.9	−7.0	0.39	0.91
4	3	−381.7	16.2	−1.05	0.54	10	10	4.0	−9.3	−0.48	0.63
4	4	264.5	−259.9	−2.66	−1.39	11	0	2.4	0.0	0.01	0.0
5	0	−222.7	0.0	0.89	0.0	11	1	−0.2	1.3	−0.09	0.01
5	1	358.9	11.7	0.30	0.98	11	2	−1.9	2.6	0.00	0.04
5	2	242.9	118.4	1.52	1.75	11	3	5.0	−1.8	−0.17	−0.00
5	3	−28.1	−111.4	−0.97	−2.99	11	4	−2.4	−4.2	0.20	−0.19
5	4	−140.6	−101.2	−2.37	0.84	11	5	−1.2	1.5	0.18	0.14
5	5	−95.2	119.1	4.86	−3.81	11	6	−4.0	−3.9	0.47	0.54
6	0	46.0	0.0	−0.02	0.0	11	7	3.7	−1.0	−0.28	−0.05
6	1	59.1	−9.0	0.32	−0.21	11	8	−0.0	−3.0	0.33	0.44
6	2	−0.1	−106.8	1.36	−0.46	11	9	−0.7	−5.3	−0.26	0.37
6	3	−243.2	61.5	2.83	1.28	11	10	−3.6	−3.8	0.80	0.36
6	4	−3.3	−26.5	0.58	−1.42	11	11	5.4	−8.7	−0.28	1.28
6	5	−0.1	−20.3	0.11	1.59	12	0	−0.5	0.0	−0.15	0.0
6	6	−102.1	−4.4	−1.01	0.30	12	1	0.3	1.1	−0.03	−0.08
7	0	71.1	0.0	−0.15	0.0	12	2	0.4	0.1	−0.13	0.05
7	1	−51.6	−52.9	−0.29	−1.68	12	3	0.2	1.9	−0.02	0.03
7	2	3.9	−27.3	−0.32	0.18	12	4	1.6	0.3	−0.15	−0.10
7	3	12.3	−7.2	0.28	0.11	12	5	0.4	−0.6	0.02	0.04
7	4	−39.9	1.4	1.85	1.01	12	6	0.1	0.4	−0.11	−0.02
7	5	0.9	17.6	−0.46	0.36	12	7	−2.3	−1.3	0.20	0.13
7	6	−4.0	−35.1	2.25	1.80	12	8	0.7	−1.3	−0.04	0.25
7	7	39.7	−47.5	−5.78	4.11	12	9	0.3	2.7	−0.13	−0.30
8	0	8.9	0.0	0.36	0.0	12	10	−0.5	−0.6	0.06	−0.07
8	1	3.9	11.1	0.24	−0.35	12	11	−4.4	4.8	0.44	−0.55
8	2	−4.6	−12.7	0.41	−0.20	12	12	−5.4	−4.6	0.80	0.40
8	3	−11.0	8.8	−0.01	−0.48	13	0	1.1	0.0	−0.10	0.0
8	4	−0.3	−15.4	−0.51	−0.34	13	1	0.7	1.8	−0.15	−0.23
8	5	6.2	8.1	0.04	−0.36	13	2	0.7	0.7	−0.00	−0.05
8	6	−5.5	19.6	0.34	0.14	13	3	−0.6	0.6	0.00	0.06
8	7	12.3	6.1	−0.01	−1.44	13	4	1.0	−0.3	−0.09	0.00
8	8	−6.8	−35.1	1.49	2.05	13	5	0.7	−0.7	−0.03	0.08
9	0	11.4	0.0	−0.31	0.0	13	6	0.9	0.9	−0.13	−0.19
9	1	7.8	−22.0	0.12	−0.08	13	7	−1.0	−0.2	0.10	0.09
9	2	3.4	14.7	−0.26	−0.01	13	8	0.8	0.1	−0.16	−0.10
9	3	−12.3	2.1	0.01	0.42	13	9	2.2	0.3	−0.20	0.06
9	4	17.0	1.2	−0.73	−0.51	13	10	3.5	3.6	−0.49	−0.45
9	5	1.2	−1.7	−0.22	−0.25	13	11	−1.5	6.9	0.17	−0.79
9	6	8.1	18.5	−1.15	−1.30	13	12	−8.5	−6.2	0.88	0.63
9	7	−9.1	18.2	1.70	−0.90	13	13	3.3	−11.4	−0.15	1.14

NOTE: Units are nT and nT/year.

of this field model is identical to that used for the Pogo(08/71) field model (Langel 1973, 1974) except that no data from 1970 were used in the derivation of Pogo(02/72). The fitting procedure used 47 485 data points that were fit with the coefficients given in Table A1 to a root mean square residual of 6.2 nT. The distribution of residuals is given in Table A2, and pertinent statistics relative to data from the three satellites in Table A3.

The model generation assumed a spheroidal Earth with mean radius of 6371.0 km, equatorial radius of 6378.16 km, and a flattening factor of 1/298.25.

Because it was not designed as a predictive

TABLE A2. Distribution of residuals

Range (nT)	−60 to −50	−50 to −40	−40 to −30	−30 to −20	−20 to −10	−10 to 0	0 to 10	10 to 20	20 to 30	30 to 40
Number of points	2	4	25	216	2562	19 113	23 692	1831	28	2

TABLE A3. Statistics for OGO 2, OGO 4, and OGO 6

	Number of points	RMS (nT)	Mean (nT)	Standard deviation about mean (nT)
OGO 2	12 773	5.17	0.263	5.16
OGO 4	18 431	6.80	0.088	6.80
OGO 6	16 281	6.25	−0.063	6.21

model, Pogo(02/72) does not include data from observatories to aid in determination of the secular variation. It is, however, suitable for some uses at times past 1971. Mead (1979) has recently evaluated four field models for the epoch 1973–1976, well past the time span of the data utilized to create the models. The models evaluated were Pogo(08/71), IGS/75 (Barraclough *et al.* 1975), AWC/75 (Peddie and Fabiano 1976), and IGRF 1975 (IAGA 1976). He concluded that the first three were all about equally accurate and much superior to IGRF 1975. Both AWC/75 and IGS/75 are slightly better than Pogo(08/71). An extension of Mead's result shows that Pogo(02/72) is of comparable accuracy to Pogo(08/71) for the interval 1973–1976.

5/9/80
HKA

NSDF datasets

main heading:

OGO SERIES ~~SCALAR~~ SCALAR MAGNETOMETER DATA, SELECTED

Dataset names:

A (1) LOW-LAT~~ITUDE~~ ~~DATA~~ DATA USED IN ~~GODDARD~~ GSFC MAGNETIC ANOMALY MAP

B (2) HIGH-LA~~TITUDE~~ DATA USED IN ~~GODDARD~~ GSFC MAGNETIC ANOMALY MAP

C (3) LOW-LAT~~ITUDE~~ AVE. ~~2x2 DEG~~ ~~ANO~~ ANOMALY FIELD + EQUIV. SOURCE ANOMALY FIELD

D (4) SELECTED POGO DATASET

We should perhaps obtain models POGO 2/72 and POGO 2/79 ?

What is title and number of (5)? (see attached page)

5/9/80
HKH

As noted in Magsat Bulletin NO. 4, paragraph "Availability of POGO DATA TO INVESTIGATORS"

(1) all global data used in Goddard mag. anomaly map between 50°N + 50°S

2 tapes OGO. LOWLAT. ASCEND (i.e. northbound)
& . DSCEND (i.e. southbound)

(2) some for N. + S. polar areas (above 50° N. +S.)

2 tapes OGO. HIGH LAT. NORTH
, SOUTH

(3) (2°) average anomaly field (+ equiv source anomaly field) (low lat., -50° → +50°)

1 tape OGO. LOWLAT. AVERAGE

[notes in parentheses not given in Magsat Bulletin]

(4) Data utilized in GSFC field modeling

SELECTED POGO DATASET

5) MGST (3/80 (-2))

forget this.

INFORMATION SHEET FOR INCOMING DATA

DATE DATA RECEIVED: _____

NSSDC ID: _____ DATE NSDF COORDINATOR CONSULTED: _____

DATE SCIENTIST NOTIFIED: _____

SOURCE:	MATERIAL RECEIVED: (NUMBER OF SHEETS OF HARDCOPY, NUMBER 100' REELS MICROFILM, NUMBER OF MAGNETIC TAPES, ETC.)
PI AND AFFILIATION:	

SATELLITE NAME/NSDF NAME: _____

EXPERIMENT NAME: _____

DATA SET FULL NAME: _____

CONTACT: _____ ACQUISITION SCIENTIST: _____

FORM THAT WILL BE ANNOUNCED IN AIM/NSDF: _____

THESE ARE: ☐ A NEW DATA SET ☐ ADDITIONS ☐ REPLACEMENTS ☐ OTHER (EXPLAIN BELOW)

ACCESSION UNIT NUMBERS: _____

REMARKS:

DATA RECEIPT NOTIFICATION SENT? ☐

_____

DATA TECHNICIAN

INFORMATION SHEET FOR INCOMING DATA

DATE DATA RECEIVED: _____

NSSDC ID: _____ DATE NSDF COORDINATOR CONSULTED: _____

DATE SCIENTIST NOTIFIED: _____

SOURCE: LANGEL	MATERIAL RECEIVED: (NUMBER OF SHEETS OF HARDCOPY, NUMBER 100' REELS MICROFILM, NUMBER OF MAGNETIC TAPES, ETC.)
PI AND AFFILIATION:	

SATELLITE NAME/NSDF NAME: _____

EXPERIMENT NAME: _____

DATA SET FULL NAME: _____

CONTACT: _____ ACQUISITION SCIENTIST: _____

FORM THAT WILL BE ANNOUNCED IN AIM/NSDF: _____

THESE ARE: ☐ A NEW DATA SET ☐ ADDITIONS ☐ REPLACEMENTS ☐ OTHER (EXPLAIN BELOW)

ACCESSION UNIT NUMBERS: _____

REMARKS:

DATA RECEIPT NOTIFICATION SENT? ☐

_____

DATA TECHNICIAN

INFORMATION SHEET FOR INCOMING DATA

NSSDC ID: _____

DATE DATA RECEIVED: _____

DATE NSDF COORDINATOR CONSULTED: _____

DATE SCIENTIST NOTIFIED: _____

SOURCE: LANGEL	MATERIAL RECEIVED: (NUMBER OF SHEETS OF HARDCOPY, NUMBER 100' REELS MICROFILM, NUMBER OF MAGNETIC TAPES, ETC.)
PI AND AFFILIATION:	

SATELLITE NAME/NSDF NAME: _____

EXPERIMENT NAME: _____

DATA SET FULL NAME: _____

CONTACT: _____ ACQUISITION SCIENTIST: _____

FORM THAT WILL BE ANNOUNCED IN AIM/NSDF: _____

THESE ARE: ☐ A NEW DATA SET ☐ ADDITIONS ☐ REPLACEMENTS ☐ OTHER (EXPLAIN BELOW)

ACCESSION UNIT NUMBERS: _____

REMARKS:

DATA RECEIPT NOTIFICATION SENT? ☐

_____

DATA TECHNICIAN

INFORMATION SHEET FOR INCOMING DATA

NSSDC ID: _____

DATE DATA RECEIVED: _____

DATE NSDF COORDINATOR CONSULTED: _____

DATE SCIENTIST NOTIFIED: _____

SOURCE: LANGEL	MATERIAL RECEIVED: (NUMBER OF SHEETS OF HARDCOPY, NUMBER 100' REELS MICROFILM, NUMBER OF MAGNETIC TAPES, ETC.)
PI AND AFFILIATION:	

SATELLITE NAME/NSDF NAME: _____

EXPERIMENT NAME: _____

DATA SET FULL NAME: _____

CONTACT: _____ ACQUISITION SCIENTIST: _____

FORM THAT WILL BE ANNOUNCED IN AIM/NSDF: _____

THESE ARE: ☐ A NEW DATA SET ☐ ADDITIONS ☐ REPLACEMENTS ☐ OTHER (EXPLAIN BELOW)

ACCESSION UNIT NUMBERS: _____

REMARKS:

DATA RECEIPT NOTIFICATION SENT? ☐

_____

DATA TECHNICIAN

4/9/81

HKH has descriptions of these 4 datasets, but they are not in serial form.

```
IEF285I   SYS1.DUMMY                                      KEPT          DDNAME=SYSLIB  -1              0 EXCPS
IEF285I   VOL SER NOS= K3ITL5.
IEF285I   SYS1.DUMMY                                      KEPT          DDNAME=SYSLIB  -2              0 EXCPS
IEF285I   VOL SER NOS= K3ITL5.
IEF285I   SYS1.FORTLIB                                    KEPT          DDNAME=SYSLIB  -3             54 EXCPS
IEF285I   VOL SER NOS= K3ITL0.
IEF285I   SYS2.FORTLIB                                    KEPT          DDNAME=SYSLIB  -4             12 EXCPS
IEF285I   VOL SER NOS= K3SYS2.
IEF285I   SYS1.PL1LIB                                     KEPT          DDNAME=SYSLIB  -5              0 EXCPS
IEF285I   VOL SER NOS= K3ITL5.
IEF285I   SYS1.FORTSSP                                    KEPT          DDNAME=SYSLIB  -6              0 EXCPS
IEF285I   VOL SER NOS= K3ITL5.
IEF285I   SYS2.COBLIB                                     KEPT          DDNAME=SYSLIB  -7              0 EXCPS
IEF285I   VOL SER NOS= M2SYS1.
IEF285I   SYS1.ALGLIB                                     KEPT          DDNAME=SYSLIB  -8              0 EXCPS
IEF285I   VOL SER NOS= K3SYS2.
IEF285I   SYS80246.T192445.RV000.YZRWPRP2.LODMOD          PASSED        DDNAME=SYSLMOD                29 EXCPS
IEF285I   VOL SER NOS= K3SCR2.
IEF285I   SYS80246.T192445.SV000.YZRWPRP2.R0000035        SYSOUT        DDNAME=SYSPRINT                2 EXCPS
IEF285I   VOL SER NOS= K3SCR5.
IEF285I   SYS80246.T192445.SV000.YZRWPRP2.R0000036        SYSOUT        DDNAME=SYSTERM                 1 EXCPS
IEF285I   VOL SER NOS= K3SCR2.
IEF285I   SYS80246.T192445.RV000.YZRWPRP2.P0000037        DELETED       DDNAME=SYSUT1                 24 EXCPS
IEF285I   VOL SER NOS= K3SCR4.
IEF285I   SYS80246.T192445.RV000.YZRWPRP2.S0000038        SYSIN         DDNAME=SYSLIN  -1              3 EXCPS
IEF285I   VOL SER NOS= K3SCR3.
IEF285I   SYS80246.T192445.RV000.YZRWPRP2.S0000038        DELETED       DDNAME=SYSLIN  -1              3 EXCPS
IEF285I   VOL SER NOS= K3SCR3.
IEF285I   SYS80246.T192445.SV000.YZRWPRP2.R0000039        DELETED       DDNAME=SYSABEND                0 EXCPS
IEF285I   VOL SER NOS= K3SCR5.
IEF373I STEP /LINK    / START 80246.2003
IEF374I STEP /LINK    / STOP  80246.2003 CPU    0MIN 00.84SEC MAIN 130K LCS    0K
- STEP 01 -     RETURN CODE = 0000                                  STEP TIME =      .20 MINS=(CPU=      .01,IO=      .19)
                                  IO IN SECS. DISK=    11.40,DRUM=      .00,TAPE=      .00,CELL=      .00,CTHR=      .13
- SURCHARGES=(DRIVES ALOC=000,TAPE MOUNTS=000,CORE=000,PAPER=000,PRIORITY=00000)SECS.    TOTAL STP TIME=      .20 MINS.  -
      XXGO       EXEC PGM=*.LINK,SYSLMOD,COND=(4,LT),REGION=70K                          00000260
      XXFT05F001 DD  DDNAME=DATA5                                                        00000270
      XXFT06F001 DD SYSOUT=&OUT,DCB=(RECFM=VBA,LRECL=137,BLKSIZE=&BLKSIZE)               00000280
      IEF653I SUBSTITUTION JCL - SYSOUT=A,DCB=(RECFM=VBA,LRECL=137,BLKSIZE=7265)
      XXFT07F001 DD SYSOUT=B,DCB=(RECFM=FB,BLKSIZE=7280,LRECL=80)                        00000290
      XXSYSPRINT DD SYSOUT=&OUT,DCB=(RECFM=VBA,LRECL=137,BLKSIZE=&BLKSIZE),              00000300
      IEF663I SUBSTITUTION JCL - SYSOUT=A,DCB=(RECFM=VBA,LRECL=137,BLKSIZE=7265),
      XX             SPACE=(CYL,(0,1)),UNIT=(DISK,3)                                     00000310
      XXSYSUDUMP DD SYSOUT=A,SPACE=(CYL,(0,5))                                           00000320
      //GO.FT08F001 DD UNIT=6250,DISP=(OLD,KEEP),LABEL=(1,BLP,,IN),
      //         DCB=(BLKSIZE=32000,RECFM=U,DEN=4),
      //         VOL=SER=JJ0020
      //GO.DATA5 DD *
      //
IEF236I ALLOC. FOR YZRWPRP2 GO
IEF237I 335   ALLOCATED TO PGM=*.DD
IEF237I 232   ALLOCATED TO FT05F001
IEF237I 237   ALLOCATED TO FT06F001
IEF237I 237   ALLOCATED TO FT07F001
IEF237I 232   ALLOCATED TO SYSPRINT
IEF237I 235   ALLOCATED TO SYSPRINT
IEF237I 237   ALLOCATED TO SYSPRINT
IEF237I 335   ALLOCATED TO SYSUDUMP
IEF237I 495   ALLOCATED TO FT08F001
```

5Φ IIA 039850
C-2/061

```
                                  RECORD      1   OF FILE    1
                                  LENGTH =     800   BYTES

    40404040  40E4E0F5  F4F04040  40404040  404040F6  40404040  4040F2F7  F6F34040  40404040  40F2F1F3   Header
    40404040  40F04BF1  F1F8F2F8  F1F5F440  40404040  40404040  40404040  40404040  40404040  40404040
    4040F34B  F9F8F9F2  4060F04B  F0F4F1F6  4040F04B  F0404040  4060F04B  F4F5F9F8  4040F04B  F2F7F9F1   Poly. fit
    4040F04B  F0404040  4060F54B  F1F3F7F5  4060F04B  F0F5F7F0  4040F04B  F0404040  40404040  40404040
    F7F8F5F6  F8F6F4F8  60F4F94B  F1F6F1F9  F3F5F44B  F0F3F9F3  F5F9F64B  F8F8F6F7  4060F04B  F4F4F1F4
    4060F04B  F5F7F3F6  40404040  404040F3  4040F04B  F0404040  4040F04B  F0404040  4040F24B  F4F6F5F1   DATA 1
    F7F8F5F7  F5F8F4F8  60F4F84B  F7F2F0F1  F3F5F44B  F1F5F4F1  F5F9F44B  F3F9F0F6  4060F04B  F5F9F7F7
    4060F04B  F4F7F6F4  40404040  404040F3  4040F04B  F0404040  4040F04B  F0404040  4040F24B  F2F3F6F9   } 2
    F7F8F5F8  F3F0F4F8  60F4F84B  F2F7F7F7  F3F5F44B  F2F6F6F6  F5F9F14B  F9F1F0F2  4060F04B  F1F7F5F8   } 3
    4060F04B  F3F7F5F2  40404040  404040F3  4040F04B  F0404040  4040F04B  F0404040  4040F24B  F5F8F6F8
                                                                                                        i
                                                                                                        N DTS
```

```
F7F8F5F9  F0F2F4F9  60F4F74B  F8F3F4F8  F3F5F44B  F3F7F6F7  F5F8F94B  F4F2F9F7  4060F04B  F0F5F0F8
4060F04B  F2F8F1F8  40404040  404040F3  4040F04B  F0404040  4040F04B  F0404040  4040F24B  F6F3F9F7
F7F8F5F9  F7F4F4F9  60F4F74B  F3F9F1F3  F3F5F44B  F4F8F4F6  F5F8F64B  F9F6F4F8  4040F04B  F7F2F6F6
4060F04B  F1F8F4F3  40404040  404040F3  4040F04B  F0404040  4040F04B  F0404040  4040F34B  F3F4F4F8
F7F8F6F0  F4F6F4F9  60F4F64B  F9F4F7F4  F3F5F44B  F5F9F0F3  F5F8F44B  F5F0F7F8  4060F04B  F2F3F4F4
4060F04B  F0F8F6F4  40404040  404040F3  4040F04B  F0404040  4040F04B  F0404040  4040F24B  F3F1F1F3
F7F8F6F1  F1F8F4F9  60F4F64B  F5F0F3F1  F3F5F44B  F6F9F3F8  F5F8F24B  F0F5F4F7  4040F04B  F8F2F4F2
4040F04B  F0F1F1F7  40404040  404040F3  4040F04B  F0404040  4040F04B  F0404040  4040F34B  F2F9F7F1
F7F8F6F1  F9F0F4F9  60F4F64B  F0F5F8F2  F3F5F44B  F7F9F5F2  F5F7F94B  F6F0F9F4  4060F04B  F5F1F1F7
4040F04B  F1F1F0F2  40404040  404040F3  4040F04B  F0404040  4040F04B  F0404040  4040F14B  F8F8F8F0
```

RECORD 37299 OF FILE 1
LENGTH = 480 BYTES

```
F6F8F2F0  F9F5F4F8  40F2F34B  F0F9F4F6  4040F14B  F7F1F5F9  F6F8F54B  F5F0F3F9  40F1F24B  F8F8F6F7
40F1F24B  F1F0F2F6  40404040  4040F2F3  4040F04B  F4F4F0F5  4060F04B  F2F0F2F2  4040F04B  F0404040
F6F8F2F1  F6F7F4F8  40F2F34B  F5F3F1F3  4040F14B  F7F5F8F3  F6F8F84B  F0F7F0F3  40F1F14B  F9F9F6F1
40F1F14B  F6F8F3F7  40404040  4040F2F3  4060F04B  F0F2F8F6  4060F04B  F7F0F2F5  4040F04B  F0404040
F6F8F2F2  F3F9F4F8  40F2F34B  F9F6F7F6  4040F14B  F8F0F1F1  F6F9F04B  F6F4F8F4  40F1F24B  F6F6F4F1
40F1F14B  F2F6F2F8  40404040  4040F2F3  4040F14B  F0F6F3F0  4040F04B  F3F5F8F0  4040F04B  F0404040
F6F8F2F3  F1F1F4F8  40F2F44B  F4F0F3F5  4040F14B  F8F4F4F3  F6F9F34B  F2F3F0F5  40F1F14B  F9F5F7F0
40F1F04B  F8F4F0F1  40404040  4040F2F3  4040F04B  F7F8F1F4  4040F04B  F0F4F5F2  4040F04B  F0404040
F6F8F2F3  F8F3F4F8  40F2F44B  F8F3F9F1  4040F14B  F8F8F8F0  F6F9F54B  F8F0F0F8  40F1F14B  F1F7F5F8
40F1F04B  F4F1F6F0  40404040  4040F2F3  4040F04B  F4F2F6F8  4060F04B  F3F4F0F4  4040F04B  F0404040
F6F8F2F4  F5F5F4F8  40F2F54B  F2F7F4F2  4040F14B  F9F3F2F2  F6F9F84B  F3F8F2F8  40F1F04B  F8F5F9F4
4040F94B  F9F9F0F9  40404040  4040F2F3  4040F04B  F5F3F8F3  4040F04B  F0404040  4040F04B  F0404040
```

37299 RECORDS IN FILE 1 OF TAPE

```
IEF142I - STEP WAS EXECUTED - COND CODE 0000
IEF285I   SYS80246.T192445.RV000.YZRWPRP2.LODMOD        PASSED          DDNAME=PGM=*.DD                0 EXCPS
IEF285I   VOL SER NOS= K3SCR2.
IEF285I   SYS80246.T192445.RV000.YZRWPRP2.S0000045      SYSIN           DDNAME=FT05F001                2 EXCPS
IEF285I   VOL SER NOS= K3SCR3.
IEF285I   SYS80246.T192445.RV000.YZRWPRP2.S0000045      DELETED         DDNAME=FT05F001                2 EXCPS
IEF285I   VOL SER NOS= K3SCR3.
IEF285I   SYS80246.T192445.SV000.YZRWPRP2.R0000040      SYSOUT          DDNAME=FT06F001                1 EXCPS
IEF285I   VOL SER NOS= K3SCR4.
IEF285I   SYS80246.T192445.SV000.YZRWPRP2.R0000041      DELETED         DDNAME=FT07F001                0 EXCPS
IEF285I   VOL SER NOS= K3SCR4.
IEF285I   SYS80246.T192445.SV000.YZRWPRP2.R0000042      DELETED         DDNAME=SYSPRINT                0 EXCPS
IEF285I   VOL SER NOS= K3SCR3.
IEF285I   SYS80246.T192445.SV000.YZRWPRP2.R0000043      DELETED         DDNAME=SYSUDUMP                0 EXCPS
IEF285I   VOL SER NOS= K3SCR2.
IEF285I   SYS80246.T192445.RV000.YZRWPRP2.R0000044      KEPT            DDNAME=FT08F001           74,602 EXCPS
IEF285I   VOL SER NOS= JJ0020.
IEF280F K 495,JJ0020,YZRWPRP2,GO
IEF373I STEP /GO       / START 80246.2003
IEF374I STEP /GO       / STOP  80246.2011 CPU    1MIN 04.14SEC MAIN 186K LCS    0K
- STEP 02 -      RETURN CODE = 0000                                STEP TIME =    13.52 MINS=(CPU=     1.06,IO=    12.46)
                                        IO IN SECS. DISK=     2.05,DRUM=      .00,TAPE=   746.14,CELL=      .00,OTHR=      .12
- SURCHARGES=(DRIVES ALOC=000,TAPE MOUNTS=000,CORE=000,PAPER=000,PRIORITY=00000)SECS.    TOTAL STP TIME=    13.52 MINS.  -
IEF285I   SYS80246.T192445.RV000.YZRWPRP2.LODMOD         DELETED
IEF285I   VOL SER NOS= K3SCR2.
IEF375I  JOB /YZRWPRP2/ START 80246.2003
IEF376I  JOB /YZRWPRP2/ STOP  80246.2011 CPU    1MIN 04.98SEC
-   SYSTEM=REL21.8F (04-01-79) K3                                                    TIME=20.11.39.60 DATE=09-02-80
- JOB 0310-                                                  TOTAL TIME =    13.73 MINS=(CPU=     1.08,IO=    12.65)
                                        IO IN SECS. DISK=    13.45,DRUM=      .00,TAPE=   746.14,CELL=      .00,OTHR=      .25
- SURCHARGES=(DRIVES ALOC=000,TAPE MOUNTS=000,CORE=000,PAPER=000,PRIORITY=00000)SECS.    TOTAL JOB TIME=    13.73 MINS.  -
  THERE WERE 01 TAPES MOUNTED FOR THIS JOB. TAPE MOUNT CHARGE WAS 00.0 MINUTES.
```

```
IEF285I    SYS1.DUMMY                                       KEPT            DDNAME=SYSLIB  -1              0 EXCPS
IEF285I    VOL SER NOS= K3ITL5.
IEF285I    SYS1.DUMMY                                       KEPT            DDNAME=SYSLIB  -2              0 EXCPS
IEF285I    VOL SER NOS= K3ITL5.
IEF285I    SYS1.FORTLIB                                     KEPT            DDNAME=SYSLIB  -3             54 EXCPS
IEF285I    VOL SER NOS= K3ITL0.
IEF285I    SYS2.FORTLIB                                     KEPT            DDNAME=SYSLIB  -4             12 EXCPS
IEF285I    VOL SER NOS= K3SYS2.
IEF285I    SYS1.PL1LIB                                      KEPT            DDNAME=SYSLIB  -5              0 EXCPS
IEF285I    VOL SER NOS= K3ITL5.
IEF285I    SYS1.FORTSSP                                     KEPT            DDNAME=SYSLIB  -6              0 EXCPS
IEF285I    VOL SER NOS= K3ITL5.
IEF285I    SYS2.COBLIB                                      KEPT            DDNAME=SYSLIB  -7              0 EXCPS
IEF285I    VOL SER NOS= M2SYS1.
IEF285I    SYS1.ALGLIB                                      KEPT            DDNAME=SYSLIB  -8              0 EXCPS
IEF285I    VOL SER NOS= K3SYS2.
IEF285I    SYS80242.T082546.RV000.YZRWPRP2.LODMOD           PASSED          DDNAME=SYSLMOD                29 EXCPS
IEF285I    VOL SER NOS= K3SCR2.
IEF285I    SYS80242.T082546.SV000.YZRWPRP2.R0000407         SYSOUT          DDNAME=SYSPRINT                2 EXCPS
IEF285I    VOL SER NOS= K3SCR5.
IEF285I    SYS80242.T082546.SV000.YZRWPRP2.R0000408         SYSOUT          DDNAME=SYSTERM                 1 EXCPS
IEF285I    VOL SER NOS= K3SCR3.
IEF285I    SYS80242.T082546.RV000.YZRWPRP2.R0000409         DELETED         DDNAME=SYSUT1                 24 EXCPS
IEF285I    VOL SER NOS= K3SCR3.
IEF285I    SYS80242.T082546.RV000.YZRWPRP2.S0000410         SYSIN           DDNAME=SYSLIN  -1              3 EXCPS
IEF285I    VOL SER NOS= K3SCR6.
IEF285I    SYS80242.T082546.RV000.YZRWPRP2.S0000410         DELETED         DDNAME=SYSLIN  -1              3 EXCPS
IEF285I    VOL SER NOS= K3SCR6.
IEF285I    SYS80242.T082546.SV000.YZRWPRP2.R0000411         DELETED         DDNAME=SYSABEND                0 EXCPS
IEF285I    VOL SER NOS= K3SCR2.
IEF373I STEP /LINK    / START 80242.2120
IEF374I STEP /LINK    / STOP  80242.2120 CPU    0MIN 00.80SEC MAIN 130K LCS    0K
- STEP 01 -      RETURN CODE = 0000                                  STEP TIME =      .20 MINS=(CPU=      .01,IC=      .19)
                                    IO IN SECS. DISK=    11.40,DRUM=      .00,TAPE=      .00,CELL=      .00,CIHR=      .12
- SURCHARGES=(DRIVES ALOC=000,TAPE MOUNTS=000,CORE=000,PAPER=000,PRIORITY=00000)SECS.    TOTAL STP TIME=      .20 MINS.  -
      XXGO     EXEC PGM=*.LINK.SYSLMOD,COND=(4,LT),REGION=70K                                    00000260
      XXFT05F001 DD  DDNAME=DATA5                                                                00000270
      XXFT06F001 DD SYSOUT=&OUT,DCB=(RECFM=VBA,LRECL=137,BLKSIZE=&BLKSIZE)                       00000280
      IEF653I SUBSTITUTION JCL - SYSOUT=A,DCB=(RECFM=VBA,LRECL=137,BLKSIZE=7265)
      XXFT07F001 DD SYSOUT=B,DCB=(RECFM=FB,BLKSIZE=7280,LRECL=80)                                00000290
      XXSYSPRINT DD SYSOUT=&OUT,DCB=(RECFM=VBA,LRECL=137,BLKSIZE=&BLKSIZE),                      00000300
      XX               SPACE=(CYL,(0,1)),UNIT=(DISK,3)                                           00000310
      XXSYSUDUMP DD SYSOUT=A,SPACE=(CYL,(0,5))                                                   00000320
      //GO.FT08F001 DD UNIT=6250,DISP=(OLD,KEEP),LABEL=(1,BLP,,IN),
      //         DCB=(BLKSIZE=32000,RECFM=U,DEN=4),
      //           VOL=SER=JJ0015
      //GO.DATA5 DD *
      //
IEF236I ALLOC. FOR YZRWPRP2 GO
IEF237I 335    ALLOCATED TO PGM=*.DD
IEF237I 235    ALLOCATED TO FT05F001
IEF237I 232    ALLOCATED TO FT06F001
IEF237I 232    ALLOCATED TO FT07F001
IEF237I 235    ALLOCATED TO SYSPRINT
IEF237I 232    ALLOCATED TO SYSPRINT
IEF237I 237    ALLOCATED TO SYSPRINT
IEF237I 335    ALLOCATED TO SYSUDUMP
IEF237I 497    ALLOCATED TO FT08F001
```

S0111A D 39851

C 21062

<

```
                                    RECORD      1  OF FILE   1
                                    LENGTH =     800  BYTES

    40404040  40F4F0F2  F2F14040  40404040  404040F4  40404040  4040F7F6  F1F04040  40404040  4040F8F8
    40404040  40F04EF0  F0F2F8F9  F2F1F740  40404040  40404040  40404040  40404040  40404040  40404040
    4040F04B  F0404040  4040F04B  F0404040  4040F04B  F0404040  4040F04B  F0404040  4040F04B  F0404040
    4040F04B  F0404040  4060F14B  F9F9F6F6  4060F04B  F0F8F9F4  4040F04B  F0404040  40404040  40404040
    F1F0F8F0  F7F1F2F6  4060F74B  F2F2F8F6  4040F04B  F0F0F2F9  F4F8F64B  F0F1F5F6  4040F44B  F1F8F7F5
    4040F44B  F1F8F4F0  40404040  4040F1F3  4040F04B  F0404040  4040F04B  F0404040  4040F143  F3F5F3F8
    F1F0F8F1  F4F1F2F6  4060F74B  F6F7F9F6  4040F04B  F0F0F5F5  F4F8F74B  F3F4F7F7  4040F34B  F8F0F4F7
    4040F44B  F1F9F3F8  40404040  4040F1F3  4040F04B  F0404040  4040F04B  F0404040  4040F04B  F9F2F0F8
    F1F0F8F2  F1F1F2F6  4060F84B  F1F3F0F3  4040F04B  F0F0F8F2  F4F8F84B  F6F9F5F3  4040F34B  F0F9F7F7
    4040F44B  F2F0F6F7  40404040  4040F1F3  4040F04B  F0404040  4040F04B  F0404040  4040F04B  F1F6F2F6
```

```
F1F0F8F2  F8F1F2F6  4060F84B  F5F8F0F8  4040F04B  F0F1F0F9  F4F9F04B  F0F4F6F9  4040F24B  F9F0F2F3
4040F44B  F2F1F6F7  40404040  4040F1F3  4040F04B  F0404040  4040F04B  F0404040  4060F04B  F0F8F5F0
F1F0F8F3  F5F1F2F6  4060F94B  F0F3F1F2  4040F04B  F0F1F3F7  F4F9F14B  F4F1F0F2  4040F34B  F1F4F4F5
4040F44B  F2F2F9F7  40404040  4040F1F3  4040F04B  F0404040  4040F04B  F0404040  4040F04B  F1F0F3F9
F1F0F8F4  F2F1F2F6  4060F84B  F4F8F1F3  4040F04B  F0F1F6F6  F4F9F24B  F7F8F9F1  4040F24B  F6F3F2F8
4040F44B  F2F4F3F7  40404040  4040F1F3  4040F04B  F0404040  4040F04B  F0404040  4060F04B  F4F6F2F1
F1F0F8F4  F9F1F2F6  4060F94B  F9F3F1F3  4040F04B  F0F1F9F5  F4F9F44B  F1F6F8F0  4040F24B  F5F3F9F1
4040F44B  F2F5F8F8  40404040  4040F1F3  4040F04B  F0404040  4040F04B  F0404040  4060F04B  F6F1F1F2
F1F0F8F5  F6F1F2F6  60F1F04B  F3F8F1F0  4040F04B  F0F2F2F5  F4F9F54B  F5F5F4F7  4040F24B  F1F9F9F2
4040F44B  F2F7F4F9  40404040  4040F1F3  4040F04B  F0404040  4040F04B  F0404040  4060F14B  F0F0F7F3
```

<

RECORD 38936 OF FILE 1
LENGTH = 720 BYTES

```
F7F4F9F9  F8F6F5F2  40F3F44B  F9F8F3F9  4040F04B  F8F8F6F6  F4F6F24B  F1F4F4F5  4060F24B  F8F3F9F8
4060F24B  F4F6F6F9  40404040  4040F2F0  4060F04B  F2F6F4F6  4040F04B  F0404040  4040F04B  F0404040
F7F5F0F0  F5F6F5F2  40F3F44B  F9F8F3F9  4040F04B  F8F8F6F6  F4F6F24B  F1F4F4F5  4060F24B  F8F3F9F8
4060F24B  F6F7F6F5  40404040  4040F2F0  4060F04B  F2F5F3F8  4040F04B  F0404040  4040F04B  F0404040
F7F5F0F1  F2F6F5F2  40F3F44B  F0F7F6F3  4040F04B  F9F2F0F9  F4F5F94B  F8F4F7F7  4060F34B  F3F5F9F4
4060F24B  F8F8F7F7  40404040  4040F2F0  4060F04B  F3F7F0F2  4040F04B  F0404040  4040F04B  F0404040
F7F5F0F1  F9F6F5F2  40F3F34B  F6F2F2F3  4040F04B  F9F3F7F3  F4F5F84B  F7F1F0F9  4060F44B  F5F3F9F1
4060F34B  F1F0F0F6  40404040  4040F2F0  4060F14B  F3F4F0F5  4040F04B  F0404040  4040F04B  F0404040
F7F5F0F2  F6F6F5F2  40F3F34B  F1F6F8F0  4040F04B  F9F5F3F3  F4F5F74B  F5F5F7F7  4060F443  F5F2F3F4
4060F34B  F3F1F5F0  40404040  4040F2F0  4060F14B  F1F1F4F0  4040F04B  F0404040  4040F04B  F0404040
F7F5F0F3  F3F6F5F2  40F3F24B  F7F1F3F5  4040F04B  F9F6F8F8  F4F5F64B  F4F9F6F1  4060F443  F3F5F9F4
4060F34B  F5F3F0F9  40404040  4040F2F0  4060F04B  F7F3F7F5  4040F04B  F0404040  4040F043  F0404040
F7F5F0F4  F0F6F5F2  40F3F24B  F2F5F8F8  4040F04B  F9F8F3F9  F4F5F54B  F4F0F2F3  4060F443  F3F3F2F0
4060F34B  F7F4F8F2  40404040  4040F2F0  4060F04B  F4F9F6F3  4040F04B  F0404040  4040F04B  F0404040
F7F5F0F4  F7F6F5F2  40F3F14B  F8F0F3F9  4040F04B  F9F9F8F6  F4F5F44B  F3F2F0F3  4060F443  F8F0F4F7
4060F34B  F9F6F6F9  40404040  4040F2F0  4060F04B  F7F5F3F8  4040F04B  F0404040  4040F04B  F0404040
F7F5F0F5  F4F6F5F2  40F3F14B  F3F4F8F9  4040F14B  F0F1F2F8  F4F5F34B  F2F5F3F9  4060F54B  F0F3F1F3
4060F44B  F1F8F6F7  40404040  4040F2F0  4060F04B  F7F6F4F0  4040F04B  F0404040  4040F04B  F0404040
```

38936 RECORDS IN FILE 1 OF TAPE

<

```
IEF142I - STEP WAS EXECUTED - COND CODE 0000
IEF285I   SYS80242.T082546.RV000.YZRWPRP2.LODMOD        PASSED          DDNAME=PGM=*.DD                0 EXCPS
IEF285I   VOL SER NOS= K3SCR2.
IEF285I   SYS80242.T082546.RV000.YZFWPRP2.S0000417      SYSIN           DDNAME=FT05F001                2 EXCPS
IEF285I   VOL SER NOS= K3SCF6.
IEF285I   SYS80242.T082546.RV000.YZRWPRP2.S0000417      DELETED         DDNAME=FT05F001                2 EXCPS
IEF285I   VOL SER NOS= K3SCR6.
IEF285I   SYS80242.T082546.SV000.YZFWPRP2.R0000412      SYSOUT          DDNAME=FT06F001                1 EXCPS
IEF285I   VOL SER NOS= K3SCR3.
IEF285I   SYS80242.T082546.SV000.YZFWPRP2.R0000413      DELETED         DDNAME=FT07F001                0 EXCPS
IEF285I   VOL SER NOS= K3SCR3.
IEF285I   SYS80242.T082546.SV000.YZFWPRP2.R0000414      DELETED         DDNAME=SYSPRINT                0 EXCPS
IEF285I   VOL SER NOS= K3SCF6.
IEF285I   SYS80242.T082546.SV000.YZRWPRP2.R0000415      DELETED         DDNAME=SYSUDUMP                0 EXCPS
IEF285I   VOL SER NOS= K3SCR2.
IEF285I   SYS80242.T082546.RV000.YZRWPRP2.R0000416      KEPT            DDNAME=FT08F001           77,876 EXCPS
IEF285I   VOL SER NOS= JJ0015.
IEF280E K 497,JJ0015,YZRWPRP2,GO
IEF373I STEP /GO       / START 80242.2120
IEF374I STEP /GO       / STOP  80242.2133 CPU    0MIN 56.42SEC MAIN 186K LCS    0K
- STEP 02 -      RETURN CODE = 0000                                STEP TIME =    13.95 MINS=(CPU=      .94,IO=    13.01)
                                IO IN SECS. DISK=     2.15,DRUM=      .00,TAPE=   778.88,CEL_=      .00,OTHR=      .12
- SUPCHARGES=(DRIVES ALOC=000,TAPE MOUNTS=000,CORE=000,PAPER=000,PRIORITY=00000)SECS.    TOTAL STP TIME=    13.95 MINS.  -
IEF285I   SYS80242.T082546.RV000.YZFWPRP2.LODMOD         DELETED
IEF285I   VOL SER NOS= K3SCR2.
IEF375I  JOB /YZRWPRP2/ START 80242.2120
IEF376I  JOB /YZRWPRP2/ STOP  80242.2133 CPU    0MIN 57.22SEC
-  SYSTEM=REL21.8F (04-01-79) K3                                                    TIME=21.33.42.26 DATE=08-29-80
- JOB 0471-                                                  TOTAL TIME =    14.15 MINS=(CPU=      .95,IO=    13.20)
                                IO IN SECS. DISK=    13.55,DRUM=      .00,TAPE=   778.88,CELL=      .00,OTHR=      .25
- SUPCHARGES=(DRIVES ALOC=000,TAPE MOUNTS=000,CORE=000,PAPER=000,PRIORITY=00000)SECS.    TOTAL JOB TIME=    14.15 MINS.  -
 THERE WERE 01 TAPES MOUNTED FOR THIS JOB.  TAPE MOUNT CHARGE WAS 00.0 MINUTES.
```

```
IEF285I   SYS1.DUMMY                                      KEPT          DDNAME=SYSLIB  -1              0 EXCPS
IEF285I   VOL SER NOS= K3ITL5.
IEF285I   SYS1.DUMMY                                      KEPT          DDNAME=SYSLIB  -2              0 EXCPS
IEF285I   VOL SER NOS= K3ITL5.
IEF285I   SYS1.FORTLIB                                    KEPT          DDNAME=SYSLIB  -3             54 EXCPS
IEF285I   VOL SER NOS= K3ITL0.
IEF285I   SYS2.FORTLIB                                    KEPT          DDNAME=SYSLIB  -4             12 EXCPS
IEF285I   VOL SER NOS= K3SYS2.
IEF285I   SYS1.PL1LIB                                     KEPT          DDNAME=SYSLIB  -5              0 EXCPS
IEF285I   VOL SER NOS= K3ITL5.
IEF285I   SYS1.FORTSSP                                    KEPT          DDNAME=SYSLIB  -6              0 EXCPS
IEF285I   VOL SER NOS= K3ITL5.
IEF285I   SYS2.COBLIB                                     KEPT          DDNAME=SYSLIB  -7              0 EXCPS
IEF285I   VOL SER NOS= M2SYS1.
IEF285I   SYS1.ALGLIB                                     KEPT          DDNAME=SYSLIB  -8              0 EXCPS
IEF285I   VOL SER NOS= K3SYS2.
IEF285I   SYS80218.T104255.RV000.YZRWPRP2.LODMOD          PASSED        DDNAME=SYSLMOD                29 EXCPS
IEF285I   VOL SER NOS= K3SCR5.
IEF285I   SYS80218.T104255.SV000.YZRWPRP2.R0000001        SYSOUT        DDNAME=SYSPRINT                2 EXCPS
IEF285I   VOL SER NOS= K3SCR2.
IEF285I   SYS80218.T104255.SV000.YZRWPRP2.R0000002        SYSOUT        DDNAME=SYSTERM                 1 EXCPS
IEF285I   VOL SER NOS= K3SCR6.
IEF285I   SYS80218.T104255.RV000.YZRWPRP2.R0000003        DELETED       DDNAME=SYSUT1                 24 EXCPS
IEF285I   VOL SER NOS= K3SCR4.
IEF285I   SYS80218.T104255.RV000.YZRWPRP2.S0000004        SYSIN         DDNAME=SYSLIN  -1              3 EXCPS
IEF285I   VOL SER NOS= K3SCR4.
IEF285I   SYS80218.T104255.RV000.YZRWPRP2.S0000004        DELETED       DDNAME=SYSLIN  -1              3 EXCPS
IEF285I   VOL SER NOS= K3SCR4.
IEF285I   SYS80218.T104255.SV000.YZRWPRP2.R0000005        DELETED       DDNAME=SYSABEND                0 EXCPS
IEF285I   VOL SER NOS= K3SCR5.
IEF373I STEP /LINK     / START 80218.1050
IEF374I STEP /LINK     / STOP  80218.1051 CPU    0MIN 01.14SEC MAIN 130K LCS    0K
- STEP 01 -      RETURN CODE = 0000                                STEP TIME =      .20 MINS=(CPU=      .01,IO=      .19)
                                    IO IN SECS. DISK=    11.40,DRUM=      .00,TAPE=      .00,CELL=      .00,OTHR=      .13
- SURCHARGES=(DRIVES ALOC=000,TAPE MOUNTS=000,CORE=000,PAPER=000,PRIORITY=00000)SECS.    TOTAL STP TIME=      .20 MINS.  -
      XXGO       EXEC PGM=*.LINK,SYSLMOD,COND=(4,LT),REGION=70K                          00000260
      XXFT05F001 DD  DDNAME=DATA5                                                        00000270
      XXFT06F001 DD SYSOUT=&OUT,DCB=(RECFM=VBA,LRECL=137,BLKSIZE=&BLKSIZE)               00000280
      IEF653I SUBSTITUTION JCL - SYSOUT=A,DCB=(RECFM=VBA,LRECL=137,BLKSIZE=7265)
      XXFT07F001 DD SYSOUT=B,DCB=(RECFM=FB,BLKSIZE=7280,LRECL=80)                        00000290
      XXSYSPRINT DD SYSOUT=&OUT,DCB=(RECFM=VBA,LRECL=137,BLKSIZE=&BLKSIZE),              00000300
      IEF653I SUBSTITUTION JCL - SYSOUT=A,DCB=(RECFM=VBA,LRECL=137,BLKSIZE=7265),
      XX             SPACE=(CYL,(0,1)),UNIT=(DISK,3)                                     00000310
      XXSYSUDUMP DD SYSOUT=A,SPACE=(CYL,(0,5))                                           00000320
      //GO.FT08F001 DD UNIT=6250,DISP=(OLD,KEEP),LABEL=(1,BLP,,IN),
      //       DCB=(BLKSIZE=32000,RECFM=U,DEN=4),
      // VOL=SER=JJ0068
      //GO.DATA5 DD *
      //
IEF236I ALLOC. FOR YZRWPRP2 GO
IEF237I 336   ALLOCATED TO PGM=*.DD
IEF237I 237   ALLOCATED TO FT05F001
IEF237I 237   ALLOCATED TO FT06F001
IEF237I 237   ALLOCATED TO FT07F001
IEF237I 232   ALLOCATED TO SYSPRINT
IEF237I 235   ALLOCATED TO SYSPRINT
IEF237I 237   ALLOCATED TO SYSPRINT
IEF237I 336   ALLOCATED TO SYSUDUMP
IEF237I 490   ALLOCATED TO FT08F001
```

SØ-11 B D39852
C21037

<

RECORD   1 OF FILE   1
LENGTH =   800 BYTES

```
40404040  40F3F9F0  F5F14040  40404040  404040F1  40404040  40404040  F2F14040  40404040  40404040
40404040  40404040  40404040  40404040  40404040  40404040  40404040  40404040  40404040  40404040
F1F4F9F7  F4F1F1F2  40F6F84B  F8F6F4F8  4040F64B  F4F5F0F4  F5F9F54E  F9F6F3F1  40F4F0F6  F2F94BF0
40404040  4040F1F7  4040F24B  F0F7F6F7  4040F64B  F5F7F0F0  40404040  40404040  40404040  40404040
F1F4F9F9  F2F1F1F2  40F6F74B  F7F2F7F0  4040F64B  F7F6F1F5  F5F8F84B  F4F1F4E3  40F4F0F5  F3F148F5
40404040  4040F1F7  4040F04B  F9F7F8F0  4040F64B  F4F8F6F2  40404040  40404040  40404040  40404040
F1F5F0F0  F5F6F1F2  40F6F64B  F8F7F1F4  4040F64B  F9F7F1F7  F5F8F24B  F8F4F1F1  40F4F0F4  F5F54BF3
40404040  4040F1F7  4040F04B  F4F3F3F3  4040F64B  F4F2F8F0  40404040  40404040  40404040  40404040
F1F5F0F1  F0F1F1F2  40F6F64B  F5F8F5F8  4040F74B  F0F3F7F6  F5F8F14B  F0F0F0F7  40F4F0F4  F2F94BF3
40404040  4040F1F7  4040F04B  F4F2F2F3  4040F64B  F4F0F9F4  40404040  40404040  40404040  40404040
```

Header
Data 1)
2.
3
4
:
NPTS

```
F1F5F0F2  F3F6F1F2  40F6F54B  F7F2F7F8  4040F74B  F2F2F4F6  F5F7F54B  F5F2F7F3  40F4F0F3  F4F64BF3
40404040  4040F1F7  4060F04B  F8F7F6F3  4040F64B  F3F5F5F9  40404040  40404040  40404040  40404040
F1F5F0F3  F8F1F1F1  40F6F44B  F8F0F4F5  4040F74B  F4F0F8F4  F5F6F94B  F7F4F0F5  40F4F0F2  F5F84BF3
40404040  4040F1F7  4060F14B  F6F4F4F4  4040F64B  F3F0F1F9  40404040  40404040  40404040  40404040
F1F5F0F5  F1F6F1F1  40F6F34B  F9F4F3F0  4040F74B  F5F6F5F4  F5F6F44B  F4F2F9F0  40F4F0F1  F7F14BF3
40404040  4040F1F7  4060F24B  F1F8F5F2  4040F64B  F2F5F4F5  40404040  40404040  40404040  40404040
F1F5F0F6  F9F6F1F1  40F6F24B  F7F9F1F9  4040F74B  F7F5F5F4  F5F5F74B  F4F8F2F4  40F4F0F0  F5F14BF3
40404040  4040F1F7  4060F14B  F7F4F4F8  4040F64B  F1F9F5F4  40404040  40404040  40404040  40404040
F1F5F0F8  F3F1F1F1  40F6F14B  F9F2F6F7  4040F74B  F8F8F5F0  F5F5F24B  F3F6F1F8  40F3F9F9  F5F74BF0
40404040  4040F1F7  4060F14B  F3F6F7F7  4040F64B  F1F5F3F9  40404040  40404040  40404040  40404040
```

RECORD 6594 OF FILE 1
LENGTH = 800 BYTES

```
F5F7F7F4  F9F4F2F7  40F7F84B  F9F7F2F9  40F5F04B  F3F4F8F1  F5F3F94B  F0F1F1F2  40F4F4F5  F4F44BF0
40404040  4040F1F0  4060F34B  F2F3F1F1  40F2F14B  F3F6F9F8  40404040  40404040  40404040  40404040
F5F7F7F5  F2F0F1F9  40F7F94B  F0F8F5F3  40F5F04B  F9F7F1F9  F5F3F94B  F7F6F4F6  40F4F4F5  F5F94BF6
40404040  4040F1F0  4060F34B  F6F5F1F0  40F2F14B  F4F0F2F7  40404040  40404040  40404040  40404040
F5F7F7F5  F4F6F1F1  40F7F94B  F1F9F6F4  40F5F14B  F6F0F8F9  F5F4F04B  F5F1F5F6  40F4F4F5  F7F54BF9
40404040  4040F1F0  4060F24B  F8F9F9F1  40F2F14B  F4F3F5F7  40404040  40404040  40404040  40404040
F5F7F7F5  F7F2F0F3  40F7F94B  F3F0F6F0  40F5F24B  F2F5F8F5  F5F4F14B  F2F7F2F2  40F4F4F5  F5F04BF8
40404040  4040F1F0  4060F34B  F5F9F2F4  40F2F14B  F4F6F8F8  40404040  40404040  40404040  40404040
F5F7F7F6  F2F3F8F7  40F7F94B  F5F2F1F0  40F5F34B  F5F9F8F4  F5F4F24B  F7F8F2F2  40F4F4F6  F2F14BF3
40404040  4040F1F0  4060F34B  F5F1F8F2  40F2F14B  F5F3F5F3  40404040  40404040  40404040  40404040
F5F7F7F6  F4F9F7F9  40F7F94B  F6F2F6F3  40F5F44B  F2F8F8F8  F5F4F34B  F5F4F3F7  40F4F4F6  F3F74BF0
40404040  4040F1F0  4060F24B  F7F3F8F9  40F2F14B  F5F6F8F7  40404040  40404040  40404040  40404040
F5F7F7F7  F0F1F6F3  40F7F94B  F8F3F1F9  40F5F54B  F7F1F1F7  F5F4F54B  F0F6F3F5  40F4F4F6  F6F64BF0
40404040  4040F1F0  4060F24B  F6F8F4F3  40F2F14B  F6F3F5F7  40404040  40404040  40404040  40404040
F5F7F7F7  F2F7F5F5  40F7F94B  F9F3F2F3  40F5F64B  F4F4F4F3  F5F4F54B  F8F2F2F3  40F4F4F6  F8F04BF1
40404040  4040F1F0  4060F24B  F6F5F8F9  40F2F14B  F6F6F9F3  40404040  40404040  40404040  40404040
F5F7F7F7  F5F3F4F7  40F8F04B  F0F3F1F0  40F5F74B  F1F9F1F9  F5F4F64B  F5F9F0F1  40F4F4F6  F9F44BF2
40404040  4040F1F0  4060F24B  F3F9F1F3  40F2F14B  F7F0F3F0  40404040  40404040  40404040  40404040
F5F7F7F7  F8F5F1F5  40F8F04B  F1F4F9F1  40F5F84B  F1F2F5F2  F5F4F74B  F5F2F3F4  40F4F4F7  F8F94BF9
40404040  4040F1F0  4060F34B  F3F8F3F3  40F2F14B  F7F4F4F3  40404040  40404040  40404040  40404040
```



```
IEF142I - STEP WAS EXECUTED - COND CODE 0000
IEF285I   SYS80218.T104255.RV000.YZRWPRP2.LODMOD        PASSED          DDNAME=PGM=*.DD                0 EXCPS
IEF285I   VOL SER NOS= K3SCR5.
IEF285I   SYS80218.T104255.RV000.YZRWPRP2.S0000011      SYSIN           DDNAME=FT05F001                2 EXCPS
IEF285I   VOL SER NOS= K3SCR4.
IEF285I   SYS80218.T104255.RV000.YZRWPRP2.S0000011      DELETED         DDNAME=FT05F001                2 EXCPS
IEF285I   VOL SER NOS= K3SCR4.
IEF285I   SYS80218.T104255.SV000.YZRWPRP2.R0000006      SYSOUT          DDNAME=FT06F001                1 EXCPS
IEF285I   VOL SER NOS= K3SCR4.
IEF285I   SYS80218.T104255.SV000.YZRWPRP2.R0000007      DELETED         DDNAME=FT07F001                0 EXCPS
IEF285I   VOL SER NOS= K3SCR4.
IEF285I   SYS80218.T104255.SV000.YZRWPRP2.R0000008      DELETED         DDNAME=SYSPRINT                0 EXCPS
IEF285I   VOL SER NOS= K3SCR3.
IEF285I   SYS80218.T104255.SV000.YZRWPRP2.R0000009      DELETED         DDNAME=SYSUDUMP                0 EXCPS
IEF285I   VOL SER NOS= K3SCR5.
IEF285I   SYS80218.T104255.RV000.YZRWPRP2.R0000010      KEPT            DDNAME=FT08F001           13,192 EXCPS
IEF285I   VOL SER NOS= JJ0068.
IEF280E K 490,JJ0068,YZRWPRP2,GO
IEF373I STEP /GO      / START 80218.1051
IEF374I STEP /GO      / STOP  80218.1054 CPU    0MIN 13.79SEC MAIN 186K LCS    0K
- STEP 02 -     RETURN CODE = 0000
                                                    STEP TIME =     2.45 MINS=(CPU=      .22,IO=     2.23)
                                IO IN SECS. DISK=     2.05,DRUM=      .00,TAPE=   132.04,CELL=      .00,OTHR=      .12
- SURCHARGES=(DRIVES ALOC=000,TAPE MOUNTS=000,CORE=000,PAPER=000,PRIORITY=00000)SECS.    TOTAL STP TIME=     2.45 MINS.  -
IEF285I   SYS80218.T104255.RV000.YZRWPRP2.LODMOD        DELETED
IEF285I   VOL SER NOS= K3SCR5.
IEF375I  JOB /YZRWPRP2/ START 80218.1050
IEF376I  JOB /YZRWPRP2/ STOP  80218.1054 CPU    0MIN 14.93SEC
-   SYSTEM=REL21.8F (04-01-79) K3                                                TIME=10.54.56.70 DATE=08-05-80
                                                    TOTAL TIME =     2.66 MINS=(CPU=      .24,IO=     2.42)
                                IO IN SECS. DISK=    13.45,DRUM=      .00,TAPE=   132.04,CELL=      .00,OTHR=      .25
- SURCHARGES=(DRIVES ALOC=000,TAPE MOUNTS=000,CORE=000,PAPER=000,PRIORITY=00000)SECS.    TOTAL JOB TIME=     2.66 MINS.  -
 THERE WERE 01 TAPES MOUNTED FOR THIS JOB. TAPE MOUNT CHARGE WAS 00.0 MINUTES.
```

5Φ-11B 039853
C21038

```
//         DCB=(BLKSIZE=32000,RECFM=U,DEN=4),
//             VOL=SER=JJ0067
//GO.DATA5 DD *
//
IEF236I ALLOC. FOR YZRWPFP2 GO
IEF237I 335   ALLOCATED TO PGM=*.DD
IEF237I 335   ALLOCATED TO FT05F001
IEF237I 336   ALLOCATED TO FT06F001
IEF237I 232   ALLOCATED TO FT07F001
IEF237I 336   ALLOCATED TO SYSPRINT
IEF237I 232   ALLOCATED TO SYSPRINT
IEF237I 235   ALLOCATED TO SYSPRINT
IEF237I 335   ALLOCATED TO SYSUDUMP
IEF237I 491   ALLOCATED TO FT08F001
```

RECORD 1 OF FILE 1
LENGTH = 800 BYTES

```
4C404040  40F3F9F1  F4F54C40  40404040  404040F2  40404040  40404040  F8F14040  404C4040  40404040
4C404040  40404040  40404040  40404C40  40404040  40404040  40404040  40404040  40404040  40404040
F7F8F6F3  F6F2F8F0  60F5F04B  F0F1F0F6  F3F5F14B  F0F1F2FC  F4F3F24B  F9F3F1F6  40F2F6FC  F8F24BF5
40404040  4040F2F7  4040F24B  F7F5F7F1  40F2F04B  F3F2F1F5  40404040  40404040  40404040  40404040
F7F8F6F5  F4F2F8F0  60F5F14B  F2F0F9F1  F3F5F14B  F0F7F3F7  F4F3F24B  F4F1F2F4  40F2F6F4  F4F94BF3
4C404040  4040F2F7  4040F24B  F7F6F7F7  40F2F04B  F3F0F3F2  40404040  40404040  40404040  40404040
F7F8F6F6  F7F7F8F0  60F5F24B  F1F0F7F9  F3F5F14B  F1F2F4F8  F4F3F24B  F1F6F2F8  40F2F6F7  F4F24BF3
40404040  4040F2F7  4040F24B  F5F9F6F0  40F2F04B  F2F8F9F0  40404040  40404040  40404040  40404040
F7F8F6F8  F1F2F8F0  60F5F34B  F0F0F6F6  F3F5F14B  F1F8F0F2  F4F3F24B  F0F2F6F4  40F2F7F0  F5F04BF3
40404040  4040F2F7  4040F14B  F7F0F9F5  40F2F04B  F2F7F4F4  40404040  40404040  40404040  40404040
F7F8F6F9  F9F2F8F0  60F5F44B  F2F0F4F8  F3F5F14B  F2F6F1F7  F4F3F24B  F0F2F4F4  40F2F7F4  F8F54BF8
40404040  4040F2F7  4040F14B  F2F9FCF5  40F2F04B  F2F5F4F2  40404040  40404040  40404040  40404040
F7F8F7F1  F2F7F8F0  60F5F54B  F1F0F3F3  F3F5F14B  F3F2F8F9  F4F3F24B  F1F5F4F5  40F2F7F8  F3F04BF3
40404040  4040F2F7  4040F04B  F8F0F2F4  40F2F04B  F2F3F8F4  40404040  40404040  40404040  40404040
F7F8F7F2  F6F2F8F0  60F5F64B  F0F0F1F6  F3F5F14B  F4F0F1F9  F4F3F24B  F4F0F8F2  40F2F8F1  F9F04BF3
40404040  4040F2F7  4040F04B  F4F7F8F3  40F2F04B  F2F2F2F1  40404040  40404040  40404040  40404040
F7F8F7F4  F4F2F8F0  60F5F74B  F1F9F8F9  F3F5F14B  F5F0F8F5  F4F3F24B  F9F1F4F8  40F2F8F6  F9F34BF3
4C404040  4040F2F7  4040F04B  F5F8F2F7  40F2F04B  F1F9F9F6  40404040  40404040  40404040  40404040
F7F8F7F5  F7F7F8F0  60F5F84B  F0F9F6F5  F3F5F14B  F5F9F6F4  F4F3F34B  F4F3F6F3  40F2F9FC  F8F74BF0
40404040  4040F2F7  4C40FC4B  F8F8F3F7  40F2F04B  F1F8F1F9  40404040  40404040  40404040  40404040
```

RECORD 5701 OF FILE 1
LENGTH = 400 BYTES

```
40F1F8F9  F1F5F0F1  60F8F04B  F0F6F1F2  40F8F34B  F5F0F4F9  F5F2F64B  F7F7F4F7  40F4F5F7  F6F94BF3
4C404040  4040F1FC  4C60FC4B  F3F8F5F2  4040F04B  F0F2F1F0  40404040  40404040  40404040  40404040
40F1F8F9  F4FCF9F3  60F7F94B  F9F6F2F6  40F8F44B  F2F6F0F7  F5F2F74B  F4F7F0F0  40F4F5F8  F2F54BF8
4C404040  4040F1F0  4040F04B  F0F2F9F4  4C40F04B  F0F9F0F5  40404040  40404040  40404040  40404040
40F1F8F9  F6F6F8F5  60F7F94B  F8F6F2F2  4CF8F54B  F0F0F1F7  F5F2F84B  F1F7F0F9  40F4F5F8  F8F04BF9
4C404040  4040F1F0  4060F04B  F6F7F7F1  4040F04B  F1F6F3F1  40404040  40404040  40404040  40404040
40F1F9F0  F1F8F6F9  60F7F94B  F6F5F6F6  40F8F64B  F4F3F9F5  F5F2F94B  F5F6F7F4  40F4F5F9  F9F14BF0
4C404040  4040F1F0  4060F14B  F0F0F4F1  4040F04B  F3F1F9F0  40404040  40404040  40404040  40404040
40F1F9FC  F4F4F6F1  60F7F94B  F5F5F1F5  40F8F74B  F1F3F6F5  F5F3F04B  I2F7F4F4  40F4F6F0  F4F64BF0
4C404040  4040F1F0  4060F04B  F6F2F8F6  4040F04B  F4F0F2F5  40404040  40404040  40404040  40404040
```

5701 RECORDS IN FILE 1 OF TAPE

```
IEF142I - STEP WAS EXECUTED - COND CODE 0000
IEF285I   SYS80219.T090205.RV000.YZRWPFP2.ICDMCD      PASSED        DDNAME=PGM=*.DD            0 EXCPS
IEF285I   VOL SER NOS= K3SCR2.
IEF285I   SYS80219.T090205.RV000.YZRWPFP2.S0000229    SYSIN         DDNAME=FT05F001            2 EXCPS
IEF285I   VOL SER NOS= K3SCR6.
IEF285I   SYS80219.T090205.RV000.YZRWPFP2.S0000229    DELETED       DDNAME=FT05F001            2 EXCPS
IEF285I   VOL SER NOS= K3SCR6.
IEF285I   SYS80219.T090205.SV000.YZRWPFP2.R0000224    SYSOUT        DDNAME=FT06F001            1 EXCPS
```

S011C
D39854
C21039

```
IEF237I 335   ALLOCATED TO PGM=*.DD
IEF237I 237   ALLOCATED TO FT05F001
IEF237I 232   ALLOCATED TO FT06F001
IEF237I 237   ALLOCATED TO FT07F001
IEF237I 232   ALLOCATED TO SYSPRINT
IEF237I 235   ALLOCATED TO SYSPRINT
IEF237I 237   ALLOCATED TO SYSPRINT
IEF237I 335   ALLOCATED TO SYSUDUMP
IEF237I 490   ALLOCATED TO FT06F001
```

RECORD 1 OF FILE 1
LENGTH = 800 BYTES

```
4C60F4F9  4BF0F0F0  404C40F0  4BFC404C  40F5F2F6  4BF6FCF2  4C40F5F0  4EFCF0FC  404040F0  4EF1F8F1
4C4040F0  4BF2F7F5  404C40F0  4BF5F7F4  404C40F0  4BF3F8F7  4C4040F0  4EF2F8F7  40404040  40404040
4C60F4F7  4EF0F0F0  404C40F0  4BFC4040  40F5F1F6  4BF4F4F1  4C40F7F1  4EFCF0FC  404C4CF0  4EF6F5F8
4C4040F0  4BF5F8F8  404040F0  4EF6F6F8  404C40F0  4EF2F5F3  4C4040F0  4EF2F0F6  40404040  40404040
4C60F4F5  4BF0F0F0  404C40F0  4BF04C4C  40F4F9F7  4BF7F8F2  4C40F5F0  4EFCF0FC  404040F0  4EF7F9F6
4C4040F0  4EF9F4F5  404040F1  4BF0F4F8  404C60F0  4BF0F8F4  4C4040F0  4EF0F4FC  404C4040  4C404040
4C60F4F3  4BF0F0F0  404040F0  4BFC4040  40F5F0F6  4EF0F2F0  4C4CF9F6  4EFCF0FC  404C4CF0  4EF7F7F5
4C4040F0  4EF8F8F9  404C40F0  4BF7F7F3  404C60F0  4BF4F3F6  404C60F0  4EF1F0F3  40404040  40404040
4C60F4F1  4BF0F0F0  404040F0  4EF04C40  40F5F1F9  4EF2F4F1  4CF1F1F7  4EF0F0FC  404C40F0  4BF3F9F6
4C4040F0  4EF4F8F3  404C40F0  4EF2F3F4  404C60F0  4BF5F3F5  4C4C60F0  4EF1F9F2  40404040  40404040
4C60F3F9  4BF0F0F0  404040F0  4BFC4C4C  40F5F2F6  4BF0F1F9  4CF1F1F7  4EFCF0FC  404040F0  4EF0F7F8
4C4060F0  4EF0F4F1  404C60F0  4BF2F4F3  404C60F0  4EF2F6F4  4C4060F0  4EF2F4F1  40404040  40404040
4C60F3F7  4BF0F0F0  404040F0  4BF04C4C  40F9F4F4  4EF3F9F0  40F1F1F1  4EFCF0FC  404060F0  4EF2F4F5
4040F0F0  4BF3F7F5  404C60F0  4BF4F3F5  404C40F0  4BF0F5F5  4C4060F0  4EF2F0F7  40404040  40404040
4060F3F5  4BF0F0F0  404040F0  4EF04040  40F5F4F0  4EF9F5F3  4CF1F1F7  4EF0F0FC  404060F0  4EF3F5F1
4040F0F0  4BF5F3F5  404C60F0  4BF4F6F1  404C40F0  4BF3F6F9  4C4060F0  4EF1F5F7  40404040  40404040
4C60F3F3  4BF0F0F0  404C40F0  4BFC4C4C  40F5F3F8  4EF4F6F5  40F1F1F9  4EFCF0FC  404060F0  4EF2F4F9
4C4060F0  4BF5F2F5  404C60F0  4BF3F3FC  404C40F0  4EF5F7F1  4C4C60FC  4EF1F3F4  40404040  40404040
4C60F3F1  4BF0F0F0  404C40F0  4BF04040  40F5F3F6  4EF7F8F9  4CF1F1F7  4EF0F0FC  404C60F0  4BF0F1F4
4C4060F0  4BF2F7F8  404060F0  4EFCF2F6  404C40F0  4EF6FCF7  4040F0F0  4EF1F8F5  404C4C40  40404040
```

RECORD 800 OF FILE 1
LENGTH = 800 BYTES

```
4040F3F1  4BF0F0F0  40F3F5F8  4BF0F0F0  40F5F5F2  4EF1F5F7  40F1F2F4  4EFCF0FC  404060F2  4BF0F1F6
4040F0F2  4EF1F5F4  4040F0F1  4BF1F7F9  404C40F1  4BF9F3F4  4C4060F0  4EF5F2F8  40404040  40404040
4040F3F3  4EF0F0F0  40F3F5F8  4BF0F0FC  40F5F3F9  4EF6F6F9  4CF1F3F9  4EF0F0FC  404060F1  4BF7F3F5
4C4060F1  4BF8F3F4  4040F0F1  4BF5F7F4  404C40F0  4EF5F5F2  4C4060F0  4EF0F5F4  40404040  40404040
4C40F3F5  4BF0F0F0  40F3F5F8  4EFCFCFC  40F5F4F8  4EF0FCF4  40F1F3F2  4EFCF0FC  404060F0  4EF8F4F0
4C4060F0  4BF8F7F4  4040F0F1  4BF4F7F7  404060F0  4EF3F5F8  4C4040F0  4EF1F1F6  40404040  40404040
4040F3F7  4BF0F0F0  40F3F5F8  4BF0F0F0  40F5F4F8  4EF0F1F4  40F1F3F7  4EFCF0FC  404060F0  4EF2F1F7
4C4060F0  4BF2F2F3  404C40F0  4EF7F5F3  404C60F0  4EF6F8F8  4040F0F0  4EF2F5F3  40404040  40404040
4040F3F9  4BF0F0F0  40F3F5F8  4BF0F0F0  40F5F4F6  4BF1F1F5  40F1F2F6  4EF0F0FC  404C40F0  4EF1F7F5
4C4040F0  4BF1F9F1  404C40F0  4BF1F5F7  404C60F0  4EF6F6F2  4C4040F0  4EF4F2F5  404C4C40  40404040
4C40F4F1  4BF0F0F0  40F3F5F8  4EFCF0FC  40F5F3F9  4BF6F2F0  40F1F1F8  4EFCF0FC  404040F0  4EF5F7F4
4C4040F0  4BF4F6F8  404060F0  4EF3F3F8  404C60F0  4EF4FCF9  4C4040FC  4EF5F1F5  404C4C40  40404040
4040F4F3  4BF0F0F0  40F3F5F8  4BFCF0F0  40F5F3F2  4BF4F4F1  40F1F1F5  4EF0F0FC  404040F0  4EF4F8F9
4C4040F0  4BF4F9F2  404060F0  4BF6F5F2  404C40F0  4BF1F2F7  4C4C40F0  4EF4F5F1  40404040  40404040
4040F4F5  4BF0F0F0  40F3F5F8  4BFCF0F0  40F5F2F7  4EF3F6F5  4CF1F0F6  4EF0F0FC  404040F0  4BF4F3F8
4C4040F0  4BF2F5F2  404C60F0  4BF6F5F6  404C40F0  4BF6F7F2  4C4040F0  4EF4F3F6  40404040  40404040
4040F4F7  4BF0F0F0  40F3F5F8  4BF0F0F0  40F5F0F6  4EF7F3F3  40F1F2F6  4EFCF0FC  404060F0  4BF0F5F7
4C4060F0  4BF1F8F2  404C60F0  4BF4F1F9  404C40F1  4BF1F4F1  4C4040F0  4EF5F1F7  40404C40  40404040
4040F4F5  4BF0F0F0  40F3F5F8  4BF0F0F0  4CF4F5F5  4EF5F0F9  4CF1F1F8  4EF0F0FC  404060F0  4BF4F3F1
4C4060F0  4BF5F7F6  404C60F0  4BF0FCF6  404C40F1  4BF2F7F1  4C4040F0  4EF5F5F4  40404040  40404040
```

5CC RECORDS IN FILE 1 OF TAPE

```
IEF142I - STEP WAS EXECUTED - COND CODE 0000
IEF285I   SYS80220.T121136.RV000.YZRWPFF2.LCDMCD        PASSED          DDNAME=PGM=*.DD              0 EXCPS
IEF285I   VOL SER NOS= K3SCR2.
```

4008 DUMP OF TAPE X441

S0-110 June 9, 1969 - ~~June~~ Nov 15, 1969

D - 39870

C - 21099

INPUT TAPE X441 ON MT1
DATA INPUT H9 FL 1 1 1

40382

FILE 1 RECORD 1 LENGTH 4008BYTES

(0)	0FA80000	0FA40000	00009DBE	034A4A29	C21A320C	422AECA2	43443888	C0000005	00000001	44557A28
(40)	00000000	00000000	00009DBE	034A5569	C21A0A0F	422AF081	43443475	00000005	00000001	445572B8
(80)	00000000	00000000	00009DBE	034A60A9	C219E211	422AF45A	43443051	00000005	00000001	44556ECA
(120)	00000000	00000000	00009DBE	034A6BE9	C219BA10	422AF82F	43442C38	00000005	00000001	44556258
(160)	00000000	00000000	00009DBE	034A7729	C219920F	422AFC00	434427FF	00000005	00000001	44555A2B
(200)	00000000	00000000	00009DBE	034A796B	C2198A07	422AFCC4	43442734	00000005	00000001	445558AE
(240)	00000000	00000000	00009DBE	034A84AA	C219E208	422EC08F	434422FE	00000005	00000001	44555D7F
(280)	00000000	00000000	00009DBE	034A8FEA	C2193A04	422E0456	43441EBA	00000005	00000001	44554D0E
(320)	00000000	00000000	00009DBE	034A9B2A	C21911FF	422B0818	43441A66	00000005	00000001	4455419E
(360)	00000000	00000000	00009DBE	034AA66A	C218E9FB	422ECBD6	434415E5	00000005	00000001	4455396F
(400)	00000000	00000000	00009DBE	034AB1AA	C218C1F2	422E0F90	434411BC	00000005	00000001	44553140
(440)	00000000	00000000	00009DBE	034ABCEA	C21899EA	422E1345	43440D08	00000005	00000001	44552911
(480)	00000000	00000000	00009DBE	034AC82A	C21871E0	422B16F7	43440892	00000005	00000001	445521A1
(520)	00000000	00000000	00009DBE	034AD36A	C21849D6	422E1AA4	434403FD	00000005	00000001	44551AEF
(560)	00000000	00000000	00009DBE	034ADEAA	C21821C8	422E1E4E	4343FF77	C0000005	00000001	44551430
(600)	00000000	00000000	00009DBE	034AE9EA	C217F9BC	422E21F3	4343FAC7	00000005	00000001	44550C0E
(640)	00000000	00000000	00009DBE	034AF52A	C217D1AC	422E2595	4343F632	00000005	00000001	44550550
(680)	00000000	00000000	00009DBE	034B006A	C217A99C	422E2932	4343F173	00000005	00000001	44549EAA
(720)	00000000	00000000	00009DBE	034B0BAA	C2178188	422E2CCB	4343ECB5	00000005	00000001	44549E7B
(760)	00000000	00000000	00009DBE	034B16EA	C2175979	422E3060	4343E7E9	00000005	00000001	44549EC9
(800)	00000000	00000000	00009DBE	034B222A	C2173165	422E33F2	4343E311	00000005	00000001	44549E17
(840)	00000000	00000000	00009DBE	034B2D6A	C217094F	422E3780	4343DE48	00000005	00000001	44549E1A6
(880)	00000000	00000000	00009DBE	034B38AA	C2166139	422E3B0A	4343D95E	00000005	00000001	44549BB3
(920)	00000000	00000000	00009DBE	034B43EA	C2168921	422E3E90	4343D467	00000005	00000001	44549442
(960)	00000000	00000000	00009DBE	034B4F2A	C2169108	422E4212	4343CF5C	00000005	00000001	44549D90
(1000)	00000000	00000000	00009DBE	034B5A6A	C21668EE	422E4591	4343CA54	00000005	00000001	44549DDE
(1040)	00000000	00000000	00009DBE	034B65AA	C21640D2	422E490C	4343C541	00000005	00000001	44549C02C
(1080)	00000000	00000000	00009DBE	034B70EA	C21618E6	422E4C84	4343C023	00000005	00000001	44549E97A
(1120)	00000000	00000000	00009DBE	034B7C2A	C215F099	422E4FF7	4343BADC	00000005	00000001	44549B386
(1160)	00000000	00000000	00009DBE	034B876A	C215C87A	422E5368	4343B5A9	00000005	00000001	44549AC16
(1200)	00000000	00000000	00009DBE	034B92AA	C215A059	422E56D5	4343B06B	00000005	00000001	44549A622
(1240)	00000000	00000000	00009DBE	034B9DEA	C2157838	422E5A3F	4343AF13	00000005	00000001	44549F70
(1280)	00000000	00000000	00009DBE	034BA92A	C2155014	422E5DA5	4343A5C1	00000005	00000001	445498BE
(1320)	00000000	00000000	00009DBE	034BB46A	C21527F0	422E6108	4343A065	00000005	00000001	445492CB
(1360)	00000000	00000000	00009DBE	034BBFAA	C214FFCA	422E6467	43439E00	00000005	00000001	44548BEA
(1400)	00000000	00000000	00009DBE	034BCAEA	C214D7A3	422E67C3	434395E3	C0000005	00000001	44548567
(1440)	00000000	00000000	00009DBE	034BD62A	C214AF7B	422E6B1C	43438FFE	00000005	00000001	44547F73
(1480)	00000000	00000000	00009DBE	034BE16A	C2148750	422E6E72	43438A7E	00000005	00000001	4454797F
(1520)	00000000	00000000	00009DBE	034BECAA	C2145F26	422E71C4	43438415	00000005	00000001	44547738C
(1560)	00000000	00000000	00009DBE	034BF7EA	C21436FA	422E7513	43437F2B	00000005	00000001	44546CDA
(1600)	00000000	00000000	00009DBE	034C032A	C2140ECC	422E7860	43437994	C0000005	00000001	44546A7A5
(1640)	00000000	00000000	00009DBE	034C0E6A	C213E69D	422E7BA9	434373D7	C0000005	00000001	44546181
(1680)	00000000	00000000	00009DBE	034C1E2A	C213AE58	422E803D	43436BDC	00000005	00000001	44545BC4
(1720)	00000000	00000000	00009DBE	034C296A	C2133626	422E837F	434366D8	C0000005	00000001	44545DD0
(1760)	00000000	00000000	00009DBE	034C34AA	C2135DF3	422E86BE	4343601E	00000005	00000001	44544CDD
(1800)	00000000	00000000	00009DBE	034C3FEA	C21335BE	422E89FA	43435A3D	00000005	00000001	44544EE9
(1840)	00000000	00000000	00009DBE	034C4B2A	C2130D87	422E8D33	43435456	C0000005	00000001	44544037
(1880)	00000000	00000000	00009DBE	034C566A	C212E550	422E9069	4343E44B	00000005	00000001	44543A43
(1920)	00000000	00000000	00009DBE	034C61AA	C212BD17	422E939C	4343483A	00000005	00000001	445435CD
(1960)	00000000	00000000	00009DBE	034C6CEA	C21294DD	422E96CC	43434234	00000005	00000001	44542FD9
(2000)	00000000	00000000	00009DBE	034C782A	C2126CA2	422E99FA	43433C0A	00000005	00000001	44542BE6
(2040)	00000000	00000000	00009DBE	034C836A	C2124464	422E9D25	434335EA	00000005	00000001	445424B0
(2080)	00000000	00000000	00009DBE	034C8EAA	C2121C26	422EA04D	43432FE6	00000005	00000001	44541DFE
(2120)	00000000	00000000	00009DBE	034C99EA	C211F3E5	422EA373	43432980	00000005	00000001	44541B06
(2160)	00000000	00000000	00009DBE	034CA52A	C211CBA4	422EA695	43432341	C0000005	00000001	445412D6
(2200)	00000000	00000000	00009DBE	034CB06A	C211A361	422EA9B5	43431CF2	00000005	00000001	44540CE2
(2240)	00000000	00000000	00009DBE	034CBBAA	C2117B1E	422EACD3	43431690	00000005	00000001	445407AD

(2360)	00000000	00000000	00009DBE	034CDDEA	C2110249	422EE61D	43430347	C0000005	00000001	4453F691
(2400)	00000000	00000000	00009DBE	034CE8AA	C210D9FF	422EB930	4342FCCA	00000005	00000001	4453F15C
(2440)	00000000	00000000	00009DBE	034CF3EA	C2108184	422EEC41	4342F63B	00000005	00000001	4453EC26
(2480)	00000000	00000000	00009DBE	034CFF2A	C2108967	422EBF50	4342EFAA	00000005	00000001	4453E633
(2520)	00000000	00000000	00009DBE	034D0A6A	C2106118	422EC25D	4342E907	00000005	00000001	4453E0FE
(2560)	00000000	00000000	00009DBE	034D15AA	C21038C9	422EC567	4342E2E3	00000005	00000001	4453DB0A
(2600)	00000000	00000000	00009DBE	034D20EA	C2101078	422EC86F	4342DBAE	00000005	00000001	4453D5D5
(2640)	00000000	00000000	00009DBE	034D2C2A	C1FE8256	422ECB74	4342D4F8	00000005	00000001	4453CFE1
(2680)	00000000	00000000	00009DBE	034D388A	C1FBBC93	422ECEC4	4342CD75	00000005	00000001	4453CAAC
(2720)	00000000	00000000	00009DBE	034D43CA	C1F93744	422ED1C5	4342C69E	00000005	00000001	4453C577
(2760)	00000000	00000000	00009DBE	034D4F0A	C1F6B1D5	422ED4C3	4342BFB6	00000005	00000001	4453BF84
(2800)	00000000	00000000	00009DBE	034D5A4A	C1F42C50	422ED7C0	4342E8C5	00000005	00000001	4453BA4E
(2840)	00000000	00000000	00009DBE	034D658A	C1F1A6B4	422EDABA	4342B1D6	00000005	00000001	4453B519
(2880)	00000000	00000000	00009DBE	034D70CA	C1EF20FC	422EDDB2	4342AADE	00000005	00000001	4453AFE4
(2920)	00000000	00000000	00009DBE	034D7C0A	C1EC9B33	422EE0A8	4342A3C8	00000005	00000001	4453AAAF
(2960)	00000000	00000000	00009DBE	034D874A	C1EA1541	422EE39C	43429CC9	00000005	00000001	4453A57A
(3000)	00000000	00000000	00009DBE	034D928A	C1E78F4E	422EE68E	4342959E	00000005	00000001	4453A045
(3040)	00000000	00000000	00009DBE	034D9DCA	C1E5093C	422EE97E	43428E73	00000005	00000001	44539B10
(3080)	00000000	00000000	00009DBE	034DA90A	C1E2830B	422EEC6C	4342874A	00000005	00000001	445395DA
(3120)	00000000	00000000	00009DBE	034DB44A	C1DFFCBC	422EEF58	43428022	C0000005	00000001	44539164
(3160)	00000000	00000000	00009DBE	034DBF8A	C1DD7668	422EF242	434278CD	00000005	00000001	44538B70
(3200)	00000000	00000000	00009DBE	034DCACA	C1DAEFF6	422EF52B	4342717B	00000005	00000001	445386FA
(3240)	00000000	00000000	00009DBE	034DD60A	C1D86966	422EF811	43426A2A	00000005	00000001	44538104
(3280)	00000000	00000000	00009DBE	034DE14A	C1D5E2C5	422EFAF6	434262BD	00000005	00000001	44537C8F
(3320)	00000000	00000000	00009DBE	034DEC8A	C1D35BFD	422EFDD9	43425BE1	00000005	00000001	44537819
(3360)	00000000	00000000	00009DBE	034DF7CA	C1D0D527	422C00B9	434253EA	00000005	00000001	445372E3
(3400)	00000000	00000000	00009DBE	034E030A	C1CE4E35	422C0399	43424C76	00000005	00000001	44536E6D
(3440)	00000000	00000000	00009DBE	034E0E4A	C1CBC72B	422C0676	434244E5	00000005	00000001	44536879
(3480)	00000000	00000000	00009DBE	034E198A	C1C94018	422C0952	43423D3A	00000005	00000001	44536402
(3520)	00000000	00000000	00009DBE	034E24CA	C1C68BDC	422C0C2D	434235A1	00000005	00000001	44535F8C
(3560)	00000000	00000000	00009DBE	034E300A	C1C43183	422C0F05	43422ECC	C0000005	00000001	44535A57
(3600)	00000000	00000000	00009DBE	034E3B4A	C1C1AA1F	422C11DC	43422640	00000005	00000001	44535EE0
(3640)	00000000	00000000	00009DBE	034E468A	C1BF22A3	422C14B1	43421E81	00000005	00000001	44535169
(3680)	00000000	00000000	00009DBE	034E51CA	C1BC9B0C	422C1785	43421ECA	00000005	00000001	44534CF3
(3720)	00000000	00000000	00009DBE	034E5D0A	C1BA134D	422C1A57	43420EF9	00000005	00000001	445347BD
(3760)	00000000	00000000	00009DBE	034E684A	C1B78B7F	422C1D28	4342071C	00000005	00000001	44534347
(3800)	00000000	00000000	00009DBE	034E738A	C1B5C3A0	422C1FF7	4341FF2E	00000005	00000001	44533F8F
(3840)	00000000	00000000	00009DBE	034E7ECA	C1B27B99	422C22C5	4341F743	00000005	00000001	44533B18
(3880)	00000000	00000000	00009DBE	034E8A0A	C1AFF37D	422C2592	4341EF5E	00000005	00000001	445335E3
(3920)	00000000	00000000	00009DBE	034E954A	C1AD6B47	422C285D	4341E761	00000005	00000001	44533224
(3960)	00000000	00000000	00009DBE	034EA08A	C1AAE301	422C2B26	4341DF42	C0000005	00000001	44532DB4
(4000)	00000000	00000000								

FILE 1 RECORD 1724 LENGTH 4008BYTES

(0)	0FA80000	0FA40000	00009E5D	0026161C	C223F95D	4291E90C	43421250	00000003	00000001	44BF346A
(40)	00000000	00000000	00009E5D	00269D1C	C225DB27	42922E14	4341D630	00000003	00000001	4491C1A3
(80)	00000000	00000000	00009E5D	0027241C	C227BDB6	42927BC8	434193F0	00000003	00000001	4494710F
(120)	00000000	00000000	00009E5D	0027AB1C	C2299FEA	4292C9DD	43414C00	00000003	00000001	44968 7ED
(160)	00000000	00000000	00009E5D	00283210	C22B8220	42932236	4340FDF0	00000003	00000001	4499C10A
(200)	00000000	00000000	00009E5D	0028BB5D	C22DEC5E	42938475	4340A8B0	00000003	00000001	4499E84C
(240)	00000000	00000000	00009E5D	00389118	C23D6568	C23CAA82	4329B720	00000003	00000001	44748CAF
(280)	00000000	00000000	00009E5D	0039193B	C23B5679	C23E989E	4328EBC0	00000003	00000001	4470C0BF
(320)	00000000	00000000	00009E5D	003CA03B	C2394758	C23AAE3E	43282370	00000003	00000001	44ECDF97
(360)	00000000	00000000	00009E5D	003D273B	C2373421	C239DA20	43275CA0	00000003	00000001	44691E73
(400)	00000000	00000000	00009E5D	003DB4FB	C2350249	C23917ED	43268E10	00000003	00000001	44E5E1EB
(440)	00000000	00000000	00009E5D	003E3BFB	C232E7A5	C2387340	4325CBE0	00000003	00000001	44E1E67C
(480)	00000000	00000000	00009E5D	003EC2FB	C230C989	C237DF7C	43250BE0	00000003	00000001	44EEE369
(520)	00000000	00000000	00009E5D	003F49FB	C22EA8BA	C2375A10	43244ED0	00000003	00000001	44598ED4
(560)	00000000	00000000	00009E5D	003FD0FB	C22C84D3	C236E104	43239510	00000003	00000001	44590DF1
(600)	00000000	00000000	00009E5D	004057FC	C22A5E21	C236720D	4322DEE0	00000003	00000001	44E6A23E
(640)	00000000	00000000	00009E5D	0040E01C	C228302C	C236CCD7	43222B30	00000003	00000001	44547BBB
(680)	00000000	00000000	00009E5D	0041695C	C225FB04	C235AE7E	43217A70	00000003	00000001	44529D61
(720)	00000000	00000000	00009E5D	0041F05C	C223CCB2	C2355BD3	4320D130	00000003	00000001	445110DC
(760)	00000000	00000000	00009E5D	004277EC	C2219C10	C2350957	43202C80	C0000003	00000001	444FCDFE

(880)	00000000	00000000	00009E5D	00440E9B	C21AF3C7	C2343FE5	431E5D00	00000003	00000001	44[illegible]
(920)	00000000	00000000	00009E5D	00449E9B	C214BAD5	C233FA89	431DCF10	00000003	00000001	444DAE8C
(960)	00000000	00000000	00009E5D	00451DBB	C2167B4E	C233BFE8	431D4EE0	00000003	00000001	444DD659
(1000)	00000000	00000000	00009E5D	00459A4B	C2143ECE	C23388BE	431CC580	00000003	00000001	444E505A
(1040)	00000000	00000000	00009E5D	00463278	C211E3F1	C2335104	431C4580	00000003	00000001	444F1FE9
(1080)	00000000	00000000	00009E5D	0046BBBB	C1F9AA11	C2331D66	431BD120	00000003	00000001	44503E5A
(1120)	00000000	00000000	00009E5D	00474288	C1D59805	C232EC5B	431B6610	00000003	00000001	44519CB8
(1160)	00000000	00000000	00009E5D	0047C9EB	C1B1713D	C232ECFD	431B0280	00000003	00000001	44534CF3
(1200)	00000000	00000000	00009E5D	004351DB	C18CEA35	C2328DE4	431AA620	00000003	00000001	44555D7F
(1240)	00000000	00000000	00009E5D	0048D9FB	C16851E7	C2325FED	431A51A0	00000003	00000001	44577A0A8
(1280)	00000000	00000000	00009E5D	0049621B	C143AA23	C2323299	431A0570	00000003	00000001	44[illegible]
(1320)	00000000	00000000	00009E5D	0049E91B	C11F42A8	C2320603	4319C230	00000003	00000001	44[illegible]
(1360)	00000000	00000000	00009E5D	004A76DB	40703080	C231D754	43198490	00000003	00000001	44[illegible]
(1400)	00000000	00000000	00009E5D	004B049A	412D52A9	C231A87F	43195040	00000003	00000001	44[illegible]
(1440)	00000000	00000000	00009E5D	004B8B9A	4151D6EC	C2317B82	4319274C	00000003	00000001	44[illegible]
(1480)	00000000	00000000	00009E5D	004C13BA	4176AE5E	C2314D7F	43190EC0	00000003	00000001	44[illegible]
(1520)	00000000	00000000	00009E5D	004C9ABA	419B3AFC	C2311EF6	4318EF30	00000003	00000001	44[illegible]
(1560)	00000000	00000000	00009E5D	004D251A	41C0B2A8	C230EE0A	4318DFF0	00000003	00000001	4472A984
(1600)	00000000	00000000	00009E5D	004DAC1A	41E53F4F	C230ECD7	4318DA10	00000003	00000001	44769B9F
(1640)	00000000	00000000	00009E5D	004E331A	42109C8E	C230B9DE	4318DCC0	00000003	00000001	447A7CF0
(1680)	00000000	00000000	00009E5D	004EBFBA	4212FD29	C230528C	4318E8E0	00000003	00000001	447E916C
(1720)	00000000	00000000	00009E5D	004F543A	42157F4E	C23C1537	4318FFE0	00000003	00000001	44[illegible]
(1760)	00000000	00000000	00009E5D	004FDC5A	4217CB4C	C22FD9EE	43191DF0	00000003	00000001	44[illegible]
(1800)	00000000	00000000	00009E5D	00506358	421A11B3	C22F9EC8	4319444C	00000003	00000001	44[illegible]
(1840)	00000000	00000000	00009E5D	0050EC9B	421C60E7	C22F58AC	431973B0	00000003	00000001	44[illegible]
(1880)	00000000	00000000	00009E5D	00517398	421EA563	C22F1240	4319AAE0	00000003	00000001	44[illegible]
(1920)	00000000	00000000	00009E5D	00520278	42210A78	C22EC241	4319EDB0	00000003	00000001	4494EBC9
(1960)	00000000	00000000	00009E5D	00528978	42234C6F	C22E70BF	431A3520	00000003	00000001	4497FBE5
(2000)	00000000	00000000	00009E5D	00531DFA	4225C67B	C22E0F6F	431A8C80	00000003	00000001	449B1965
(2040)	00000000	00000000	00009E5D	0065683A	42411BDC	42692F57	43309120	00000003	00000001	44[illegible]
(2080)	00000000	00000000	00009E5D	0066B1D9	423C53E9	42EC2355	43325710	00000003	00000001	44A2D08C
(2120)	00000000	00000000	00009E5D	00684FF9	42366AF7	42EEA37E	433476A0	00000003	00000001	449CA3AE
(2160)	00000000	00000000	00009E5D	00696EB9	42322040	42EFF4FB	4335F3E0	00000003	00000001	449EFC14
(2200)	00000000	00000000	00009E5D	006ACB79	422D0E6E	42712A3C	4337A510	00000003	00000001	44[illegible]
(2240)	00000000	00000000	00009E5D	006BBB19	422994F4	4271D5C7	4338C270	00000003	00000001	44[illegible]
(2280)	00000000	00000000	00009E5D	006CB3B9	4225FC63	42726D3B	4339DEF0	00000003	00000001	44830D51
(2320)	00000000	00000000	00009E5D	006D7779	42232964	4272D530	433AFE10	00000003	00000001	447E[illegible]3C
(2360)	00000000	00000000	00009E5D	006E5F38	421FD390	4273421E	433BAA0C	00000003	00000001	44783BAA
(2400)	00000000	00000000	00009E5D	006F58F8	421C3DFB	4273A973	433CA310	00000003	00000001	447234B7
(2440)	00000000	00000000	00009E5D	00703218	42192270	4273F9A1	433D6FEC	00000003	00000001	446D5BD4
(2480)	00000000	00000000	00009E5D	00711008	4215F453	42744443	433E34D0	00000003	00000001	446BEC95
(2520)	00000000	00000000	00009E5D	0071D918	42131A2B	427481ED	433EDB40	00000003	00000001	446[illegible]333
(2560)	00000000	00000000	00009E5D	0072CE58	41F9E10A	4274C7C3	433F9850	00000003	00000001	44623793
(2600)	00000000	00000000	00009E5D	00738A39	41CF427D	4274F9D5	43401DF0	00000003	00000001	446[illegible]F8B
(2640)	00000000	00000000	00009E5D	00747889	419944D2	42753E15	4340B92C	00000003	00000001	445F2B30
(2680)	00000000	00000000	00009E5D	00755899	4166B1C4	42756C18	43413BD0	00000003	00000001	445F04A0
(2720)	00000000	00000000	00009E5D	00760939	413EDC8F	427599B4	43419830	00000003	00000001	445F9888
(2760)	00000000	00000000	00009E5D	00760638	41144CC4	4275C11D	4341F0AC	00000003	00000001	446[illegible]92E
(2800)	00000000	00000000	00009E5D	007777F8	C113AD14	4275E9CE	434239E0	00000003	00000001	44629314
(2840)	00000000	00000000	00009E5D	007817B8	C1379035	42760E6C	43427330	00000003	00000001	44648[illegible]C0
(2880)	00000000	00000000	00009E5D	00788BB8	C15FF528	4276[illegible]11	4342AA10	00000003	00000001	44672251
(2920)	00000000	00000000	00009E5D	00797118	C18503D0	4276EEFD	4342D380	00000003	00000001	44[illegible]D7AA
(2960)	00000000	00000000	00009E5D	007A2AB8	C1AE9D81	42768BD2	4342F760	00000003	00000001	446D2C38
(3000)	00000000	00000000	00009E5D	007AD378	C1D462FF	4276E5F9	43430E80	00000003	00000001	44706938
(3040)	00000000	00000000	00009E5D	007B6D99	C1F6DD48	4276DDF4	43431B30	00000003	00000001	44737D89
(3080)	00000000	00000000	00009E5D	007C0219	C2118110	42770615	43432040	00000003	00000001	4476[illegible]AAB
(3120)	00000000	00000000	00009E5D	007C9C39	C213A830	427731B0	43431DD0	00000003	00000001	4479C177
(3160)	00000000	00000000	00009E5D	007D39E9	C215DB2F	42776[illegible]C	43431310	00000003	00000001	447D10CF
(3200)	00000000	00000000	00009E5D	007DC9B9	C217DDC8	42778E17	43430220	00000003	00000001	448C15C2
(3240)	00000000	00000000	00009E5D	007E5BF8	C219E84B	4277BEF8	4342E9F0	00000003	00000001	448[illegible]1E6E
(3280)	00000000	00000000	00009E5D	007EED18	C21BEEBD	4277F29B	4342CAC0	00000003	00000001	448[illegible]1838
(3320)	00000000	00000000	00009E5D	007F82B8	C21E0534	42782B8[illegible]	4342A370	00000003	00000001	448[illegible]18E5
(3360)	00000000	00000000	00009E5D	00801AF8	C2200F99	427[illegible]6752	43427560	00000003	00000001	448[illegible]F57C
(3400)	00000000	00000000	00000000	00000000	00000000	00000000	00000000	00000000	00000000	00000000

```
(  3520)  00000000  00000000  00000000  00000000  00000000  00000000  00000000  00000000  00000000  00000000
(  3560)  00000000  00000000  00000000  00000000  00000000  00000000  00000000  00000000  00000000  00000000
(  3600)  00000000  00000000  00000000  00000000  00000000  00000000  00000000  00000000  00000000  00000000
(  3640)  00000000  00000000  00000000  00000000  00000000  00000000  00000000  00000000  00000000  00000000
(  3680)  00000000  00000000  00000000  00000000  00000000  00000000  00000000  00000000  00000000  00000000
(  3720)  00000000  00000000  00000000  00000000  00000000  00000000  00000000  00000000  00000000  00000000
(  3760)  00000000  00000000  00000000  00000000  00000000  00000000  00000000  00000000  00000000  00000000
(  3800)  00000000  00000000  00000000  00000000  00000000  00000000  00000000  00000000  00000000  00000000
(  3840)  00000000  00000000  00000000  00000000  00000000  00000000  00000000  00000000  00000000  00000000
(  3880)  00000000  00000000  00000000  00000000  00000000  00000000  00000000  00000000  00000000  00000000
(  3920)  00000000  00000000  00000000  00000000  00000000  00000000  00000000  00000000  00000000  00000000
(  3960)  00000000  00000000  00000000  00000000  00000000  00000000  00000000  00000000  00000000  00000000
(  4000)  00000000  00000000
```

FILE	INPUT RECS.	DATA RECORDS INPUT	MAX. SIZE	READ ERROR SUMMARY PERM	ZERO B	SHORT	UNDEF.	INPUT RETRIES #RECS.	TOTAL#
1	1724	1725	4008	0	0	0	0	3	9

EOJ DUMP STOPPED AFTER FILE 1 # OF PERMANENT READ ERRORS 0

START TIME 07/23/80 09:15:20 STOP TIME 07/23/80 09:16:24

$$
$ASS IN MT3
```
```